

CONFORMATIONAL AND PHASE TRANSITIONS OF BRUSH-LIKE
MACROMOLECULES AT INTERFACES

Jamie Boyce Arnold

A dissertation submitted to the faculty of the University of North Carolina at Chapel Hill in
partial fulfillment of the requirements for the degree of Doctor of Philosophy in the
Department of Chemistry

Chapel Hill
2008

Approved by

Advisor: Sergei Sheiko

Michael Rubinstein

Ed Samulski

Tom Baer

John Papanikolas

© 2008
Jamie Boyce Arnold
ALL RIGHTS RESERVED

ABSTRACT

JAMIE B. ARNOLD: Conformational and Phase Transitions of Brush-like Macromolecules at Interfaces
(Under the direction of Sergei S. Sheiko)

Flexible molecular brushes have exhibited extraordinary conformational and phase behavior that is largely a result of their brush-like architecture. The interaction between the densely grafted side chains controls both the conformation of the flexible backbone (hence molecular shape) and the intramolecular interactions (hence ordering and mixing). The unusual behavior of molecular brushes was especially evident when studying either single adsorbed molecules or dense monolayers on substrates. Molecular imaging by atomic force microscopy in combination with Langmuir-Blodgett monolayer characterization and replication via a PFPE-based soft-lithography technique proved to be an invaluable tool to characterize molecular weight distributions, individual branch size distributions, and conformational transitions of individual brush-like macromolecules. These molecules were observed to undergo discrete conformational transitions in response to changes of substrate area and substrate chemical composition. The transitions depended on the details of the molecular branching architecture as well as the molecular chemical composition. In addition to the molecular properties, the brush architecture stabilized the ordering of disk-like macromolecules and enhanced the mixing of two otherwise immiscible polymers. Not only did they mix, but they also exhibited an ordered structure of alternating hydrophilic and hydrophobic molecules.

In memory of my dear friend
Laurie McCauley

ACKNOWLEDGEMENTS

I want to thank my mom and dad, Toby and Julie Boyce, for always encouraging me no matter what decisions I made, even when I decided to go to graduate school and you weren't even sure what that meant! Laurie, thanks for being proud of me and encouraging me—it meant more than you know.

Mr. Burner, thank you for encouraging me to take AP chemistry, for seeing something in me that I didn't yet see in myself.

Dr. Seidman, thank you for showing me the excitement of physical chemistry and for teaching me classes when I was the only student taking them.

Dr. Mattson, thank you for helping me to think outside the box and for showing me that I usually am not. Thank you for teaching me how to make a solution and properly clean glassware, among many other invaluable, while seemingly ordinary skills a chemist should have.

Stephanie Canyon—without your encouragement I may never have attended graduate school at all. Thank you for helping me to see things in myself that I could not yet see.

Laurie and Greg McCauley—what an amazing friendship that developed from me tutoring Scott and Lauren! Thank you for your overflowing encouragement and your prayers for “finishing well.” My life has been forever changed by our vivid friendship.

To Isaac LaRue—your surprising combination of patience and candor helped me immensely to persevere in the early years of research. Thank you for your help.

Sam Lord, your genuine love for science was inspiring and encouraging. Thank you for inadvertently spawning the lab cake-cooking contest.

Frank Sun, you often made coming to lab much more fun than it otherwise would have been. Thank you also for your candor and for your help in giving me fresh perspective on my projects.

Sherryl Yu, Mike Barrett, and Hui Xu, thank you for all your help in just learning instrumental techniques, discussing research problems, and then just having fun. I couldn't have asked for a better lab group.

Dr. Rubinstein, thank you for asking the hard questions. The fear of them made me be better prepared for seminars and conferences and made me think more thoroughly about my research.

Sergei, thank you so much for introducing me to the wonders of polymer physics and AFM. Thank you for helping me to learn how to communicate science in a way that people can understand and be interested in. Your patience toward me has seemed bottomless, and I appreciate it so much and recognize that it was often practiced in the face of some amount of irrationality on my part. ☺ Thank you for always trying to fully communicate a concept, making sure that it was rightly understood. It has been, on the whole, a pleasure working in your lab.

Charles, what a life we have begun together. Thank you for bearing with me in these final hours of graduate work and being proud of me. Your constant presence and support is a new luxury I pray I will never take for granted.

And, of course, I must thank my God and Savior, Jesus Christ, who led me here and gave me this task. I thank him for sustaining me and giving me everything that I have needed to complete the work I had to complete. I am thankful for the many experiences I have had during this time, though many of them painful. I have been changed by the experiences of the past six years in ways I could not have anticipated and am grateful for it. And I am also thankful for the order and complexity in the universe and on our little planet that makes science possible and fascinating. “The boundary lines have fallen for me in pleasant places; surely I have a delightful inheritance.” Psalm 16.6

TABLE OF CONTENTS

LIST OF TABLES.....xi

LIST OF FIGURES.....xii

Chapters

1	INTRODUCTION.....	1
1.1	Introduction of the Problem.....	1
1.2	Biological Brushes.....	4
1.3	Synthetic Molecular Brushes.....	7
1.4	Synthesis of Molecular Brushes.....	9
1.5	Conformation of Brush-like Macromolecules.....	12
1.5.1	Brush Conformation in Solution.....	12
1.5.2	Brush Conformation on Surfaces.....	15
1.6	Fundamental Issues.....	21
1.7	Experimental Challenges.....	21
2	SINGLE MOLECULE CHARACTERIZATION OF COMPLEX MACROMOLECULES: THE DIMENSIONS, CONFORMATION, AND ORDERING OF MULTI-ARM BRUSHES.....	24
2.1	Addressing the Challenges of Complicated Molecules.....	24
2.2	The Necessity of Molecular Imaging.....	26

2.3	The Characterization of Single-molecule Dimensions.....	28
2.3.1	Confirming the Synthesis of Star-like Molecular Brushes.....	28
2.3.2	Molecular Weight Characterization.....	30
2.3.3	Molecular Weight Distribution.....	32
2.3.4	Arm-length Distribution.....	33
2.3.5	Conclusions for Single-molecule Characterization.....	36
2.4	Conformational Transition and Surface Ordering of the Four-arm Brush.....	37
2.4.1	Conformational Transitions.....	37
2.4.2	Ordering of Four-arm Macromolecules.....	40
2.5	Conclusions.....	46
3	THE EVALUATION OF THE ACCURACY OF AFM USING MOLECULAR REPLICATION.....	48
3.1	A Shortcoming of Tapping Mode AFM.....	48
3.2	Curable PFPE-Based Molecule Replication.....	50
3.3	Replicating Single Molecules Using the Soft Lithography Technique.....	53
3.4	Analysis and Discussion.....	56
3.4.1	Masters and Replicates.....	56
3.4.2	Considering the Surface Properties of PFPE.....	61
3.5	Conclusions.....	63
4	COMPARING THE CONFORMATIONAL BEHAVIOR OF HYDROPHILIC AND HYDROPHOBIC MACROMOLECULAR BRUSHES.....	65
4.1	The Conformational Transitions of Brush Polymers.....	65
4.2	The Illusive Cylindrical Conformation.....	67

4.3	Synthesis and Characterization.....	69
4.4	Results and Discussion.....	71
4.4.1	The Stability of PDMA Monolayers at the Air-Water Interface: Linear and Brush-like Macromolecules.....	71
4.4.2	Conformational Transitions.....	78
4.4.3	Discussion.....	84
4.5	Copolymer Brushes.....	87
4.5.1	Characterization.....	87
4.5.2	Results and Discussion.....	87
4.6	Conclusions.....	91
5	THE MIXING OF CHEMICALLY DIFFERENT MACROMOLECULAR BRUSHES.....	93
5.1	Polymer Mixing.....	93
5.2	Polymers Studied.....	96
5.3	The Phenomenon.....	98
5.3.1	Linear Polymer Mixing.....	98
5.3.2	Brush Polymer Mixing.....	101
5.4	Effects on Mixing.....	103
5.4.1	Brush Mixtures with Varying Side Chain Lengths.....	103
5.4.2	Linear and Brush Mixtures.....	107
5.5	Mixing Kinetics and Analysis of Ordering.....	109
5.6	Discussion.....	114
5.7	Conclusion.....	116
6	Conclusion.....	118

REFERENCES.....118

LIST OF TABLES

2.1	Molecular Weight Data for Backbones and Brushes.....	33
2.2	Length Characterization from AFM Measurements.....	34
3.1	Areas and Heights for Single Collapsed Molecules and Drops Determined from AFM Height Images.....	59
3.2	Heights for Extended Linear Brush and Collapsed Four-arm Brush Determined from AFM Height Images.....	60
4.1	Molecular Characterization by MALLS-GPC and AFM-LB Techniques.....	70
4.2	Length Data for Compressed and Uncompressed Brush Monolayers.....	83
4.3	Characterization Data for Copolymer Brushes.....	87
5.1	Molecular Weight Data for Polymers Studied.....	97

LIST OF FIGURES

Figure	
1.1	Examples of Trichomes.....4
1.2	Structure of a Proteoglycan Aggregate.....7
1.3	The Variety of Brush Structure.....8
1.4	Three Synthetic Strategies for Brushes.....10
1.5	Surface Conformations of Brushes.....16
1.6	Equilibrium Spreading.....17
1.7	AFM Images of Brush Surface Conformations.....19
2.1	Multi-arm Brush Synthetic Scheme.....29
2.2	AFM Height Images of Multi-arm Brushes.....30
2.3	Schematic of the Langmuir-Blodgett (LB) Trough.....31
2.4	LB Monolayer Transfer onto a Solid Substrate.....32
2.5	Schematic for the Conformational Transition of a Multi-arm Brush Molecule Caused by Two-dimensional Compression.....38
2.6	LB Isotherm for the Four-arm Brush.....39
2.7	AFM Height Images of the Four-arm Brush Conformational Transition.....40
2.8	2D Power Spectral Density of Monolayers of Globular Molecules.....42
2.9	Angular Dependence of the 2D Power Spectral Density Function.....42
2.10	Radial Correlation Function and Amplitude Decay.....43
2.11	Orientalional Order Function.....45
2.12	Exponential and Power Law Fits for G_646
3.1	Scheme of Collapsed Brush Molecule.....50

3.2	Perfluoropolyether.....	51
3.3	Soft Lithography Process.....	52
3.4	AFM of the Replication of Single Collapsed Molecules.....	53
3.5	AFM of the Replication of Droplets.....	54
3.6	AFM of the Replication of Extended Molecules.....	55
3.7	AFM of the Replication of Collapsed Star Molecules.....	56
3.8	The Contact Angle of the Cap.....	62
4.1	Conformational Diagram for Cylindrical Brushes.....	66
4.2	Compressed Brush Conformations.....	67
4.3	Linear PDMA Consecutive Isotherms.....	72
4.4	Pressure Limited Consecutive Isotherms of Linear PDMA.....	72
4.5	Consecutive PDMA Brush Isotherms.....	75
4.6	Monitoring of the a/w Interface for Adsorbing Molecules.....	76
4.7	PBA Brush Isotherm and Corresponding AFM Height Images	79
4.8	PDMA Brush Isotherm and Corresponding AFM Height Images.....	81
4.9	Dependence of Intermolecular Distance with Compression.....	82
4.10	Molecular Parking.....	84
4.11	Conformational Changes of PBA-PDMA Copolymer Brushes.....	88
4.12	Dependence of Intermolecular Distance on MMA.....	89
4.13	Copolymer and Homopolymer Isotherms.....	90
5.1	Possible States of Two-Component Mixing.....	92
5.2	Chemical Structures of the Monomers Used.....	98
5.3	Linear Mixtures from Premixed Solutions.....	99

5.4	PDMA Domain Size in Linear Mixture with Time.....	100
5.5	AFM Height Images of Mixed Monolayers at Different Lateral Pressures.....	102
5.6	Phase Contrast Between PBA and PDMA.....	102
5.7	AFM Height Images of Mixed Monolayers with Different Side Chain Length PBA Brushes.....	104
5.8	Intermolecular Distances of All Species in Monolayers with Different Side Chain Length PBA Brushes.....	105
5.9	AFM Images for Mixed Monolayers with Different Side Chain Length PDMA Brushes.....	106
5.10	Intermolecular Distances Between All Species with Different Side Chain Length PDMA Brushes.....	106
5.11	AFM Height and Phase Image of Linear PDMA with PBA Brushes.....	107
5.12	Monolayers of Various Linear Polymers Mixed with PDMA Brush.....	108
5.13	The Dependence of PDMA Brush Intermolecular Distance on the Molecular Weight of the Linear Polymer.....	109
5.14	AFM Height Images of Brush Monolayers Mixed with Time.....	110
5.15	Fractions of Like and Unlike Polymer Pairs in Monolayers at Different Pressures and Times.....	112
5.16	Intermolecular Distances Between All Species in the Premixed Brush Monolayer.....	113
5.17	Scheme of Polymer Brushes at the Air/Water Interface.....	115

CHAPTER 1

INTRODUCTION

1.1 Introduction of the Problem

From cleaning teeth to painting walls, brushes are used in nearly all aspects of life. The brush form is ubiquitous because of its functionality, which is imparted by the flexible bristles that are densely tethered to a substrate. This dense grafting gives the brush shape persistence even in the case of flexible substrates. The brush morphology also provides a large surface-to-volume ratio, increasing the mass-loading of a fluid such as for a paint brush.

Similar principles are relevant for molecular brushes. If there was a molecule with a flexible backbone decorated with densely grafted long side chains, this brush-like macromolecule would adopt the shape of a semi-flexible cylinder possessing a high density of functional groups. However, in contrast to colloidal brushes on a rigid substrate, conformation of molecular brushes with a flexible backbone is a subject to change. The flexible substrate (backbone) must follow the self-organization of the tethered side-chains that may alter in response to variations in the surrounding environment. A common example of this is a brush-like protein aggregate known as proteoglycan found in joint cartilage. Proteoglycan changes shape with upon compression, resulting in an increase of osmotic pressure that resists joint deformation and wear (see the following section). These molecules give cartilage its impact resistance and a lack of them is known to contribute to the onset of osteoarthritis. The concept of super-functional and shape-persistent

macromolecules, which could also switch its shape and maintain shape persistence in multiple conformations, inspired polymer chemists. Synthetic molecules have been designed that change shape with changes in their environment (temperature, pH, ionic strength) as well as respond to an external field. Such stimuli responsive molecules can be used as small containers for drug delivery, fragrance in health and beauty products, or other similar applications. One of the many examples is a 32-arm star core-shell molecule having a hydrophobic poly(n-butyl acrylate) core and a hydrophilic poly(ethylene glycol) methyl ether methacrylate shell.¹ These molecules were able to carry a hydrophobic load as unimolecular containers (i.e. without aggregating) in an aqueous solution. Cylindrical polymer brushes have been used to make water-soluble nanowires of a similar core-shell structure, by crosslinking the inner block of diblock side chains.² While these nanowires were rigid and did not have a variable conformation, their unique chemical structure allowed them to exhibit lyotropic liquid crystalline-like behavior. In a sense, this gives the system as a whole a conformational variability. Demonstrating further utility, shape persistent molecules can self-organize on surfaces, resulting in bottom-up lithography, the feature size of which is only limited by the size of the molecules. Brush-like macromolecules with the switchable and persistent shapes can be viewed as peculiar mesoscopic building blocks for the construction of larger structures and functional systems. These applications depend on being able to control the molecule's shape or conformation.

The conformation of brush-like macromolecules depends on their architecture and chemical composition. The architecture comprises branching topology, grafting density, and

¹ Kreutzer, G. *et al. Macromolecules* **2006**, *39*, 4506.

² Yuan, J.; Xu, Y.; Walther, A.; Schumacher, M.; Schmalz, H.; Müller, A.H.E. *Polym. Prepr. (Am. Chem. Soc., Div. Polym. Chem.)* **2008**, in press

length of the side chains. The chemical composition determines molecular interactions and chain flexibility. The side chains can be hydrophilic or hydrophobic, stiff or flexible. Because of these variables it is necessary to thoroughly study and understand their conformational behavior both as single molecules and in assemblies. In an effort to reach this goal, four main studies are reported here:

- Development of molecular imaging and image analysis techniques for characterization of individual branched macromolecules
- The conformation and ordering of star-like brush molecules at interfaces.
- The control of conformation: a comparative study of hydrophilic and hydrophobic brushes
- The architecture-induced mixing in a monolayer of hydrophilic and hydrophobic brushes

An important aspect of this research is the characterization of brush-like macromolecules that includes the molecular weight distribution of the backbones and side chains, and the molecules' particular conformation. The characterization of such complex architectures is challenging and requires using a combination of techniques. In addition to conventional gel permeation chromatography and light scattering techniques, molecular imaging and image analysis techniques have been developed for the characterization of molecules on surfaces. Two newly developed methods will be discussed: the combination of Langmuir-Blodgett monolayer sample preparation with imaging by atomic force microscopy (AFM) and the combination of PFPE-based soft lithography/replication with imaging by AFM. These two methods increase the amount of accurate data collected compared with traditional polymer

characterization techniques. In addition, characterization was done with some of the traditional techniques, including gel permeation chromatography and laser light scattering.

1.2 Biological Brushes

Brush structures are one of the most typical morphologies found in nature. Macroscopic brushes such as trees and hair allow for dense packing of functional species within shape-persistent, though flexible, objects. More biological brushes can be found on a microscopic scale. Plants have microscopic brush-like structures known as trichomes on their leaves. These trichomes help the plant by reducing water loss,

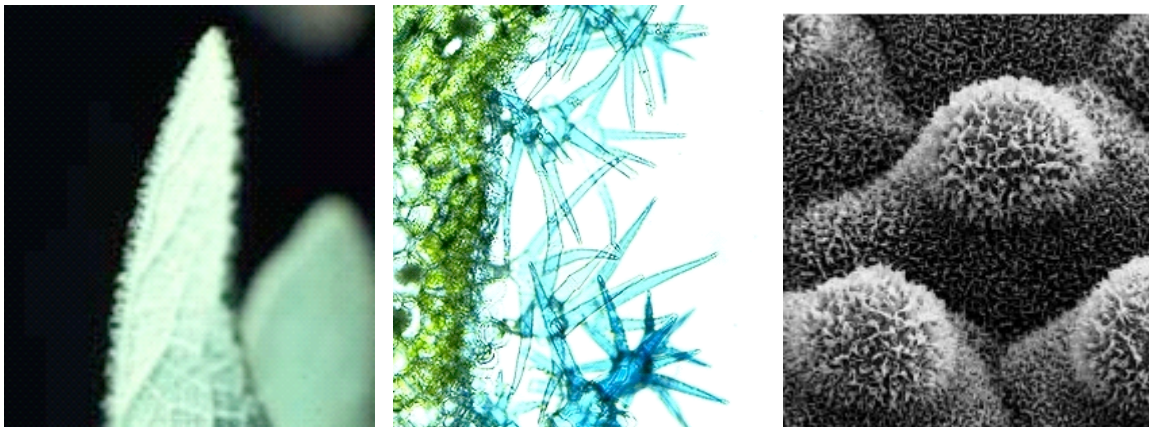


Figure 1.1^{3,4} Examples of Trichomes Trichomes on the leaves of plants can be a macro- or microscopic brush structure designed for the protection and viability of the leaf (left and middle). Microscopic roughness combined with even smaller hairy structure makes lotus leaves superhydrophobic and, therefore, self-cleaning (right).

regulating temperature and protecting it from insects and disease. Covering a surface in bristles also alters its wettability and can result in a surface that is self-cleaning. This effect

³ <http://botweb.uwsp.edu/Anatomy/non-secretorytrichomes.htm> (accessed September 2005).

has been studied with lotus leaves and has been termed the “lotus effect.”⁴ Surface roughness combined with a hairy structure on a smaller scale makes lotus leaves superhydrophobic and allows water droplets to pick up debris as they roll off the leaves.

Tethered hair-like microscopic structures are also found in the human body. Known as cilia these structures are found in and on a variety of organs and pathways including the sinuses, airways, kidney tubules, fallopian tubes, ears, and eyes. Sometimes their purpose is simply to protect cell surfaces, but other times they serve some more complicated function such as detecting sound in the ears or moving mucous through the lungs. Cilia in the lungs beat between 1000-3000 times per minute, moving mucous with trapped contaminants and bacteria out of the lungs. This process is regulated not only by the movement of the tethered brush-like cilia, but also by the viscoelastic properties of mucous, one of the components of which is a molecular brush called mucin.^{5,6} Mucous that is too viscous or not viscous enough can not be propelled by cilia causing serious health problems, such as cystic fibrosis.

Progress in microscopic techniques led to the discovery of molecular brushes such as proteoglycans that represent another major class of biomolecules in addition to DNA and proteins.^{7,8} Proteoglycans consist of a protein backbone with polyelectrolyte carbohydrate side chains. These brush-like molecules are found in many places in the body performing

⁴ Barthlott, W.; Neinhuis, C. *Planta* **1997**, *202*, 1.

⁵ Bansil, R.; Stanley, E.; LaMont, J.T. *Annu. Rev. Physiol.* **1995**, *57*, 635.

⁶ Bromberg, L.E.; Barr, D.P. *Biomacromol.* **2000**, *1*, 325.

⁷ Seog, J.; Dean, D.; Plaas, A.H.K.; Weng-Palms, S.; Grodzinsky, A.J.; Ortiz, C. *Macromolecules* **2002**, *35*, 5601.

⁸ Essentials of Glycobiology; Varki, A.; Cummings, R.; Esko, J.; Freeze, H.; Hart, G.; Marth, J., Eds.; Cold Spring Harbor Laboratory Press: Cold Spring Harbor, NY, 1999.

various functions, such as cell to cell signaling, joint lubrication and cell surface protection.⁹⁻

¹¹ In one of the most well-studied examples, proteoglycans, as one of the main components of cartilage, act as a water sponge and result in the shock absorbing and lubricating functions of cartilage.¹²⁻¹⁴ This is possible because of the high charge density per unit length the dense brush structure affords which results in a high osmotic pressure upon compression.¹⁵ It is believed that the functional properties of proteoglycans are a direct result of their brush-like structure, which insures a high density of charged groups per unit length.

⁹ Kaneider, N.C.; Dunzendorfer, S.; Wiedermann, C.J. *Biochemistry* **2004**, *43*, 237.

¹⁰ Scott, J.E. *Biochemistry* **1996**, *35*, 8795.

¹¹ Jay, G.D.; Haberstroh, K.; Cha, C.-J. *Connet. Tissue. Res.* **1992**, *28*, 71.

¹² Chen, L.; Yang, B.L.; Wu, Y.; Yee, A.; Yang, B.B. *Biochemistry* **2003**, *42*, 8332.

¹³ Li, Z.; Hou, W.-S.; Bromme, D. *Biochemistry* **2000**, *39*, 529.

¹⁴ Simon, W.H. *J. Biomech* **1971**, *7*, 379.

¹⁵ Khalsa, P.S.; Eisenberg, S.R. *J. Biomechanics* **1997**, *30*, 589.

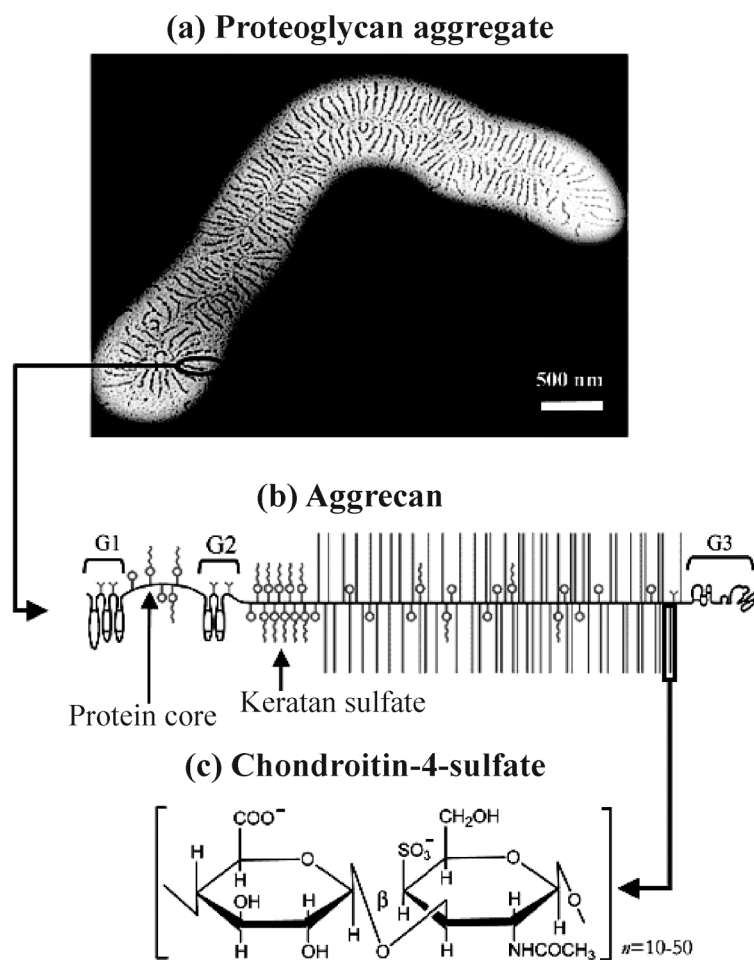


Figure 1.2⁷ Structure of a Proteoglycan Aggregate AFM height image of a proteoglycan aggregate reveals its brush-like structure. Its many carbohydrate side chains are grafted to a protein backbone.

1.3 Synthetic Molecular Brushes

The peculiar structure and functional properties of proteoglycans has inspired the synthesis of polymers with similar architectures. These synthetic counterparts are known as cylindrical brush polymers due to their appearance: each has a linear polymer backbone with many grafted side chains. Proteoglycans perform important functions made possible by their architecture; similarly, the structure of brush polymers is likely to effect interesting functional properties. The architecture of cylindrical brush polymers can vary being densely or loosely grafted, having flexible or stiff side chains, being homopolymers or copolymers.

These variables affect their properties, but it is the relatively dense grafting that has the greatest effect on the structure and properties of brush polymers.

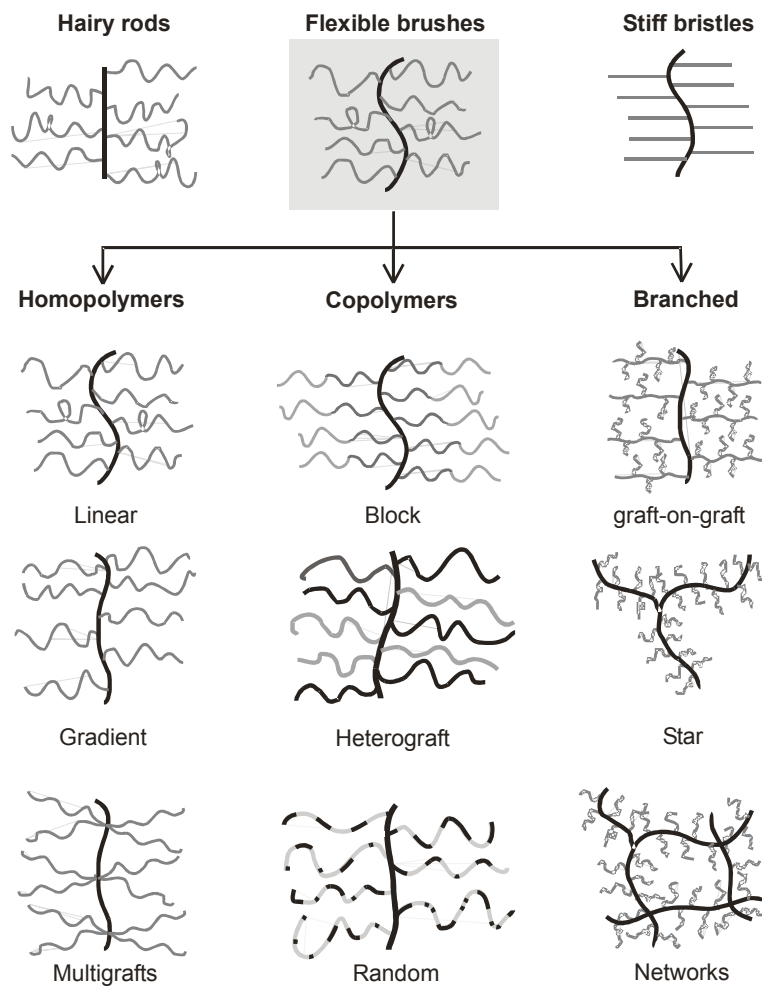


Figure 1.3¹⁷ The Variety of Brush Structure Synthetic brush polymers can vary widely in basic structure (planar, cylindrical or spherical), as well as in the smaller architectural details. In addition, the chemical composition of molecular brushes can be altered to tailor the properties and functionality of the molecule.

1.4 Synthesis of Molecular Brushes¹⁶⁻¹⁸

Polymer brushes have been synthesized by a variety of techniques in an effort to gain greater control over composition and architecture in order to obtain well-defined macromolecules. For useful brush synthesis it is important to control the grafting density, the ratio of side chain and backbone degrees of polymerization, and the polydispersities of the backbone and side chains. However, controlling these parameters has proven a challenge because of steric hindrance during synthesis.

There are three methods used to synthesize cylindrical brush polymers: “grafting through” (the polymerization of macromonomers), “grafting to” (the addition of already polymerized side chains to a backbone), and “grafting from” (the polymerization of side chains from a macroinitiator backbone). Each of these methods controls different molecular parameters well, but each also has significant disadvantages. Often multiple synthetic approaches are combined in order to synthesize more challenging architectures that cannot be achieved with only one technique. Each technique has been tested using multiple polymerization routes including anionic polymerization, ring-opening metathesis polymerization, conventional and controlled radical polymerization, different coupling reactions (“click chemistry”), and miniemulsion polymerization. Not all of these techniques

¹⁶ Sheiko, S.S.; Sumerlin, B.S.; Matyjaszewski, K. *Prog. Poly. Sci.* **2008**, (*submitted*) (and references therein)

¹⁷ Boyce, J.R.; Sun, F.C.; Sergei, S.S. in “Responsive Polymer Materials: Design and Applications” by Sergei Minko (Ed.), 1-26 (**2006**). (and references therein)

¹⁸ Sumerlin, B.S.; Matyjaszewski, K. in “Macromolecular Engineering: Precise Synthesis, Materials Properties, Applications” by Krzysztof Matyjaszewski, Yves Gnanou, and Ludwik Leibler (Eds.), v.2, 1103-1136 (**2007**). (and references therein)

have been successful in creating well-defined brush molecules with backbones much longer than the side chains.

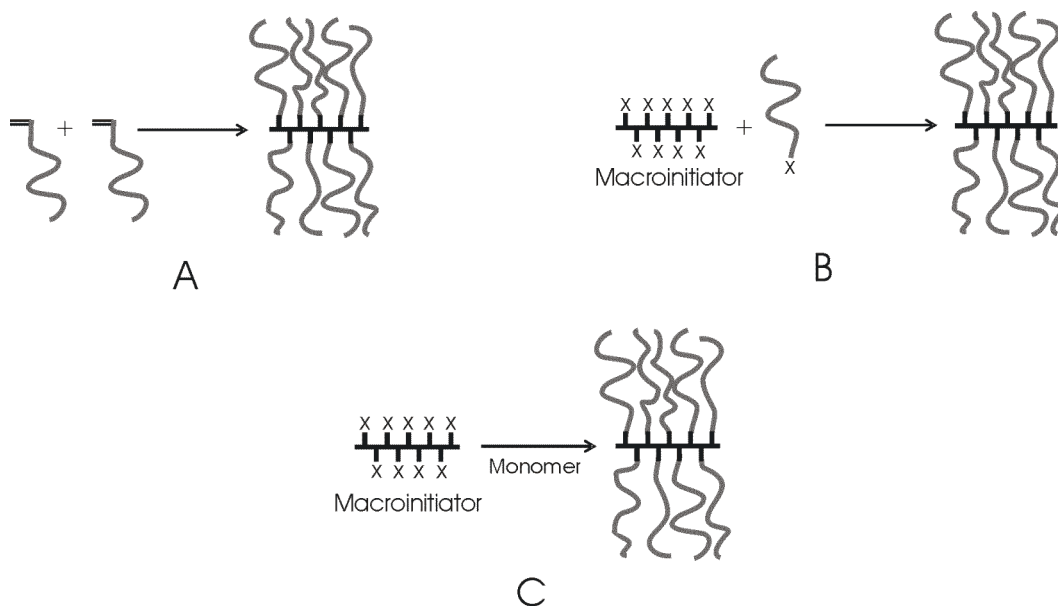


Figure 1.4¹⁷ Three Synthetic Strategies for Brushes Schematics of grafting through (A), grafting to (B), and grafting from (C)

The first brushes were synthesized by Tsukahara by the “grafting through” method. While this attempt was successful, the resulting brushes were ill-defined, the synthesis was poorly controlled, and gelation occurred at high conversion. Since that time many new methods have been developed each with its own strengths and weaknesses. In general, “grafting through” allows for excellent control of grafting density and side-chain length, since the side chains are polymerized and can be characterized prior to brush synthesis; however, the degree of polymerization of the backbone depends on the macromonomer type and length and is low due to steric hindrance at the propagating chain end and the concentration of polymerizable end groups. Anionic and radical polymerization of macromonomers has been used to synthesize brushes, but with poor to moderate control of molecular weight and success only at low conversions. Ring-opening metathesis

polymerization has had more success due to the larger spacing between side chains because of the ring opening, and ring strain adds the thermodynamic driving force for polymerization. Controlled/living methods have also been used for “grafting through,” but with limited control of parameters, with some exceptions using atom transfer radical polymerization (ATRP). The ATRP method resulted in a brush with a molecular weight that increased linearly with conversion up to high degrees of polymerization with a narrow molecular weight distribution (MWD).

“Grafting to” employs end functionalized side chains that react with corresponding functional groups on a backbone. One of the benefits of this approach is that the side chains and backbone are synthesized separately before brush synthesis, and can be well-characterized. Often this type of brush synthesis utilizes supramolecular assembly via secondary interactions such as hydrogen bonding, coordination, and ionic interactions to assemble molecules. The weakness of the “grafting to” method is that as side chains are attached, they sterically hinder the attachment of more chains resulting in a lower grafting density. The most efficient methods that have been used to prepare brushes using this method are nucleophilic substitution and click chemistry (copper(I)-catalyzed azide-alkyne coupling). Nucleophilic substitution is hampered by side reactions, while the success of the click chemistry route depends heavily on the size of the side chain monomers. A modular approach with chlorosilane chemistry has been used to make multifunctional branch points resulting in brushes with multiple side chains from the same grafting site, increasing the complexity of the architecture.

“Grafting from” employs a backbone macroinitiator with a predetermined number of initiation sites from which side chains are polymerized. With this approach steric hindrance

is less of a problem and higher grafting densities can be achieved, although compared to “grafting through,” it provides less control over side chain length and grafting density. How well these parameters are controlled is a function of the initiation efficiency. This is why “grafting from” with ATRP has been used the most successfully to synthesize brushes with as high as 100% grafting density. “Grafting from” results in well-defined molecules with long backbones, high grafting densities and narrow MWD without fractionation. It also lends itself to even more complicated architectures such as stars and brushes with gradient grafting density, as well as copolymers, such as core-shell type molecules and heterograft molecules (molecules with more than one type of side chain).

1.5 Conformation of Brush-like Macromolecules

The conformation of a brush-like molecule is determined by the competition between the entropic elasticity of the flexible backbone and the steric repulsion of the densely grafted side chains. As a result of the chemical connectivity, molecules adopt a cylindrical conformation. However, this conformation may change in response to the surrounding environment, which effectively changes the interaction between the densely grafted side chains. The possible environments include solvents and substrates. As such, one should separately consider brushes in solution and brushes on surfaces.

1.5.1 Brush Conformation in Solution

Because of their unique architecture, cylindrical brush polymers behave differently in solution than their linear counterparts.¹⁹ In solution, brush molecules can contract from a rod

¹⁹ Burchard, W. *Adv. Polym. Sci.* **1999**, *143*, 113.

to a globule with changes in temperature, solvent quality, or pH depending on their chemical composition. Their dense grafting causes them to have a worm-like shape, rather than the coil of a linear polymer. One of the most unique properties of brush polymers is their ability to change length and stiffness with changes in solvent quality, characterized by length per monomer (l_m) and persistence length (l_p), respectively. These parameters are affected by the degree of polymerization of the side chains and the grafting density of the backbone.

Currently, the effect of the molecular composition on these parameters is not completely understood and recent literature on the subject is sometimes contradictory. Several theories have been proposed relating l_p to side-chain length. If l_p increases more quickly than the brush diameter D , lyotropic ordering of cylindrical brush polymers in solution is expected.^{20,21} One theory suggests that the ratio of l_p to D is approximately constant, meaning that l_p increases proportionally to the dimensions of the side chains.²² This is in agreement with some computer simulations, although they also predict that l_p/D levels off with side chain length.^{23,24} Lyotropic ordering would not be possible in such a system, though it is expected for brushes with stiff^{25,26} and bulky^{27,28} side chains. It has also been theoretically

²⁰ Onsagar, L. *Ann. N.Y. Acad. Sci.* **1949**, *51*, 627.

²¹ Khokhlov, A.R.; Semenov, A.N. *Physica A* **1981**, *108*, 546.

²² Birshtein, T.M.; Borisov, O.V.; Zhulina, E.B.; Khokhlov, A.R.; Yurasova, T.A. *Polym. Sci. U.S.S.R.* **1987**, *29*, 1293.

²³ Saariaho, M.; Ikkala, O.; Szleifer, I.; Erukhimovich, I.; ten Brinke, G. *J. Chem. Phys.* **1997**, *107*, 3267.

²⁴ Rouault, Y.; Borisov, O.V. *Macromolecules* **1996**, *29*, 2605.

²⁵ Saariaho, M.; Subbotin, A.; Szleifer, I.; Ikkala, O.; ten Brinke, G. *Macromolecules* **1999**, *32*, 4439.

predicted that the l_p/D ratio increases with the length of the side chains as $l_p/D \sim N^{9/8}$, where N is the degree of polymerization of the side chains.²⁹ If this relation is physically true, lyotropic ordering is asymptotically expected because the persistence length increases with the side-chain length faster than the brush diameter.

Experimental results have also proven inconclusive, although they have led to new insights into brush conformation. Several light and neutron scattering measurements showed that both l_m and l_p increased with increasing side chain length and increasing side chain solvent quality.³⁰⁻³⁴ Other scattering experiments showed that neither l_p nor l_m depend on the side chain length.³⁵ Recent experiments have confirmed that l_m is not dependent upon side

²⁶ Subbotin, A.; Saariaho, M.; Stepanyan, R.; Ikkala, O.; ten Brinke, G. *Macromolecules* **1999**, *32*, 4439.

²⁷ Elli, S.; Ganazzoli, F.; Timoshenko, E.G.; Kuznetsov, Y.A.; Connolly, R. *J. Chem. Phys.* **2004**, *120*, 6257.

²⁸ Percec, V.; Ahn, C.-H.; Ungar, G.; Yeardley, D.J.P.; Möller, M.; Sheiko, S.S. *Nature* **1998**, *391*, 161.

²⁹ Fredrickson, G.H. *Macromolecules* **1993**, *26*, 2825.

³⁰ Fischer, K.; Schmidt, M. *Macromol. Rapid Commun.* **2001**, *22*, 787.

³¹ Gerle, M.; Fischer, K.; Roos, S.; Müller, A.H.E.; Schmidt, M.; Sheiko, S.S.; Prokhorova, S.; Möller, M. *Macromolecules* **1999**, *32*, 2629.

³² Fischer, K.; Schmidt, M. *Macromol. Rapid Commun.* **2001**, *22*, 787.

³³ Gerle, M.; Fischer, K.; Roos, S.; Müller, A.H.E.; Schmidt, M.; Sheiko, S.S.; Prokhorova, S.; Möller, M. *Macromolecules* **1999**, *32*, 2629.

³⁴ Lecommandoux, S.; Chécot, F.; Boralí, R.; Schappacher, M.; Deffieux, A. *Macromolecules* **2002**, *35*, 8878.

³⁵ Rathgeber, S.; Pakula, T.; Wilk, A.; Matyjaszewski, K.; Beers, K.L. *J. Chem. Phys.* **2005**, *122*, 124904/1.

chain length, but that l_p increases with increasing side chain length in theta and good solvents.^{36,37} These discrepant results illustrate the need for continued study to rightly understand the connection between architecture and functionality or behavior for molecular brushes. Beyond changes in contour length, macromolecular brush polymers also undergo a conformational transition from a rod-like to a globular shape in solution, similar to that of linear polymers, with changes in solvent quality.^{38,39} Cylindrical brush molecules, stabilized by their many side chains, remain in solution as single molecules longer than linear chains even when collapsed. Similar stability during conformational changes has also been observed on surfaces.⁴⁰

1.5.2 Brush Conformation on Surfaces

On surfaces, the conformation of brush molecules depends on the interaction of the side chains with the surface. Interfacial interactions along with the substrate confinement results in a larger variety of conformations compared to those in solution. Depending on the fraction and distribution of adsorbed side chains, the molecules can have extended, curved, or collapsed conformations (see Fig. 1.5). Imaging by atomic force microscopy (AFM) is a simple route for determining conformation, measuring contour length, radius of gyration,

³⁶ Terao, K.; Nakamura, Y.; Norisuye, T. *Macromolecules* **1999**, *32*, 711.

³⁷ Nakamura, Y.; Wan, Y.; Mays, J.W.; Iatrou, H.; Hadjichristidis, N. *Macromolecules* **2000**, *33*, 8323.

³⁸ Li, C.; Gunar, N.; Fischer, K.; Janshoff, A.; Schmidt, M. *Angew. Chem. Int. Ed.* **2004**, *43*, 1101.

³⁹ Tsubaki, K.; Kobayashi, H.; Sato, J.; Ishizu, K. *J. Colloid Interface Sci.* **2001**, *241*, 275.

⁴⁰ Neugebauer, D.; Carson, B.E.; Sheiko, S.S.; Matyjaszewski, K. *Polym. Prep. (Am. Chem. Soc., Div. Polym. Chem.)* **2003**, *44*, 510.

persistence length, as well as getting more complicated information about rheological properties, ordering and patterning of polymer brush molecules.

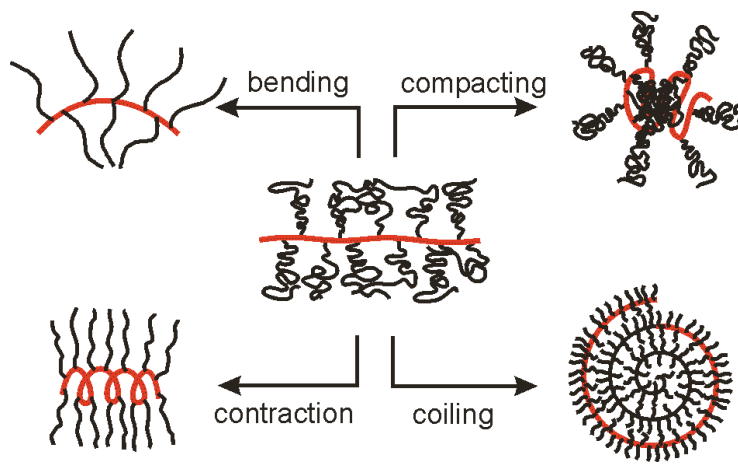


Figure 1.5 Surface Conformations of Brushes The brushes with their responsive conformations make ideal molecular actuators. The following conformational changes lead to the following mechanical actions within an individual brush molecule: bending, contraction, compacting, and coiling.

Unlike simple fluids that rapidly reach one of two simple equilibrium conformations (i.e. drops or disks (Fig. 6a)) when adsorbed on a surface, polymer brushes have a covalently bound architecture that restricts their conformation leading to more complex morphologies formed on longer time scales (Fig. 6b). A brush adsorbed to a surface adopts a conformation in response to the interplay between the intramolecular and surface forces.⁴¹⁻⁴⁴ The conformational transformation of large polymer molecules can be a slow process potentially leading to non-equilibrium and metastable structures. Moving a brush molecule from solution

⁴¹ Saariaho, M.; Ikkala, O.; ten Brinke, G. *J. Chem. Phys.* **1999**, *110*, 1180.

⁴² Khalatur, P.; Khokhlov, A. R.; Prokhorova, S. A.; Sheiko, S. S.; Moller, M.; Reineker, P.; Shirvanynts, D.; Starovoitova, N. *Eur. Phys. J. E* **2000**, *1*, 99.

⁴³ Prokhorova, S. A.; Sheiko, S. S.; Mourran, A.; Moller, M.; Beginn, U.; Zipp, G.; Ahn, C.-H.; Percec, V. *Langmuir* **2000**, *16*, 6862.

⁴⁴ Potemkin, I. I.; Khokhlov, A. R.; Reineker, P. *Eur. Phys. J. E* **2001**, *4*, 93.

to a surface breaks its cylindrical symmetry resulting in a partitioning of the side chains. One partition corresponds to adsorbed and desorbed side chains. The other partition results from the adsorption of the side chains on different sides of the backbone. Because the side chains can distribute differently with respect to the surface plane and the backbone, a variety of conformations is possible. The ratio of the fraction of side chains adsorbed to the surface (ϕ_a) to the fraction of side chains desorbed from the surface (ϕ_d) is the largest factor determining the surface conformation, as well as the fraction of side chains to the right (ϕ_R) and left (ϕ_L) of the backbone. The four experimentally observed surface macromolecular brush conformations correspond to four different ratios of ϕ_a to ϕ_d and ϕ_R to ϕ_L .

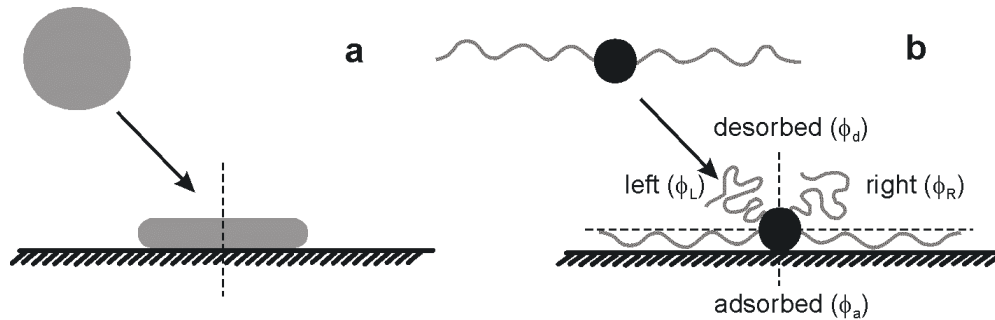


Figure 1.6¹⁰ Equilibrium Spreading Cross-section of the adsorption of simple liquids and molecular brushes. (a) A drop of simple fluid can easily adopt a variety of equilibrium shapes (shown here is the pancake). (b) The conformation of adsorbed molecular bottlebrush is confined by its interconnectivity and determined by the ratio of ϕ_a to ϕ_d .

On high energy surfaces side chains are strongly adsorbed to the surface and two brush conformations are observed, one that corresponds to $\phi_a > \phi_d$ and $\phi_R \approx \phi_L$, and a second that corresponds to $\phi_a > \phi_d$ and $\phi_R \neq \phi_L$. The first is a plate-like conformation, typically with the backbone and side chains almost fully extended. The desorbed side chains coil back onto the backbone forming a raised cap. The second case is an equilibrium version of the first and

forms by a process known as spontaneous curvature.⁴⁵ In order to gain entropy, some side chains flip from one side to the other causing an uneven distribution along the backbone and curvature toward the side with fewer side chains.

On low energy surfaces side chains no longer adsorb strongly resulting in $\phi_a < \phi_d$, with two conformations observed in this regime. The side chains gain entropy by desorbing from the surface at the expense of surface contacts. Because there are so few side chains adsorbed to the surface, in the first conformation the backbone is able to collapse forming a globular conformation. This conformation is very well documented and understood.^{46,47} The second conformation seen on low energy surfaces is a cylindrical one.⁴⁸ While the mechanism of this conformation is much less understood, the desorbed side chains behave in such a way as to keep the backbone extended.

⁴⁵ Potemkin, I.I.; Khokhlov, A.R.; Sheiko, S.S. *Macromolecules* **2004**, *37*, 3918.

⁴⁶ Gallyamov, M.O.; Tartsch, B.; Khokhlov, A.R.; Sheiko, S.S.; Börner, H.G.; Matyjaszewski, K.; Möller, M.; *Macromol. Rapid Comm.* **2004**, *25*, 1703.

⁴⁷ Sun, F.; Sheiko, S.S.; Moller, M.; Beers, K.; Matyjaszewski, K. *J. Phys. Chem. A* **2004**, *108*, 9682.

⁴⁸ Xu, H.; Shirvanyants, D.; Beers, K.L.; Matyjaszewski, K.; Dobrynin, A.V.; Rubinstein, M.; Sheiko, S.S.; *Phys. Rev. Lett.* **2005**, *94*, 237801.

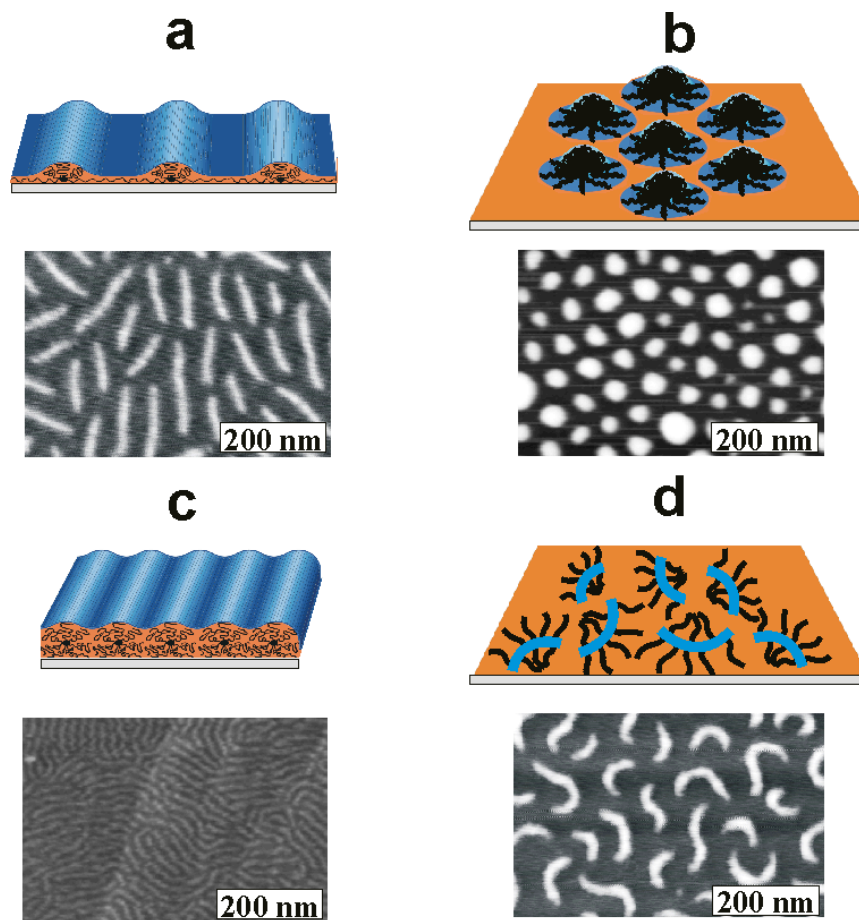


Figure 1.7¹⁷ AFM Images of Brush Surface Conformations The four distinct conformations have been observed on surfaces. The conformations occur due to variations in the number of adsorbed and desorbed side chains: (A) rod-like ($\phi_a \cong 1$), (B) globular ($\phi_a < 1$), and (C) cylindrical ($\phi_a \ll 1$). The conformation in (D) is when spontaneous curvature occurs due to an uneven distribution of the side chains ($\phi_R \neq \phi_L$). The micrographs corresponding to the schematics show the monolayer structure of the same brush molecules ($N_{\text{backbone}} = 567$, $N = 51$) measured by AFM under different surface conditions.

The conformations described above apply to brushes that have relatively long side chains and are densely grafted. Changing the grafting density, side chain length, or side chain chemical composition changes the interaction of the brush with the substrate, and therefore the conformation.⁴⁹ This effect can be compared to the conformations described above which are dependent upon the fraction of adsorbed and desorbed side chains.

⁴⁹ Sheiko, S.S.; Prokhorova, S.A.; Beers, K.A.; Matyjaszewski, K.; Potemkin, I.I.; Khokhlov, A.R.; Möller, M. *Macromolecules* **2001**, *34*, 8354.

However in the case of grafting density the number of side chains adsorbed to the surface is restricted by architecture. For example, on a high energy surface a brush with a higher grafting density will adopt a plate-like conformation, whereas a brush with a relatively low grafting density will have a globular conformation simply due to the fact that it has fewer side chains.

As previously mentioned, the complex interactions between the backbone and side chains and the dependence of those interactions on the environment makes the molecules responsive to changes in the environment. On surfaces this translates into changes in surface interaction or spreading parameter. Rod-to-globule transitions have been observed due to compression of monolayers as well as a decrease in surface energy. Exposing adsorbed molecules to solvent vapors of varying solvent quality has also induced this rod-to-globule transition as well as spontaneous curvature of molecules. Copolymer brushes have shown interesting conformational behavior. Heterograft brushes with poly(butyl acrylate) and poly(ethylene oxide) side chains shortened and eventually collapsed when placed in solvents with decreasing solvent quality with respect to the PBA.⁴⁰ Molecules could be designed to respond to temperature, pH, ionic strength, or surface interactions, as well as light or magnetic fields. Triggering shape variations by external stimuli would make molecular brushes useful for such applications as molecular sensors or molecular motors.

1.6 Fundamental Issues

The physical understanding of the conformational behavior of molecular brushes is one of the biggest remaining challenges. There continues to be ambiguity regarding the conformation of brushes in solution as well as on surfaces, particularly with respect to the backbone and side chains as separate components. How each of these parts responds to the environment and how they then interact with each other, results in the final conformation of the brush. It is known that certain stimuli, such as changes in the surrounding environment, can switch the conformation of a molecule. However, the way molecular brushes respond to stimuli remains largely unknown. Indeed, the cylindrically-shaped macromolecules can undergo multiple changes in different dimensions, such as longitudinal contraction, diameter increase, collapse into a globule, and sheet-like arrangements. The conformational transition might be continuous or discrete. Furthermore, which stimuli and the extent of the stimuli's effect on the switching are also not all known. Apart from the conformation as a single molecule, there is a great set of problems on the arrangement of the molecules in dense materials such as melts, films, and monolayers. How the molecules are affected by stimuli while they are in dense forms, and how intermolecular interactions change their conformational behavior has hardly been broached. Most studies of brushes up to this point have been single molecule or dilute systems.

1.7 Experimental Challenges

The complexity of the brush results in behavior that is very different from that of their linear counterparts. This is due to the many tethered side chains, which drive the behavior of these molecules. This results in a great diversity of new molecular conformations and

unusual phase (ordering and mixing) behaviors. The conformational and phase behavior depend not only on architecture, but also on the chemical structure of the branches and the underlying substrate. New experimental approaches are required to visualize and understand the molecular picture of these complex systems. Because of these special circumstances, experimental studies of macromolecular brushes require approaches that resolve the behavior of single molecules in varying environments. This work evolved through the following experimental steps:

- The development of molecular imaging and image analysis techniques for characterization
- The molecular-scale study of conformational and ordering behavior in direct space
- The molecular-scale study of their mixing behavior in the presence of other molecules, both of similar composition and architecture and different.

These issues will be addressed here via several means. The use of molecular imaging has been broadened for the analysis of molecular brushes by employing AFM in combination with quantitative Langmuir-Blodgett sample preparation technique. In addition, molecular replication using newly developed perfluoropolyether-based soft lithography has allowed the more accurate characterization of molecular dimensions for soft liquid-like molecules and droplets.^{50,51} The tethering of many side chains to one backbone results in a molecule that responds very differently than linear molecules to environmental changes. The molecular

⁵⁰ Rolland, J.P.; Van Dam, R.M.; Schorzman, D.A.; Quake, S.R.; DeSimone, J.M.; *J. Am. Chem. Soc.* **2004**, *126*, 2322.

⁵¹ Rolland, J.P.; Hagberg, E.C.; Denison, G.M.; Carter, K.R.; DeSimone, J.M.; *Angew. Chem. Int. Ed.* **2004**, *43*, 5796.

resolution attainable with AFM allows for the study of ordering and conformational transitions of assemblies of molecules. Here the surprisingly opposite conformational behavior of hydrophilic and hydrophobic macromolecular brushes will be reported and compared. The mixing and ordering of chemically different polymers as a result of the brush-like architecture of at least one of the components will also be addressed. It will be made clear in the following studies that architecture of molecules is incredibly important and has a huge impact on the resulting behavior and activity of the molecule.

CHAPTER 2

SINGLE MOLECULE CHARACTERIZATION OF COMPLEX

MACROMOLECULES: THE DIMENSIONS, CONFORMATION, AND ORDERING

OF MULTIARM BRUSHES

2.1 Addressing the Challenges of Complicated Molecules⁵²

One of the goals in modern synthetic polymer chemistry is to prepare polymers with controlled molecular weight and well-defined architecture. Controlled/living radical polymerization (CRP) provides a route to polymers with well-defined molecular weight and narrow molecular weight distributions, as well as with various architectures. Atom transfer radical polymerization (ATRP) is among the most efficient CRP methods and has been successfully applied to the synthesis of linear, hyperbranched, comb-like, and star-like structures. Densely grafted brush polymers are among the most intriguing macromolecular structures and ATRP lends itself to their synthesis. ATRP has been successfully used to synthesize linear brushes with various chemical compositions.⁵³⁻⁵⁷ To attempt even greater

⁵² Matyjaszewski, K.; Qi, S.; Boyce, J.R.; Shirvanyants, D.; Sheiko, S.S. *Macromolecules* **2003**, *36*, 1843.

⁵³ Beers, K.L.; Gaynor, S.G.; Matyjaszewski, K.; Sheiko, S.S.; Möller, M. *Macromolecules* **1998**, *31*, 9413.

⁵⁴ Matyjaszewski, Krzysztof; Qin, Shuhui; Boyce, Jamie R.; Shirvanyants, David ; Sheiko, Sergei S. *Macromolecules* **2003**, *36*, 1843.

⁵⁵ Zhang, M.; Breiner, T.; Mori, H.; Müller, A.H.E. *Polymer* **2003**, *44*, 1449.

molecular complexity, a series of brushes were synthesized with a star-like backbone having two, three, and four arms. The synthesis of such a complicated molecule begs confirmation on a variety of levels: the number of arms of the backbone, the grafting efficiency of side chains from these unusual backbones, and the molecular weight distribution of the individual arms along with entire molecules. In order to determine if the synthesis was “successful,” all variables of the molecules need to be determined including total backbone length, individual arm length, side chain length, and total molecular weight. Traditional polymer characterization techniques such as gel permeation chromatography (GPC) or viscometry do not provide this level of discrimination. GPC is an excellent example to demonstrate the weaknesses of these types of solution studies. Calibration of GPC is based on linear standards of some particular polymer, such as polystyrene or poly(methyl methacrylate). Molecular weights are determined by how quickly these linear polymers elute through columns packed with a porous material. Branched molecules are more compact than linear polymers of corresponding mass, i.e. have a smaller hydrodynamic volume, and therefore elute more slowly returning underestimated molecular weights. Using GPC with a light scattering detector, one can obtain relatively accurate information about the molecular weight distribution and the molecular dimensions in solution. However, the method becomes less accurate when analyzing large molecules ($qR_g > 1$) and molecules with complex architecture. It also gives no information about the number and length of branches or comparison of backbone to side chain lengths. This inability to distinguish the backbone from the branches (side chains and arms) is why solution studies of branched

⁵⁶ Qin, S.; Matyjaszewski, K.; Xu, H.; Sheiko, S.S. *Macromolecules* **2003**, *36*, 605.

⁵⁷ Neugebauer, D.; Zhang, Y.; Pakula, T.; Matyjaszewski, K. *Polymer* **2003**, *44*, 6863.

macromolecules have serious limitations. Scattering techniques can be helpful for determining an average molecular weight, however, they fail to characterize both intramolecular dimensions (branches and side chains) and overall conformation. Even well-planned out scattering experiments cannot fully separate the backbone from the many massive side chains.

AFM imaging overcomes all the limitations of other characterization techniques because the molecules become visible. The backbone, individual arms, and side chains can be seen and measured separately in direct space. Imaging reveals both the size and the overall conformation of the molecule. When combined with an appropriate substrate and sample preparation technique, one can even retrieve information about the solution conformation of brush molecules by AFM. The high resolution that AFM imaging provides makes possible the detailed characterization and analysis necessary for confirming the synthesis of and understanding the behavior of macromolecular brush polymers.

2.2 The Necessity of Molecular Imaging

The sophisticated architecture of cylindrical macromolecular brushes requires special analytical techniques, which allow accurate characterization of their branched architecture. In the case of linear brushes, it is necessary to measure the backbone separately from the side chains. In the case of multiarm brushes, it is desirable to measure the length distribution of the individual arms separately from the total size. Such characterization is hardly possible via traditional polymer characterization techniques, such as NMR, light scattering, and GPC. Here, molecular imaging is the most effective method for characterizing and analyzing brush molecules, because the branches can be resolved. Resolution of each separate component of

the molecule facilitates accurate analysis, which is important in order to understand behavior and confirm the synthesis. Confirming the synthesis allows a definite connection to be made between the functional properties of the molecules and their chemical and structural composition, furthering the base of knowledge from which to design functional molecules for specific applications. In addition to verifying synthetic strategies, molecular visualization enables accurate and quantitative measurements of molecular weight, size, and conformation. The unique advantage of molecular imaging is that one obtains molecular dimensions in direct space affording more opportunities for statistical analysis. The pictorial resolution also allows fractionation of the visualized molecules by size, branching topology, and chemical composition as well as sorting out irrelevant species.

There are few imaging techniques, such as fluorescence and electron microscopy, that were developed to explore single molecules. However, optical techniques fail to achieve nanometer resolution of flexible polymer chains with a persistence length below 100 nm. Electron microscopy needs special imaging conditions that may perturb or even damage the native molecular structure. Due to the nanometer lateral and vertical resolution, AFM demonstrates its unique advantage as it allows the imaging of molecules in great detail, including the contour length and the local curvature. The technique does not require any sample modifications and allows imaging under ambient conditions.

Molecular imaging allows quantitative measurements of the following characteristics: molecular weight, the contour length, 2D radius of gyration, local curvature, and persistence length,. In addition to lateral dimensions, AFM can also provide data about the height of a molecule giving access to the three-dimensional conformation. The 3D capability is a unique property of AFM, although it is a less accurate quantity with soft materials (see chapter 3).

Specific molecular conformations can be quantified in part because of the 3D information, and thus conformational and/or phase changes can be observed with the appropriate sample preparation. Furthermore, higher multimolecular structures and self-assembly can be analyzed for intermolecular distance and patterning. This is possible not only because individual molecules are resolved, but also because polymers of different chemical compositions can often be distinguished through phase imaging because of differences in physical properties.

AFM provides the most direct and facile route to the observation, characterization and behavior analysis of cylindrical macromolecular brushes.

2.3 The Characterization of Single-molecule Dimensions

2.3.1 Confirming the Synthesis of Star-like Molecular Brushes

A series of two, three, and four-arm macromolecular brushes was synthesized via ATRP by first polymerizing a poly(2-bromopropionyloxyethyl methacrylate) multiarm macroinitiator from a multifunctional core and then grafting poly(*n*-butyl acrylate) side chains from this macroinitiator. The backbone macroinitiator for the four-arm brush was synthesized by ATRP of 2-(trimethylsilyloxy)ethyl methacrylate using the tetrafunctional ($f = 4$) initiator pentaerythritol tetrakis(2-bromoisobutyrate), followed by the esterification of the backbone macroinitiator precursor with 2-bromopropionyl bromide. The PBA side chains were then grown from this initiator by ATRP using copper(II) bromide as a catalyst. Molecules with functionalities of two and three were also synthesized in the same manner, from initiators of corresponding functionality.

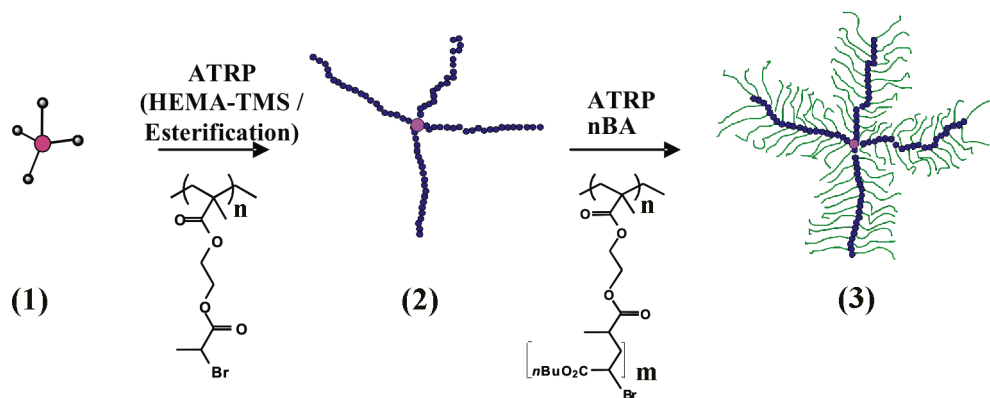


Figure 2.1 Multi-arm Brush Synthetic Scheme The cartoon illustrates the synthetic scheme and molecular structure of multi-arm molecular brushes (3). This particular scheme corresponds to four-arm brushes ($f = 4$). A branching core of functionality $f = 4$ (1) was used to prepare a 4-arm BPEM macroinitiator (2) followed by the grafting from of nBA side chains.

A monolayer of each of the star brush samples was prepared on the LB trough and imaged by AFM. The first step to confirming the synthesis was merely to visually inspect the images to see if the molecules had the correct number of branches. The height images in Figure 2.2 show that the individual molecules and their branches can be clearly distinguished. The majority of the molecules grown from the tetrafunctional initiator had four arms, however some molecules had only three and there were even a few linear molecules. Some of the molecules had arms of different lengths. Similarly, the three arm brush sample contained mostly molecules with three arms, but some linear molecules were also present. There was also some polydispersity in the length of the arms. The “branches” of the two-arm brush could be distinguished by an indentation in the backbone; however this was not visible when the sample was a monolayer. The two-arm brush also had varying arm lengths. The length data for all three samples, including a comparison to a linear sample are presented in Table 2.2.

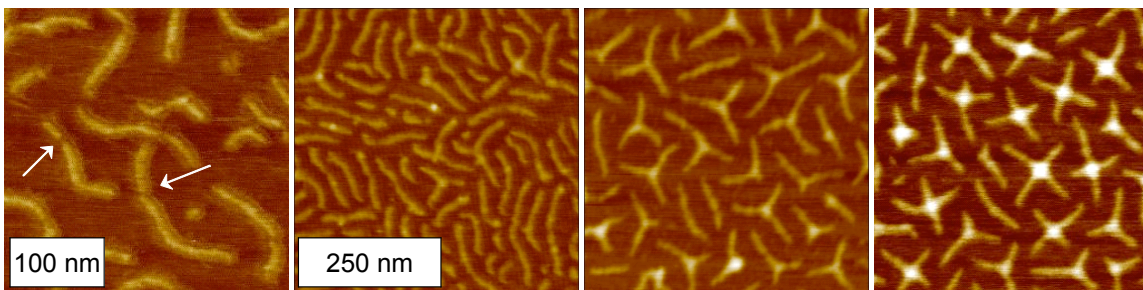


Figure 2.2 AFM Height Images of Multi-arm Brushes AFM height images reveal the structure of multiarmed brush polymers. The branching center of spin cast two arm molecules (far left) are visible as a notch in the molecule. This notch is not as easily visible in the monolayer (second from left). AFM images of LB monolayers of two arm, three arm and four arm molecules (left to right) show discrepancies in the number of arms per molecule and polydispersity in the arm length.

2.3.2 Molecular Weight Characterization

Combining AFM with Langmuir-Blodgett monolayer preparation adds another powerful dimension to brush analysis by providing a route for molecular weight analysis. LB monolayers are prepared by spreading polymer from a solution onto the surface of a shallow trough of water. This surface is bound by two barriers that can move together, decreasing the surface area available to the polymer. In this way monolayers can be formed and compressed to induce phase or conformational transitions. Monolayers are transferred by pulling a hydrophilic substrate vertically up through the layer (the “Z” method) and can then be imaged. The molecular weight determination is based on molecular imaging, which allows counting of individual molecules and accurate measurement of the number of molecules per unit area of an LB monolayer. From the mass per unit area, where M is the total mass of polymer applied to the trough, S is the surface area of the trough, and T is the transfer ratio

$$m = \frac{M}{ST} \quad (1)$$

and the number of molecules per unit area, where N is the number of molecules per image area, A ,

$$\sigma = \frac{N}{A} \quad (2)$$

the number-average molecular weight can be readily calculated:

$$M_n \equiv \frac{M}{N} = \frac{m}{\sigma} \quad (3)$$

Although the AFM measurements are done on a solid substrate, the number density is close to that on the water surface since the transfer ratio is always almost one. The transfer ratio is separately measured. Typically it varies from 0.9 to 1. The transfer ratio is the ratio of the actual mass transferred to a solid substrate to the mass of the water-supported monolayer.

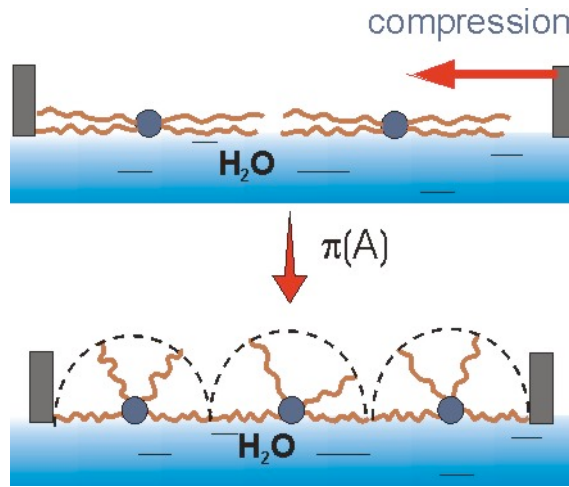


Figure 2.3 Schematic of the Langmuir-Blodgett (LB) Trough The movable barriers of the LB trough facilitate monolayer formation on the water surface after molecules are deposited.

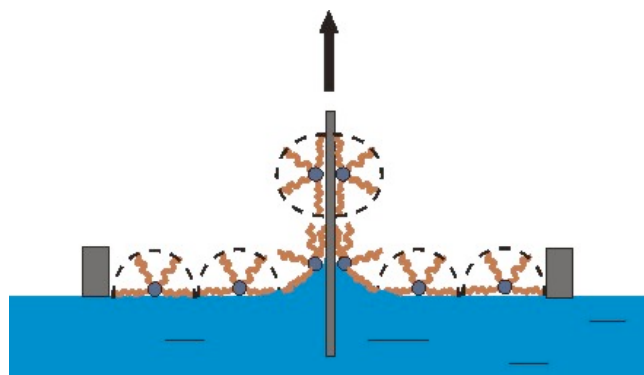


Figure 2.4 LB Monolayer Transfer onto a Solid Substrate Z type deposition of hydrophilic portion of molecules onto a hydrophilic substrate from the water surface.

2.3.3 Molecular Weight Distribution

The macroinitiator molecular weights were determined by GPC with a multiangle laser light scattering detector (MALLS) and the degrees of polymerization of the backbones were calculated. The final brush molecular weights were determined by both the AFM-LB method and GPC-MALLS. Assuming 100% grafting density (a side chain on every monomer unit of the backbone), the degree of polymerization of the side chains was calculated from the MW of the brush and the macroinitiator. These molecular weight data are reported in Table 2.1.

Table 2.1 Molecular Weight Data for Backbones and Brushes

Sample	macroinitiator ^a		brushes			degrees of polymerization	
	$M_n \times 10^5$	PDI	$M_n^b \times 10^6$	$M_n^c \times 10^6$	PDI ^b	n_n^d	m_n^e
1-arm (linear)	1.5	1.4	2.7	2.5	1.3	567	35
2-arm	1.9	1.3	1.1	1.8	1.3	720	17
3-arm	2.1	1.1	2.7	2.8	1.3	790	26
4-arm	2.8	1.1	5.5	6.0	1.3	1100	41

^aDetermined from MALLS-GPC in THF, $dn/dc=0.084$

^bDetermined from MALLS-GPC in THF, $dn/dc=0.068$

^cThe number average molecular weight was determined by AFM-LB from the mass per unit area ($m = \frac{M}{ST}$) and the number of molecules per unit area ($\sigma = \frac{N}{S}$) as $M_n \equiv \frac{M}{N} = \frac{m}{\sigma}$.

^dNumber average degree of polymerization of the macroinitiators: $n_n = \frac{M_n}{M_0}$, where $M_0 = 265$ g/mol is the molar mass of BPEM.

^eNumber average degree of polymerization of the side chains:

$$m_n = \frac{M_n^{brush} - M_n^{macroinitiator}}{n_n \cdot m_0}, \text{ where } m_0 = 128 \text{ g/mol is the molar mass of BA}$$

2.3.4 Arm-length Distribution

Along with being convenient and reliable for molecular weight determination, AFM enables accurate measurements of the molecular length. For the star-like brushes, one can measure the length of the arms separately from the length of the entire molecule. This demonstrates the strong advantage of AFM compared to other techniques such as light scattering and viscosity measurements that give average molecular dimensions. The information about the arm-length distribution is important for gaining insight into the synthetic process by which the arms grow. Table 2.2 summarizes the obtained results. The length polydispersity index, $PDI_L=L_w/L_n$, of the arms was determined to be about 1.15 for

every sample. The same PDI_L was measured for the linear molecules. This was expected because the macroinitiator, i.e. backbone, for each sample was synthesized in the same manner. Looking one step further at the whole molecule, the total length polydispersities determined by AFM decreased with increasing functionality from 1.15 to 1.04. The lowest polydispersity was found for the four-arm brushes. This had direct effects on the multimolecular structuring of the molecules, which will be discussed later.

Table 2.2 Length Characterization from AFM Measurements

Sample	Individual Arm		Entire Brush Molecule			
	L_n (nm) ^a	PDI_L ^b	L_n (nm) ^a	PDI_L ^b	Theoretical PDI_L ^c	l_m (nm) ^d
1-arm	130 ± 5	1.15 ± 0.08	130 ± 5	1.15 ± 0.08	1.15	0.23 ± 0.03
2-arm	69 ± 2	1.2 ± 0.2	137 ± 3	1.1 ± 0.2	1.075	0.19 ± 0.03
3-arm	55 ± 2	1.15 ± 0.08	165 ± 4	1.05 ± 0.08	1.050	0.21 ± 0.03
4-arm	64 ± 2	1.15 ± 0.08	256 ± 4	1.04 ± 0.08	1.038	0.23 ± 0.03

^a) L_n - number average molecular length

^b) $PDI_L = \frac{L_w}{L_n}$ - length polydispersity index

^c) Determined from eq. 4

^d) $l_m = \frac{L_n}{N_n}$ - length per monomeric unit, where N_n is the number average degree of polymerization of the backbone.

One should note that the PDI_L values determined from the length distribution are lower than PDI values from the mass distribution measured by GPC (Table 2.1). The disagreement may be caused by fundamental differences in the size analysis by the GPC-MALLS and the AFM-LB techniques. GPC blindly measures all species that are injected into the separation columns. The species may include a large variety of side products such as

small fractions of unreacted macroinitiators, individual side chains, and crosslinked molecules. In contrast, AFM is based on real space analysis, which enables selecting only the “right” species, i.e. multiarm brush molecules that possess a characteristic shape.

Table 2.2 also shows theoretical values of PDI that were calculated assuming random growth of the arms. Based on this assumption, one can readily calculate the polydispersity index of a star molecule, $PDI = PDI_{star}$. Indeed, if one assumes that the molecular weight

distribution of arms is given by a normalized function, $\rho(M)$ (i.e., $\int_0^{\infty} \rho(M) dM = 1$), such that

$\rho(M) = 0$ for all $M < 0$, the corresponding distribution of a star-shaped molecule containing f arms ($\rho(M)_{star}$) of arbitrary chosen lengths reads as a series of f auto-convolutions

$\rho(M)_{star} = \rho(M) * \rho(M) \dots \rho(M)$, where $\rho(M) * \rho(M) \equiv \int \rho(\mu) \rho(M - \mu) d\mu$. From the

definition of PDI ($PDI = \frac{\rho^{(2)}(M)}{(\rho^{(1)}(M))^2}$, where $\rho^{(i)}(M)$ denotes the i_{th} moment of the

corresponding distribution), the PDI_{star} can be calculated as

$$PDI_{star} = \frac{PDI_{arm}}{f} + \frac{f-1}{f} \quad (4)$$

For example, it is easy to show that for $f = 2$

$$\rho^{(2)}(M)_{star} = \int \{\rho(M) * \rho(M)\} M^2 dM = \iint \rho(\mu) \rho(M - \mu) M^2 d\mu dM = 2\rho^{(2)}(M) + 2(\rho^{(1)}(M))^2$$

For any arbitrary integer value of f one obtains,

$$\rho^{(2)}(M)_{star} = f \cdot \rho^{(2)}(M) + f \cdot (f-1) \cdot (\rho^{(1)}(M))^2, \text{ from which eq (4) follows directly.}$$

The equation is also consistent with the Flory-Schulz theory for condensation polymerizations, which proceed in a random fashion.^{58,59}

⁵⁸ Shulz, G.V.Z. *Phys. Chem.* **1939**, **B43**, 25.

Also noted in Table 2.2 is the length per monomeric unit (l_m), which is a measure of the extension of the arms. Values of l_m cannot exceed 0.25 nm, which corresponds to the monomer length of a fully extended carbon chain in the all-trans conformation. All the samples have similar l_m , meaning that the backbones are equally extended on the substrate, which further substantiates our analysis by AFM.

2.3.5 Conclusions for Single-molecule Characterization

Visualization by AFM of this series of star brush polymers provided important information about their synthesis and enabled accurate characterization of their size/dimensions:

1. The syntheses resulted in brush molecules with multiple arms. The majority of molecules in all cases had the anticipated number of arms, with side chains grown from them (as evidenced by the molecular weights). Thus, the syntheses were successful.
2. Not all molecules had the correct number of arms. This points to some type of termination occurring during the synthesis of the macroinitiator. Without visualization there would be no way to know about these missing arms.
3. The PDI of the individual arms for every star brush and the linear brush was approximately 1.15. This confirms that the polymerization proceeded in a similar fashion for every sample despite the increase in functionality.
4. The total PDI of each sample decreased with increasing functionality, being consistent with random growth, which is expected for radical polymerization.
5. All of the AFM-LB molecular weight values were within 10% of the GPC-MALLS values except for the two arm molecules. AFM-LB allows a sort of “fractionation” of the desired

⁵⁹Schaeffgen, J. R.; Flory, P. J. *J. Am. Chem. Soc.* **1948**, *70*, 2709.

molecules. GPC measures everything including side products from the synthesis. The flexibility of the AFM-LB technique could allow it to be used with even larger or more complicated molecules that GPC would not be able to measure.

2.4 Conformational Transition and Surface Ordering of the Four-arm Brush⁶⁰

2.4.1 Conformational Transitions

As shown previously for linear brush molecules⁶¹, 2D compression causes partial desorption of side chains, which is followed by the coiling of the otherwise extended backbone (Fig. 2.5). In the case of linear brush molecules, one observes a transition from a ribbon-like to a globular conformation characterized by a semi-spherical shape. Unlike linear brushes the star-like brushes form a disk-like shape with a height much smaller than its diameter, because the backbone is somewhat constricted by the branching (Fig. 2.5b,c). Note that the side chains undergo only partial desorption. Those side chains which remain adsorbed on the substrate form a dense corona around the coiled part, and thus control the surface arrangement of the adsorbed molecules. Here, only the results for the four-armed brush will be reported, since the behavior of the two-arm brushes is identical to that of linear molecules reported earlier⁶¹, and the three-arm molecules behave similarly to the four-arm ones.

⁶⁰ Boyce, J.R.; Shirvanyants, D.; Sheiko, S.S.; Ivanov, D.A.; Qin, S.; Börner, H.; Matyjaszewski, K. *Langmuir* **2004**, *20*, 6005.

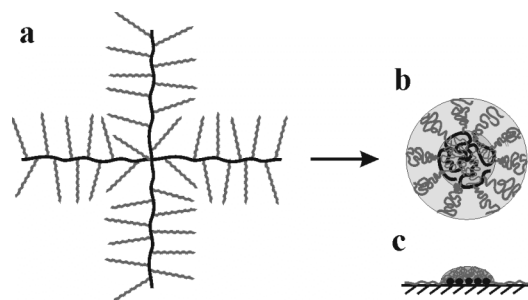


Figure 2.5 Schematic for the Conformational Transition of a Multi-arm Brush Molecule Caused by Two-dimensional Compression As opposed to the hemispherical (globular) conformation of compressed linear brush molecule⁶¹, multi-arm brushes undergo a transition from an extended conformation (a) to a disk-like conformation (b,c). The (b) and (c) show overhead and side views of the disk-like conformation, where the backbone remains adsorbed to the substrate.

A monolayer of the four-arm brush was imaged by AFM at three different degrees of compression. Figure 2.6 shows the surface pressure-molecular area isotherm for the four-arm brush. Similar to other fluids, compression of the multiarm brushes was reversible, as expected for equilibrium spreading. However, the isotherm has characteristics that distinguish it from conventional liquids. The pressure onset occurred at a mean molecular area of approximately 14,000 nm² and rose until an area of 8000 nm² where the pressure reached a plateau of 22.5 mN/m. This plateau continues to about 5600 nm² where a second plateau at 23.5 mN/m is observed. Similar behavior was observed for linear brushes ($f = 1$).⁶¹ In order to study the conformational changes occurring upon compression, four samples were transferred onto mica at different degrees of compression. Letters on the isotherm indicate molecular areas where the samples were taken.

⁶¹ Neugebauer, D.; Zhang, Y.; Pakula, T.; Sheiko, S.S.; Matyjaszewski, K. *Macromolecules* **2003**, *36*, 6746.

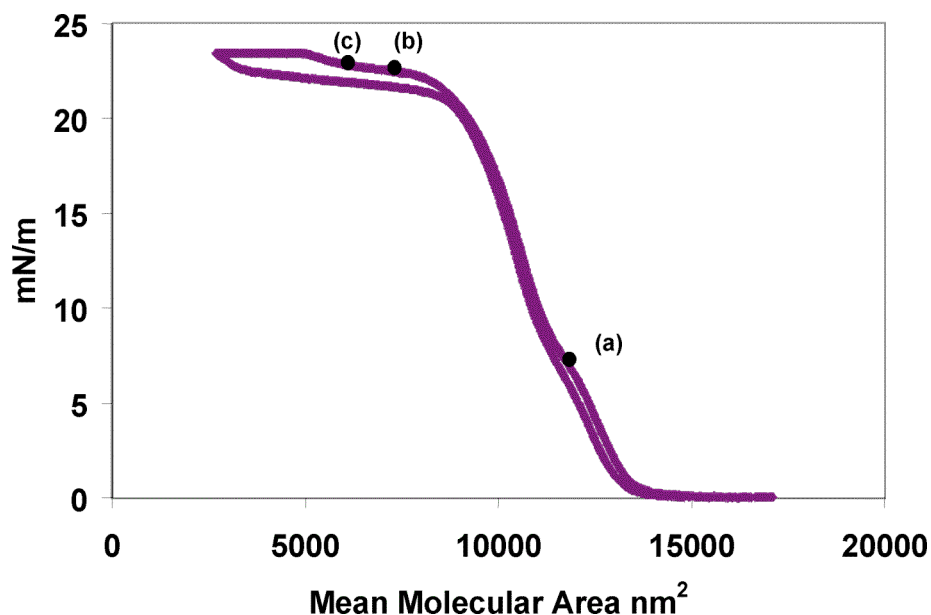


Figure 2.6 LB Isotherm for the Four-arm Brush The surface pressure-molecular area isotherm for the four-armed brush was measured at $T=23^{\circ}\text{C}$. The mean molecular area was determined for the number average molecular weight $M_n=6.0 \times 10^6$ g/mol obtained by AFM-LB. The mean molecular area is the average area of a single brush molecule on the water surface. The points on the compression isotherm indicate compressions at which a monolayer was transferred onto mica for AFM studies. Each point corresponds to an AFM image in Figure 2.7.

Figure 2.7 shows molecular conformations depicted by AFM during the transition for the four-arm brush. At a molecular area of $12,000 \text{ nm}^2$ (Fig. 2.7a) all of the arms are fully extended. As the molecules were compressed to a molecular area of 7200 nm^2 (Fig. 2.7b), the arms began to shorten and the middle of the molecules slightly increased in height. At this area, there is a coexistence of extended molecules and disk-like molecules, as well as some that appear to be in a transient state. At a molecular area of 6200 nm^2 (Fig. 2.7c), all molecules were disk-like (Fig. 2.7d) with a height much smaller than its diameter (Fig. 2.7e).

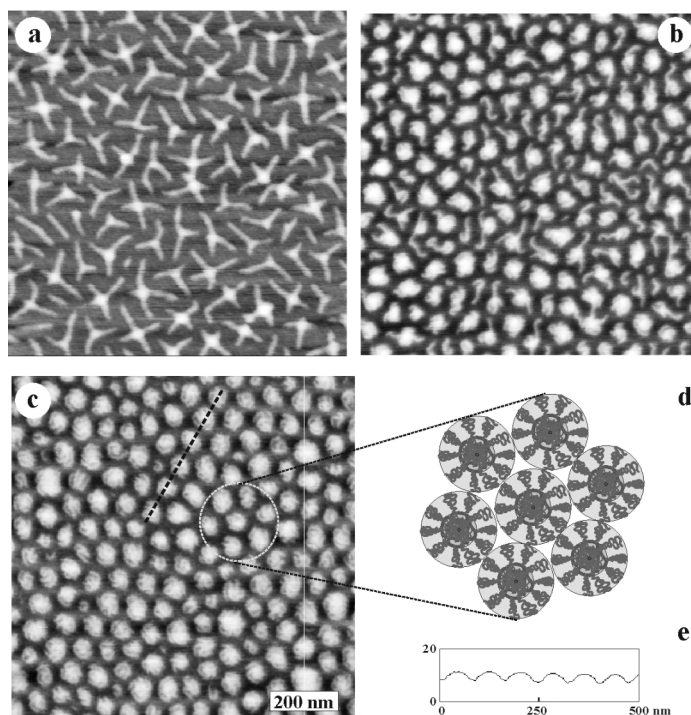


Figure 2.7 AFM Height Images of the Four-arm Brush Conformational Transition
 AFM records the transition of the four-arm brush from a star-like to a disk-like conformation. The transition was caused by lateral compression of monolayer films on the surface of water. The height images correspond to the different degrees of compression depicted in Figure 2.6. The cartoon in (d) shows hexagonal ordering of disk-like molecules stabilized by the steric repulsion of adsorbed side chains. The cross-sectional profile in (e) was measured along the dashed line in (c).

2.4.2 Ordering of Four-arm Macromolecules

At low pressures, star-like molecules are disordered because of the flexible nature of the arms, which results in the irregular shape of adsorbed molecules. Once the molecules transform from an extended to a disk-like conformation, they also gain local hexagonal order, which is stabilized by the steric repulsion of adsorbed side chains. Regions of short-range hexagonal order are clearly seen in the AFM images (see Figure 2.7c). The observed order is consistent with the lower polydispersity of the four-arm brushes.

One can compare the ordering behavior of the four-arm brushes ($PDI_L = 1.04$) and linear brushes ($PDI_L = 1.15$). Figure 2.8 shows larger scale images of compressed monolayers

of linear brushes in globular conformation (Fig. 2.8a) and four-arm brushes in the disk-like conformation (Fig. 2.8b). Visual comparison of the images of the linear and four-arm compressed brushes reveals that the monolayer of the four-arm molecules is more ordered. In the insets in Figure 2.8, there are small domains with nearly perfect hexagonal order that are also evidenced by the 2D power spectral density, $P_2(\underline{s})$, where \underline{s} is the 2D reciprocal space vector. The $P_2(\underline{s})$ of the four-arm brush demonstrates a well defined six-fold symmetry, whereas the linear brush has a less defined pattern indicating less order. The observed modulation in the scattering intensity vanishes in large samples. Figure 2.9 shows the angular dependence of the radial-averaged intensity $I(\phi)$ for $1 \times 1 \mu\text{m}^2$ and $5 \times 5 \mu\text{m}^2$ AFM images. This function was calculated as

$$I(\phi) = \int P_2(s, \phi) ds \quad (5)$$

where the integration is performed in the range of s corresponding to the first-order diffraction peak (see insets in Fig. 2.8). The smaller areas clearly show distinct peaks separated by 60 degrees (Fig. 2.9a). However, even for the larger area, one can distinguish peaks also located 60 degrees apart (Fig. 2.9b).

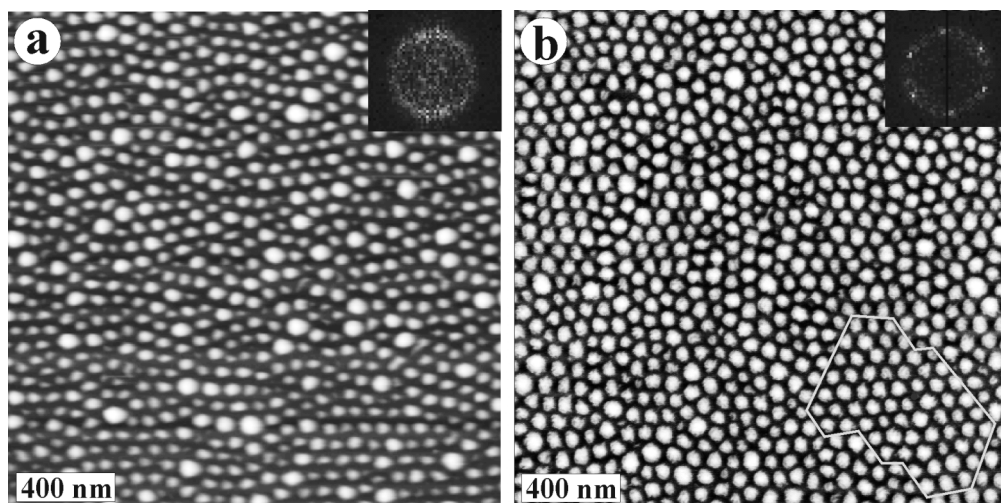


Figure 2.8 2D Power Spectral Density of Monolayers of Globular Molecules Height images of the compressed linear brush (a) and four-arm brush (b). The highlighted area in (b) shows a domain with nearly perfect hexagonal order. The insets show the 2D power spectral density measured for $1 \times 1 \mu\text{m}^2$ areas of the monolayers. Six peaks are clearly visible in the four-arm PSD indicating the presence of orientational and translational order in the system.

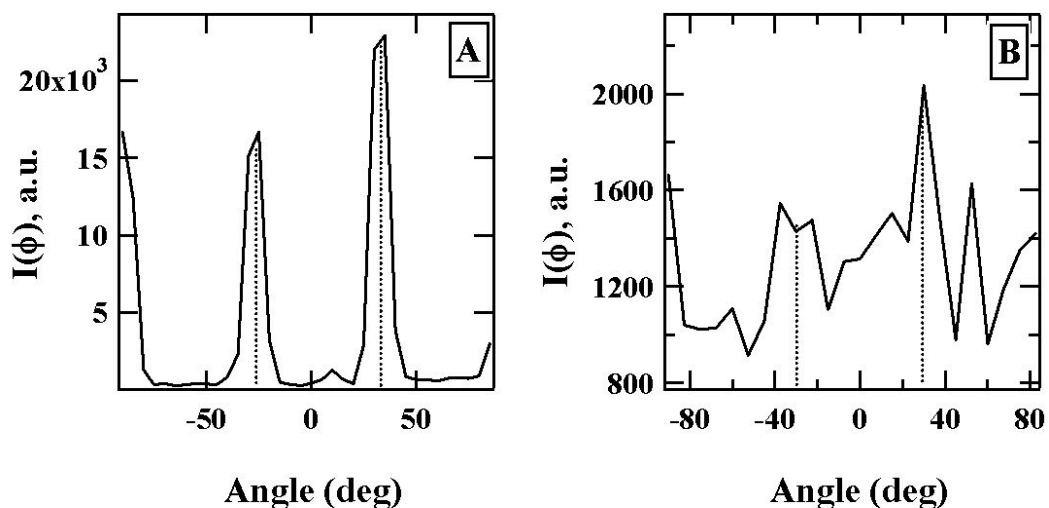


Figure 2.9 Angular Dependence of the 2D Power Spectral Density Function $P_2(s)$ calculated according to eq. (5). A-B correspond to AFM images of the four-arm brushes with sizes of 1×1 and $5 \times 5 \mu\text{m}^2$, respectively. The presence of the characteristic hexagonal pattern, which is very clear for the smaller image, can still be detected for the larger-scale image.

To characterize quantitatively the degree of order, one has to analyze the translational and orientational correlations of the AFM images and calculate the corresponding correlation lengths. The radial translational correlation function $C(R)$ was obtained from the 2D scattering function as described previously.⁶²

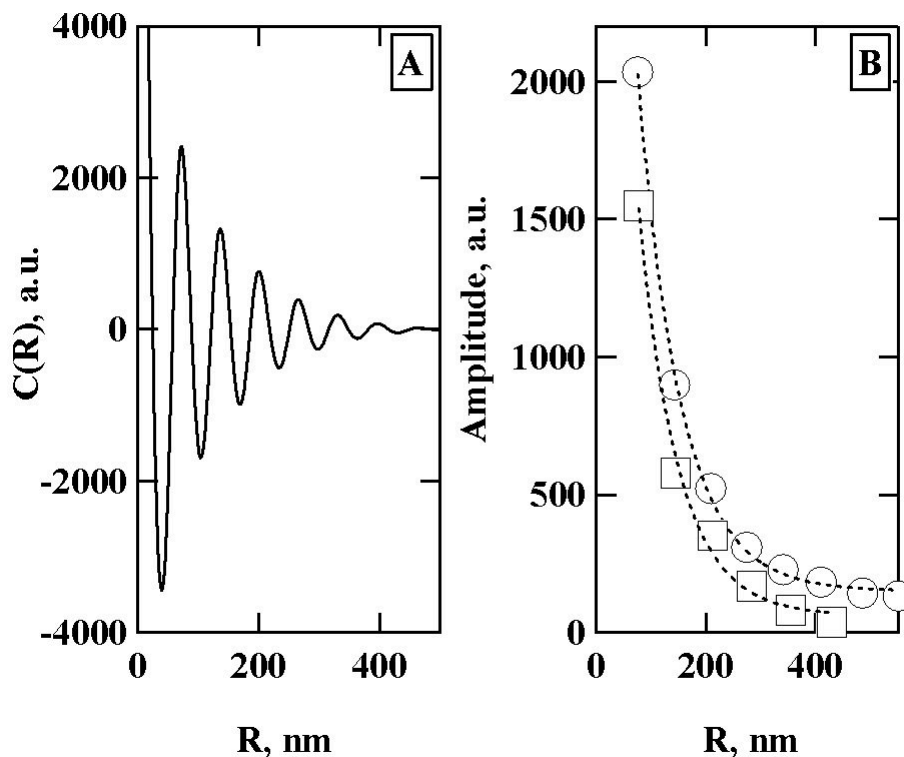


Figure 2.10 Radial Correlation Function and Amplitude Decay A: Radial correlation function exemplified for the case of the four-armed brush molecule ($1 \times 1 \mu\text{m}^2$ image); B: The decays of the amplitude of the secondary maxima of $C(R)$ as a function of distance for four-armed (circles) and linear brushes (squares) were fitted by an exponential function to obtain the translational correlation lengths $\xi_T = 76 \text{ nm}$ and 72 nm for the four-arm and linear brush, respectively.

⁶² Basire, C.; Ivanov, D.A. *Phys. Rev. Lett.* **2000**, 85, 5587.

Although the radial correlation function in Figure 2.10a shows 5 to 6 secondary maxima, the translational correlation length (ξ_T) was determined to be only about 76 nm, or one intermolecular distance, for the four-arm brush and 72 nm for the linear brush. This indicates that both the four-arm and linear molecules are fairly disordered. The obtained result seems counterintuitive because AFM images in Figures 2.7c and 2.8b reveal local hexagonal packing of the four-arm molecules. The relatively rapid decay of the correlation function can be explained not only by translational disorder of the molecules but also by the distribution of their sizes and irregularity of their shape. In such cases of partially disordered 2D systems, an in depth analysis of orientational correlations between the molecular centers of mass would be more relevant. For example, hexatic phases demonstrate perfect hexagonal order despite local defects that result in low ξ_T .

Figure 2.11 shows the orientational correlation functions recovered from $1 \times 1 \mu\text{m}^2$ AFM images of linear and four-arm brush molecules. In contrast to the translational correlations, the orientational correlations were analyzed in real space. The data points in Figure 2.11 were obtained by first recording the positions of the center of mass of individual molecules, and then correlating angles between nearest-neighbor bonds and the axis x . A detailed description of the analysis can be found in research papers and textbooks⁶³⁻⁶⁵. The data in Figure 2.11 demonstrate exponential decay of orientational order, which for the linear molecules tends to zero at large distances. By fitting the data points with the orientational

⁶³ Nelson, D.R.; Rubinstein, M.; Spaepen, F. *Phil. Mag. A* **1982**, *46*, 105.

⁶⁴ Cha, M.C., Fertig, H.A. *Phys. Rev. B* **1994**, *50*, 14368.

⁶⁵ Chaikin, P.M.; Lubensky, T.C. "Principles of Condensed Matter Physics" Cambridge, Univ. Press, 1995.

correlation function for an amorphous phase, $G_6 \sim \exp\left(\frac{-r}{\xi_6}\right)$, one can determine the orientational correlation length (ξ_6), which measures the long-range correlation of the orientation of local hexagonal axes. ξ_6 was determined to be approximately 740 nm, which is about 10 intermolecular distances. In contrast, the linear compressed brush has a correlation length of only 130 nm, or 2 intermolecular distances.

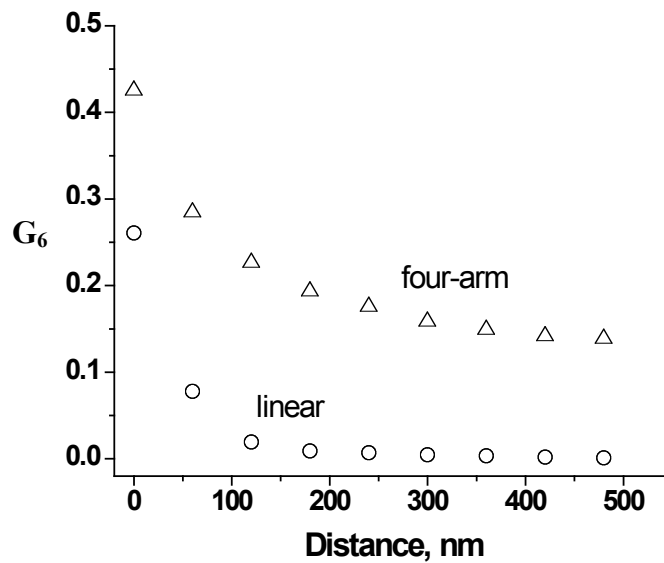


Figure 2.11 Orientational Order Function The orientational correlation function decays exponentially to a finite number on a short-range scale for the four-arm brush, but decays to zero for the linear brush. For larger AFM images, both functions tend to zero at large distances.

Because the data for the star-like molecules does not go to zero even at relatively large distances, the data was fit a power law to determine if this ordering was more like that of a hexatic phase (see Figure 2.12). The power law fit was a slightly better fit than that of the exponential, having an $R^2 = 0.980$ compared to 0.970 for the exponential. Therefore, the

collapsed star-like molecules could be more like a hexatic phase with short-range order, than like an amorphous phase.

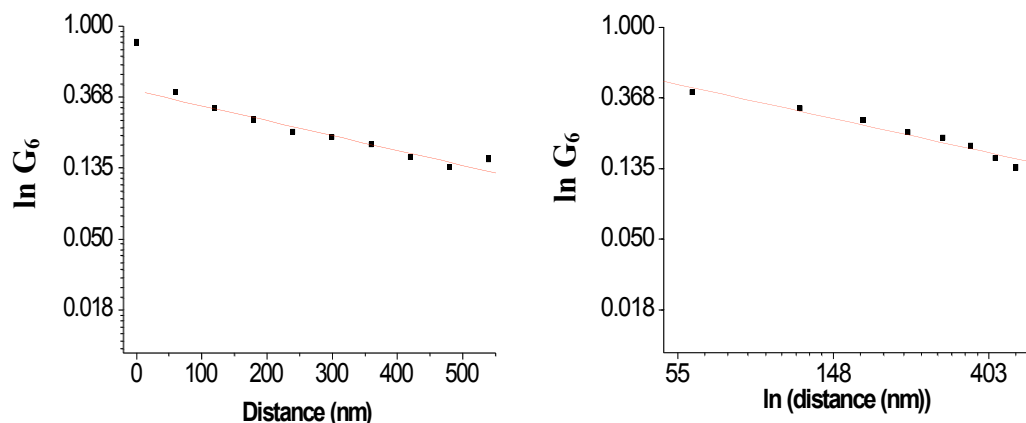


Figure 2.12 Exponential and Power Law Fits for G_6 The orientational correlation function for the collapsed star-like molecules was better fit with a power law function (right) than with an exponential (left), the power law fit having an $R^2 = 0.980$ versus 0.970 for the exponential.

The increase in ordering from the linear brush to the four-arm brush is consistent with the decrease in polydispersity, the linear brush having a PDI of 1.15 and the four-arm brush having a PDI of 1.04. Polydispersity can be defined as the relative standard deviation of the mass distribution, which can be calculated from the PDI as

$$RSD_m = \sqrt{PDI - 1} \times 100\% \quad (6)$$

For hard spheres, various computer simulations show that a terminal size RSD, above which no crystallization can occur, is in the range of 5-15% of the average sphere diameter. For hard disks, this terminal value for 2D crystallization is 8% of the average disk radius.⁶⁶⁻⁶⁸

⁶⁶Santen, L.; Krauth, W. Los Alamos National Laboratory, Preprint Archive, Condensed Matter (2001), 1-4, arXiv:cond-mat/0107459.

Since the mass of a sphere is proportional to its radius cubed ($m \sim r^3$) and the mass of a disk is proportional to the square of its radius ($m \sim r^2$), the relative standard deviation for the radius (RSD_r) can be calculated as $0.33 \cdot RSD_m$ and $0.5 \cdot RSD_m$, for the spherical and disk-like conformations, respectively. Therefore, for the compressed linear brush ($PDI = 1.15$, $RSD_m = 39\%$) one obtains $RSD_r = 13\%$, whereas the disk-like conformation of the four-arm brush ($PDI = 1.04$, $RSD_m = 20\%$) gives $RSD_r = 10\%$. Since both values are higher than the 8% terminal RSD, one should not observe long-range hexagonal order for either linear or four-arm brushes. Although the ordering theories lend insight into the reason for increased orientational ordering with the four-arm brushes, the compressed polymer molecules cannot be regarded as hard objects. The ordering behavior of the soft brush-like objects needs further investigation.

2.5 Conclusions

Molecular imaging combined with the LB technique proves a powerful method not only for the confirmation of the synthesis of architecturally complicated molecules such as multiarm brush polymers, but also for the determination of their molecular weights and polydispersities. The length distribution of individual arms was characterized separately from the total molecular size and shown to be consistent with the method of synthesis. Absolute molecular weights of complex macromolecules were measured with unprecedented precision by combining AFM imaging with quantitative LB film sample preparation.

⁶⁷ Kofke, D.A.; Bolhuis, P.G. *Phys. Rev. E* **1999**, *59*, 618.

⁶⁸ Bartlett, P. *J. Chem. Phys.* **1998**, *109*, 10970.

The LB technique also made it possible to observe and quantitatively analyze the conformation and ordering of monomolecular layers. Lateral compression of the star-like brushes caused a transition from an extended ribbon-like conformation to a compact disk-like conformation. Once the molecules transform from an extended to a disk-like conformation, they also gain local hexagonal order stabilized by the steric repulsion of adsorbed side chains. The orientational order of brush molecules in a compressed monolayer increases with decreasing polydispersity as expected. Even though the multi-arm macromolecules demonstrate very low polydispersity (PDI=1.04), this was not sufficient to attain long-range ordering of the disk-like molecules.

CHAPTER THREE
THE EVALUATION OF THE ACCURACY OF AFM USING MOLECULAR
REPLICATION

3.1 A Shortcoming of Tapping Mode AFM

The strength of AFM is its superior subnanometer spatial resolution both in lateral and height dimensions. One of the weaknesses of AFM is that it is an intrusive technique, which unlike optical imaging techniques may damage samples. In “contact mode,” the tip is in permanent contact with the sample, potentially causing both indentation and wear of the sample as it scans along the sample surface. In “tapping mode,” the tip oscillates at a high frequency in the kHz range intermittently striking the sample. Even though the contact is not permanent, the tip may deform soft samples and potentially even drag weakly bound species (particles and molecules) from their substrate. Many adjustments can be made during imaging to minimize the applied force, such as changing the drive amplitude or imaging in liquids. Even after making these adjustments, a significant level of deformation occurs with soft samples in the vertical dimension, particularly in the nanometer range.

Under static conditions, sample indentation can be estimated from the Johnson-Kendal, and Roberts (JKR) Model using the following equation $\delta = \frac{a^2}{R} \left[1 - \frac{2}{3} \left(\frac{a_0}{a} \right)^{3/2} \right]$, where a is the contact area and a_0 is the contact area at zero external force.

⁶⁹ The latter is defined as $\alpha_0 = \frac{6\pi R^2 W}{K}$, where $R \sim 10$ nm is the tip radius, $K \sim 1$ GPa elastic modulus of the sample, and $W \sim 10$ - 100 mJ/m² is the work of adhesion. In the case $a = a_0$, this gives deformation on the order of 1 nm, which can reach 10 nm for soft rubber-like samples and non-zero forces. For dynamic systems (tapping-mode scanning of viscoelastic polymers), it is significantly more challenging to estimate the extent of deformation, which depends on the tapping frequency, surface friction, and viscoelastic properties of the sample. Particularly challenging is the deformation of soft nanoparticles and single molecules with dimensions ranging from 1-10 nm that are deposited on a rigid substrate. The nm proximity of the substrate is another factor which is difficult to calculate. Therefore, it was necessary to evaluate the sample deformation by designing a method to obtain the true height of the molecules.

When studying polymers with glass transition temperatures well below room temperature, this deformation needs to be considered and taken into account. Poly(n-butyl acrylate) (PBA) ($T_g = -56^\circ\text{C}$) macromolecular polymer brushes fall into this category. The fraction of side chains adsorbed to and desorbed from the substrate determines the resulting conformation. At large fractions of adsorbed chains (strong adsorption), molecules have an extended ribbon-like conformation. At lower fractions, brush-like macromolecules adopt a disk-like shape with a cap of desorbed side chains (Figure 3.1), stabilized by a corona of the few adsorbed side chains. In order to understand the conditions for and mechanism of conformational change, it is necessary to know exactly what fractions of side chains are in which locations. For polymer brushes, missing vertical data means missing a key piece in the conformation puzzle. Therefore, in order to properly understand the conformation of polymer

⁶⁹ Israelachvili, J. Intermolecular & Surface Forces 2nd ed., Academic Press: London, 2006.

brushes, it is essential to know the relative location of all the side chains. Because PBA is above T_g at room temperature, any desorbed side chains form a dense mound on top of the backbone. The height of this mound is proportional to the fraction of desorbed side chains, which is why it is necessary to know it accurately.

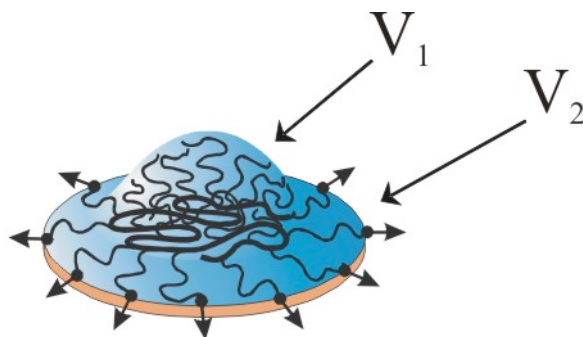


Figure 3.1 Scheme of Collapsed Brush Molecule The collapsed brush molecule consists of a cap of desorbed side chains of volume $V_1 = \pi \left(Rh^2 - \frac{1}{3}h^3 \right)$, which is for a slice of a sphere, sitting on a single layer of side chains, called the corona, of volume $V_2 = \pi r^2 h$. The area per molecule can also be determined from LB experiments, knowing the mean monomeric area and the number of monomers per molecule.

The contact nature of the AFM technique that causes problems for soft samples is actually a benefit for hard samples. Because the tip makes contact with the sample, an accurate height can be measured for a rigid object. If a soft sample can somehow be made hard without altering its dimensions, then an accurate three-dimensional picture can be obtained. Replication of a soft sample into a hard form would resolve this issue.

3.2 Curable PFPE-Based Molecule Replication

In order to obtain accurate dimensions of soft PBA macromolecular brushes via AFM, a soft lithography technique was employed to produce a rigid replicate of the original molecules. This recently developed high fidelity technique uses a low viscosity,

photocurable perfluoropolyether (PFPE) precursor (see Figure 3.2) that results in a mold with very low adhesion and low solvent permeability.⁷⁰⁻⁷² The particular advantage of this technique is its ability to mold freely-lying, weakly adhering, and soft particles. Here this technique is applied to replicate the most delicate of samples, single molecules and liquid drops. This technique allowed the reproduction of soft particles with high fidelity in order to verify dimensions provided by AFM.

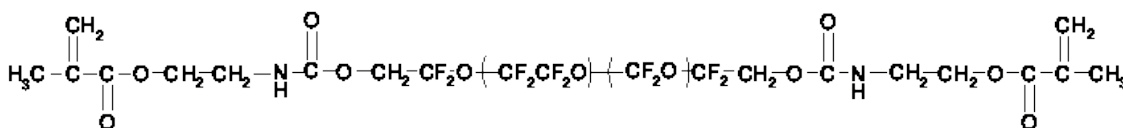


Figure 3.2 Perfluoropolyether Chemical structure of the perfluoropolyether unit prior to functionalization into precursor.

The technique includes 3 stages: (i) master preparation, (ii) mold fabrication, and (iii) making a replica of the master. A sample is prepared on a flat substrate. In order to contain the liquid precursor, a gasket is placed over the sample. The PFPE precursor is poured over the sample to cover it. The sample is cured in a UV oven ($\lambda = 365$ nm) under nitrogen. The nitrogen purging reduces reactions with oxygen that would otherwise quench cross-linking reactions. The UV radiation activates a photoinitiator that initiates cross-linking of the PFPE precursor, yielding an elastomeric mold of the sample. The mold is removed from the sample substrate and gently cleaned with an appropriate solvent, if necessary. To create a

⁷⁰ Rolland, J.P.; Van Dam, R.M.; Schorzman, D.A.; Quake, S.R.; DeSimone, J.M.; *J. Am. Chem. Soc.* **2004**, *126*, 2322.

⁷¹ Rolland, J.P.; Hagberg, E.C.; Denison, G.M.; Carter, K.R.; DeSimone, J.M.; *Angew. Chem. Int. Ed.* **2004**, *43*, 5796.

⁷² Maynor, B.W.; LaRue, I., Hu, Z., Rolland, J.P.; Pandya, A.; Fu, Qiang; Liu, Jie; Spontak, R.J.; Sheiko, S.S.; Samulski, R.J.; Samulski, E.T.; DeSimone, J.M.; *Small* **2007**, *3*, 845.

replicate the clean mold is pressed into an organic photopolymer resin, trimethylpropane triacrylate on a glass slide, and the sandwich is cured in a UV oven under nitrogen. Because the mold is made of low surface energy PFPE, mold release is not a problem. Many high fidelity replicates have been made by this technique from silicon masters, as well as replicates of freely-lying particles. However, two issues need to be considered when applying liquid PFPE to soft polymeric materials: (i) swelling and (ii) alteration of the surface energy. Swelling is very low due to poor mixing of fluorinated compounds with organic compounds. However, the change of the interfacial energy in presence of the low surface-energy PFPE might be significant. This effect will be analyzed in Section 3.4.2.

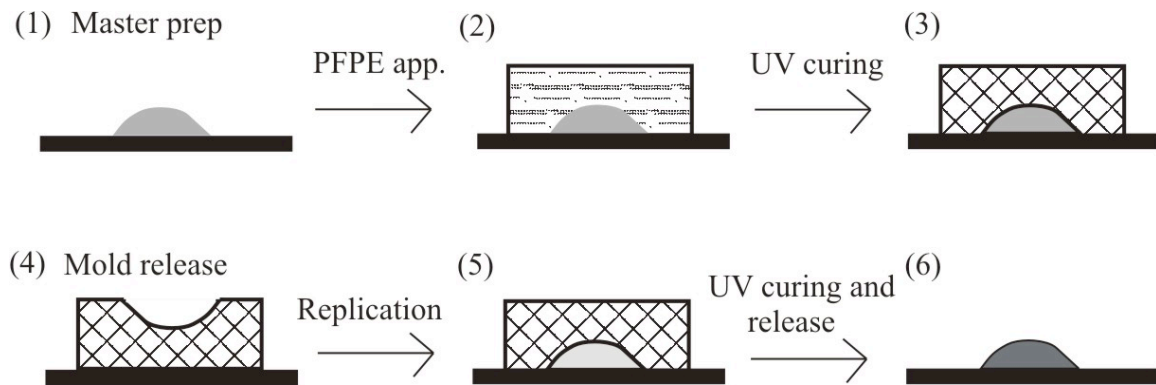


Figure 3.3 Soft Lithography Process The replication process begins by covering the master (1) with PFPE precursor (2), UV curing it to an elastomer (3), releasing the mold (4), then using the mold to make a replicate from TMPTA (5) and (6).

3.3 Replicating Single Molecules Using the Soft Lithography Technique

Four different PBA brush samples were used to test this combined AFM-replication method: a collapsed linear brush, drop-like aggregates of a linear brush, an extended linear brush, and a four-armed star brush. The linear sample used was a very well-characterized PBA linear brush polymer with $DP_{\text{backbone}} = 450$, $DP_{\text{side chain}} = 55$, and $M_n = 3.26 \times 10^6$ g/mol. As with other PBA brushes, it makes a rod-to-globule phase transition upon lateral compression of a monolayer.⁷² A monolayer of the brush was prepared on an LB trough and compressed slightly beyond the rod-to-globule transition point, which means single collapsed molecules were present as well as some small multimolecular aggregates. This layer was transferred to a mica substrate and imaged by

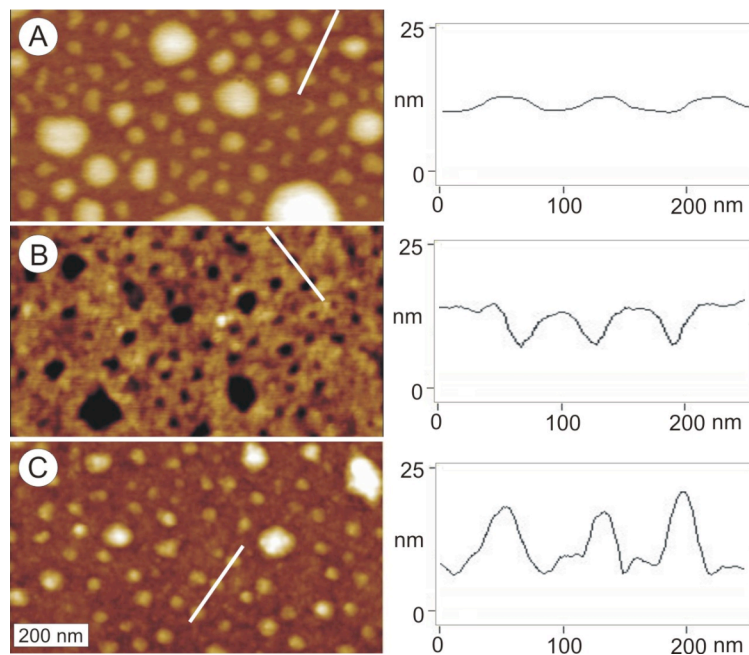


Figure 3.4 AFM of the Replication of Single Collapsed Molecules The replication process of single collapsed PBA brush molecules was followed by AFM. The height images for the master (A), mold (B), and replicate (C) are shown above. The white lines in the images indicate where height profiles of the molecules (mold and replicated molecules) were taken. The corresponding height profiles are seen to the right of the images.

AFM (See Fig. 3.4A). It was then replicated by the PFPE-based soft lithography method. Master, mold, and replicate were each imaged by AFM and analyzed in order to determine replication fidelity.

To expand this technique to a second morphology, small fluid droplets of these same PBA brushes were also replicated. Exposing a spin cast sample of the molecules to methanol vapor for about ten minutes causes them to aggregate into droplets. The droplets were on the order of 100 nm, increasing the scale of the sample features in both the lateral and vertical dimensions. Figure 3.5 shows AFM height images of all steps of the replication process for the droplets, master template (A), mold (B) and replicate (C).

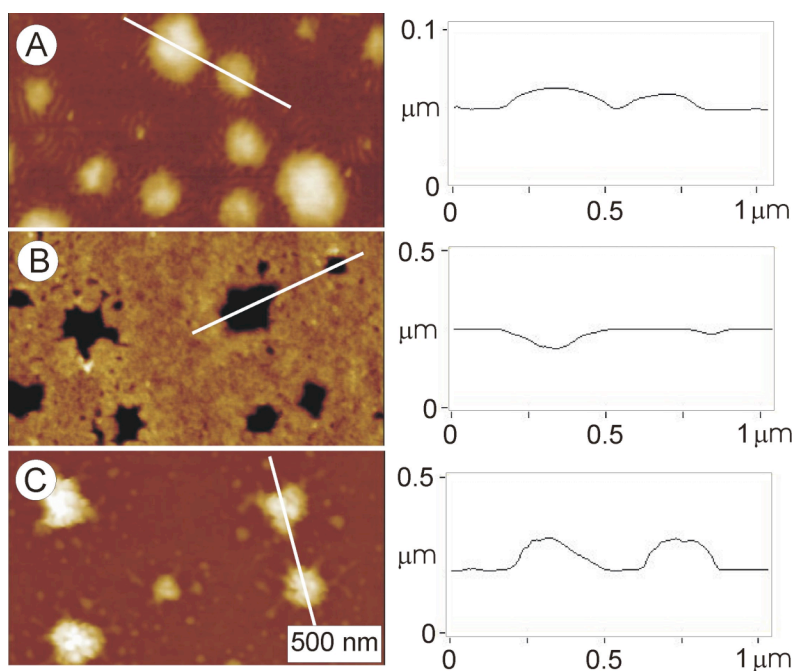


Figure 3.5 AFM of the Replication of Droplets Soft multimolecular drops were also molded and replicated with significant fidelity. The process was followed by AFM with height images of master (A), mold (B), and replicate (C). The white lines on the AFM images correspond to the height profiles to the right. Contact areas were consistent through each step, while heights were underestimated for both the master and mold. When comparing profiles, please note that the height scale for the master profile is one fifth that of the mold and replicate.

The collapsed molecular conformations and aggregates have significantly larger vertical dimensions than the extended conformation of the molecule. In the extended conformation the width and height of the backbone, in general, are much smaller than for collapsed molecules. Therefore it may be more difficult to replicate due to the smaller feature sizes. To test this, the same molecules used in the previous examples were also replicated in an extended conformation. A monolayer was formed on the LB trough at low pressure so that all molecules were extended. This sample was transferred to mica, imaged by AFM (Figure 3.6(A)), molded (B), and replicated (C).

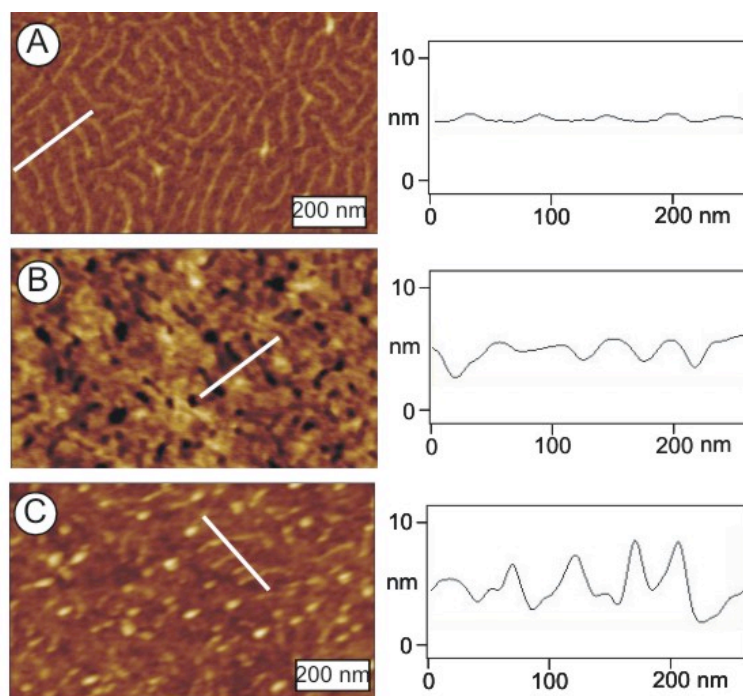


Figure 3.6 AFM of the Replication of Extended Molecules A monolayer of extended PBA brush molecules (A) was molded and replicated using the soft lithography technique. This sample had very small feature sizes (<10 nm), some of which replicated well. However, this sample exhibited some significant alteration in conformation from the master to the mold.

Increasing the complexity of the molecular architecture poses a different challenge for this technique. The same four-arm star molecules from chapter 2 were also used to test

the replication technique. A monolayer of them was first compressed slightly beyond the phase transition point on an LB trough, so that all the molecules were collapsed. This film was transferred to mica and imaged by AFM (Figure 3.7(A)), molded (B), and replicated (C).

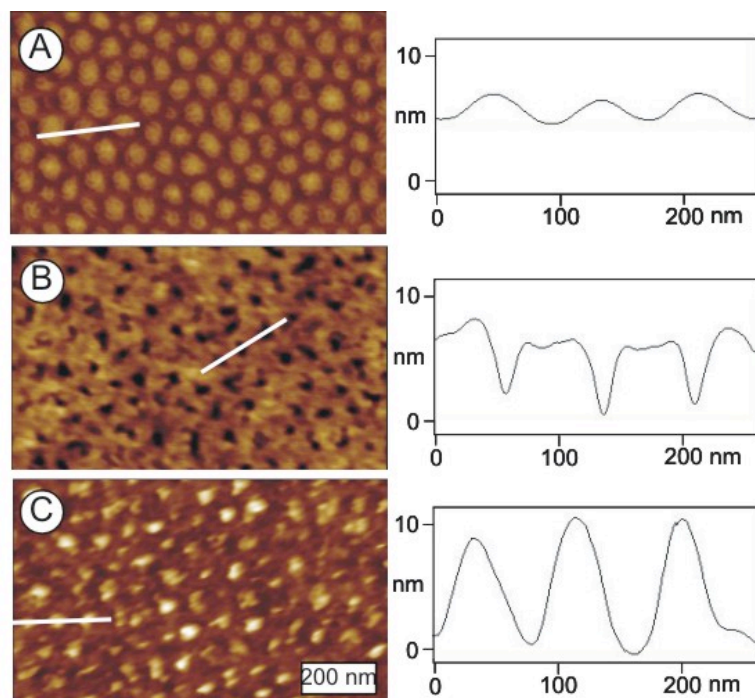


Figure 3.7 AFM of the Replication of Collapsed Star Molecules Collapsed four arm star molecules were molded and replicated. In the master (A), the arms appear to be wrapped around one another in a tight disk. In the mold (B) and replicate (C), many of the arms seem to be protruding from the center of the molecule.

3.4 Analysis and Discussion

3.4.1 Masters and Replicates

Qualitatively, AFM height images of the mold and replicate show that both the single collapsed molecules and the aggregates were successfully replicated with high fidelity. In addition, linear brush molecules and four-arm brushes were also replicated with some level of fidelity. The heights for each step of the replication process for the collapsed linear

brushes and aggregates were measured by AFM and are summarized in Table 3.1. The same information for the linear brushes and four-arm brushes can be found in Table 3.2.

The single collapsed molecules will be considered first. The height of the molecules increases from master to mold. This expected inconsistency is a result of the significant deformation of the molecules in the master by the AFM tip. The replicate molecule height was even greater than the depth of the mold wells. The less expected discrepancy between mold and replicate is due to the AFM tip not fully probing the wells of the mold. Variations in tip shape and scanning force set limitations on the characterization of holes. These two issues are not easily resolved, nor are their effects easily quantifiable. Therefore, having the rigid replicate becomes extremely important in gaining a full understanding of the conformation and dimensions of the molecules. AFM provides accurate height measurements for rigid materials, therefore the replicate measurements provide a true height for the original molecules. Contact areas for the master molecules, mold wells, and replicate molecules were consistent, verifying the fidelity of the replication process and giving further confidence to the replicate height being the true height (see Table 3.1).

In order to further validate the measured replicate heights, a calculated height was determined. Using the molecular weight of the molecule and the polymer density ($\rho = 1.09 \text{ g/cm}^3$), a volume of 4970 nm^3 was determined for a single molecule. The shape of the collapsed molecules correspond best to the top slice of a sphere, the equation for the volume of which is

$$V = \pi \left(Rh^2 - \frac{1}{3} h^3 \right) \quad (1)$$

where V is volume, R is the radius of the sphere from which the slice was taken, and h is the height of the slice. R can be calculated from the height of the slice and r, the radius of the slice:

$$R = \frac{1}{2} \left(\frac{r^2}{h} + h \right) \quad (2)$$

Because the molecules were in a dense film, the corona of side chains surrounding the molecules was not molded. Therefore, they should not be included in the calculation for the height. The footprints of the collapsed molecules were not all perfectly circular, so the average radius, r, was calculated back from the average contact area of the cap. In house software was used to determine the areas from which the radii were calculated. The average radius for the single collapsed molecules was 18.9 nm. The average volume of the molecule had to be adjusted to exclude the corona. A fully extended PBA chain is approximately 0.6 nm thick on a surface. This height and the intermolecular distance were used to determine the volume of the disk of chains upon which the cap sits. This corrected volume was 4031 nm².

The height determined by solving equations 1 and 2 for h is 5.4 nm, which is about 32% smaller than the measured average height of the replicated molecules. While assuming circular footprints and semi-spherical shapes are reasonable, these do not describe every molecule and could be the source of the discrepancy between the calculated and measured heights.

Table 3.1 Areas and Heights for Single Collapsed Molecules and Drops Determined from AFM Height Images

sample	single collapsed molecules		multimolecular drops	
	molecular area (nm ²)	height (nm)	area (nm ²)	height (nm)
master	990 ± 30	2.3 ± 0.1	49000 ± 2000	18.0 ± 0.5
mold	1120 ± 40	5.1 ± 0.2	45000 ± 2000	29 ± 1
replicate	1120 ± 30	7.5 ± 0.3	38300 ± 2000	90 ± 3
calculated (master)	-	5.4*	-	-
calculated (replicate)		7.0-8.6**		

*calculated from the measured molecular volume and molecular area assuming bulk density for both (Section 3.4.1)

**scaling calculation which considers the effect of the PFPE precursor on the wetting properties of the PBA master (see section 3.4.2)

The droplets exhibited a pattern of heights similar to that of the single molecules, with the replicate having the largest height, followed by the mold and the master (see Table 3.1). Again, there is evidence for deformation of the droplets by the AFM tip and problems with the tip fully probing the mold wells. The surface contact area for the droplets decreases slightly from master to replicate. There are some small, but noticeable changes that occur during the molding of the droplets. Protrusions coming from the droplets become more pronounced resulting in a jagged circumference. Some satellite molecules that were around the original droplets become globular during replication. The addition of PFPE to the polymer sample results in a slight decrease in the spreading parameter of the brush molecules. The conformation of brush molecules is very sensitive to spreading parameter, such that even a small change could result in a rod-to-globule transition.⁶

The extended single molecule sample also showed some indication that the PFPE could be causing a change in conformation due to a change in spreading parameter. The extended master is a monolayer in which every molecule is extended. The mold and

replicate show a number of small round holes/objects that very likely could be collapsed molecules. Some other explanation is possible, such as air bubbles or contamination of some variety, but these seem unlikely since nothing similar was observed with other samples. As with the previous samples discussed, the average height of the molecules, wells, and replicate molecules increased significantly (see Table 3.2). The heights reported were the average heights measured for extended molecules, excluding the globular objects in the mold and replicate.

Table 3.2 Heights for Extended Linear Brush and Collapsed Four-arm Brush Determined from AFM Height Images

Sample	<u>extended linear</u> height (nm)	<u>four-arm</u>
master	0.66 ± 0.02	2.55 ± 0.06
mold	1.74 ± 0.06	5.1 ± 0.2
replicate	4.5 ± 0.2	10.9 ± 0.3

The four arm molecules also showed some signs of possible conformational change from the master during the replication process. While some arms were visibly collapsed around the molecule in the master (see Fig. 3.7 (A)), the resolution of this type of sample depends greatly on the sharpness of the tip and the imaging conditions. It is equally probable to get an image of these collapsed molecules that looks much like a collapsed linear molecule, without great enough resolution to see the individual arms. When the arms are visible, they appear to be curled around and the molecule as a whole looks like a relatively solid disk. In the mold and replicate of this sample, the molecule appears smaller and less uniform in shape. There are protrusions and the backbones of the molecules are much more

pronounced. This discrepancy between master and replicate could be due to one of two factors. The first is that the AFM tip may be greatly deforming the molecules in the master, making them appear more smooth and regular than they really are. The second is that these molecules may be responding to the application of the PFPE precursor, collapsing even further. The now familiar pattern of height increase from master to replicate was exhibited by this sample as well, confirming that the actual molecules, at the least in the vertical dimension, are deformed by the AFM tip.

3.4.2 Considering the Surface Properties of PFPE

Considering the discrepancies between the measured and calculated heights for the collapsed single molecules as well as significant differences between some masters and replicates in this study, it seems right to consider the system more quantitatively in order to estimate the actual effect of the PFPE precursor on one of these soft masters (collapsed single brush macromolecules). The effect of the PFPE on the height of the collapsed linear brush can be estimated using scaling theory and a simplified model of the molecule, assuming a hemi-cylindrical cap. The balance of forces acting on the cap of desorbed (though remaining tethered) side chains includes the surface tension term, f_{surf} , (3) and the chain stretching term, f_{elast} , (4)

$$f_{surf} = (\gamma - \gamma \cos\theta) \cdot d \cong 1/2 \gamma \theta^2 \cdot d \cong 1/2 \gamma \left(\frac{h}{R}\right)^2 \cdot d \quad (3)$$

$$f_{elast} = \frac{\partial F_{elast}}{\partial R} = \frac{1}{2} kT \frac{R}{Nb^2} \quad (4)$$

where γ is the surface energy of the polymer, θ is the contact angle of the cap on the corona, d is the distance between graft sites, R is the radius of the cap, h is the height of the cap, k is

Boltzmann's constant, T is the temperature, N is the degree of polymerization of the side chain, and b is the size of a Kuhn monomer.

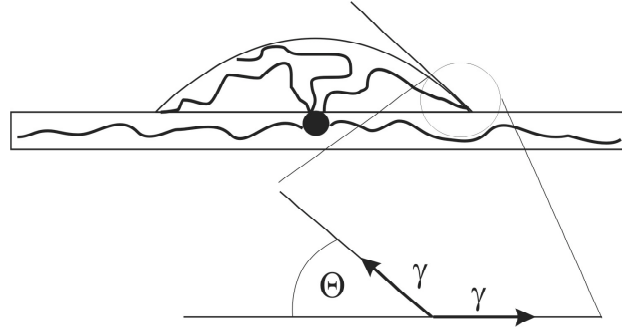


Figure 3.8 The Contact Angle of the Cap The side chains that are not adsorbed to the substrate form a cap on top of the adsorbed chains due to elasticity. Here, for simplicity, a hemi-cylindrical shape is assumed, the cap having a contact angle of θ with the corona.

Because mass is conserved, the following expression is true for a hemi-cylindrical cap:

$$V \cong Nb^3 \cong Rhd \quad (5)$$

Using this and balancing the previous two equations and solving for height, the following expression is determined:

$$h \sim \frac{N^{2/5}}{\gamma^{1/5} d^{4/5}} \quad (6)$$

This means that the height decreases with interfacial energy as $h \sim \gamma^{-1/5}$, or

$$\frac{h_1}{h_2} = \left(\frac{\gamma_2}{\gamma_1} \right)^{1/5} \quad (7)$$

This would mean that a decrease by a factor of 2 in the interfacial energy would result in an increase of 15% in the height. Using $\gamma_{\text{PBA/PFPE}} = \gamma_{\text{PBA}} + \gamma_{\text{PFPE}} - 2(\gamma_{\text{PBA}}\gamma_{\text{PFPE}})^{1/2}$ and $\gamma_{\text{PBA}} = 36 \text{ mJ/m}^2$ and $\gamma_{\text{PFPE}} = 10\text{-}16 \text{ mJ/m}^2$, an interfacial energy of 4 - 8.1 mJ/m^2 is calculated. The PBA cap in the PFPE environment would increase 1.3 - 1.6 times in height. Therefore, our

previously calculated height for single collapsed molecules of 5.4 nm would increase to 7.0 – 8.6 nm. Table 3.1 shows a measured replicate height of 7.5 nm, which falls right in this range, giving good agreement.

These calculations and their correlation with the replicate measurements strongly suggest that the PFPE is causing the PBA to dewet more from the surface, which results in a change in its conformation as represented by the height. This change, however, can be estimated and, thus, an original height deduced.

3.4 Conclusions

This new method was able to address the accuracy of the characterization of fluid objects by AFM by combining the technique with a PFPE-based soft lithography. By replicating several morphologies of cylindrical brush polymers above their T_g with a rigid polymer, heights were determined by eliminating the deformation caused by the AFM tip. As such, this combination method enabled the more accurate characterization of the vertical dimensions of brush-like macromolecules in these various morphologies. Broadening the use of AFM as a quantitative analytical tool for soft objects and fluid morphologies is a benefit for a wide range of fields.

The fidelity of PFPE-based lithography was also evaluated in application to soft nano-objects. It was found that the addition of PFPE decreased the spreading parameter of the system, altering the conformation of the original sample, including causing an increase in the actual height. In addition, over the course of many trials it was determined that this process is very sensitive to changes in the PFPE precursor. Slight alterations in the

formulation affected the reproducibility of the process. It will be necessary to better understand the process on a molecular level in order to make it more generally applicable.

CHAPTER 4

COMPARING THE CONFORMATIONAL BEHAVIOR OF HYDROPHILIC AND HYDROPHOBIC MACROMOLECULAR BRUSHES

4.1 The Conformational Transitions of Brush Polymers

Because of their unusual molecular architecture, brush-like macromolecules can adopt a variety of conformations on a surface (see Figure 4.1). Each of these conformations differs in symmetry, the number of monomeric contacts with the surface, and chain extension. Therefore, each conformation occupies a different surface area, which results in differences in the interaction energy. The conformational entropy also changes, as different conformations allow for different amounts of extension of the backbone and side chains. Akin to a gas-liquid phase transition with increasing pressure, a conformational change may proceed like a phase change, signified by an abrupt shape change and the coexistence of the two distinct shapes at a constant pressure and temperature. In a similar fashion, conformational transitions are caused by changes in the energetic and entropic contributions to the molecular free energy. This type of language is frequently used in the field of Langmuir monolayers, in which molecules in a “gas”-like sub-monolayer state are compressed to a “liquid” and then sometimes to a “solid,” each state consisting of the molecules in a certain orientation and packing.

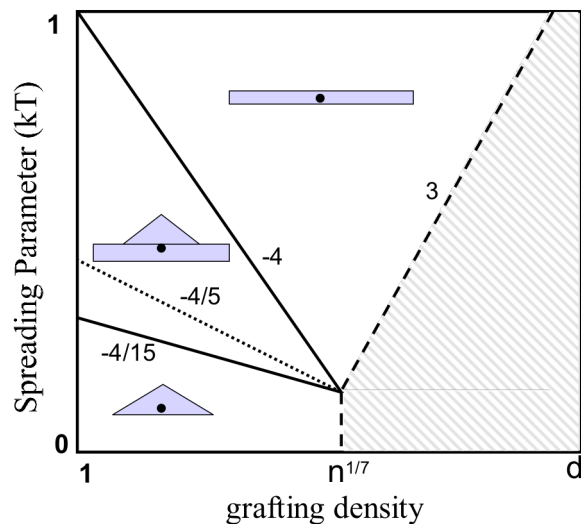


Figure 4.1⁷³ Conformational Diagram for Cylindrical Brushes The surface conformation of a cylindrical brush molecule depends on the grafting density as well as on the interaction energy with the surface. Theoretical investigations have predicted three possible conformations. The schemes correspond to a simplified cross-sectional view, the small black dot being the backbone and the blue being the side chains.

It is important to remember that highly branched molecules on surfaces are not true 2D systems. Their branches can be in or out of the plane of the surface as they are adsorbed to or desorbed from the surface. This is particularly true upon lateral compression as the area per molecule decreases and branches are forced to desorb. Macromolecular brushes respond to pressure in two ways, by transforming from a ribbon-like conformation to either a globular or a cylindrical one. Which conformation is taken depends on the interaction between the side chains and the interaction between the side chains and the surface. In forming a globule the molecule loses energy as the number of surface contacts decreases, but it gains energy because of increased attractive monomer-monomer contacts. The molecule gains entropy with the collapse of the backbone and some of the side chains. The cylindrical shape is less

⁷³ Zhulina, E.; Randell, G.; Rubinstein, M. *in preparation*

understood. It may be favored by repulsive interactions between side chains. The compressed side chains would gain some entropy, although it seems that the number of surface contacts would decrease.

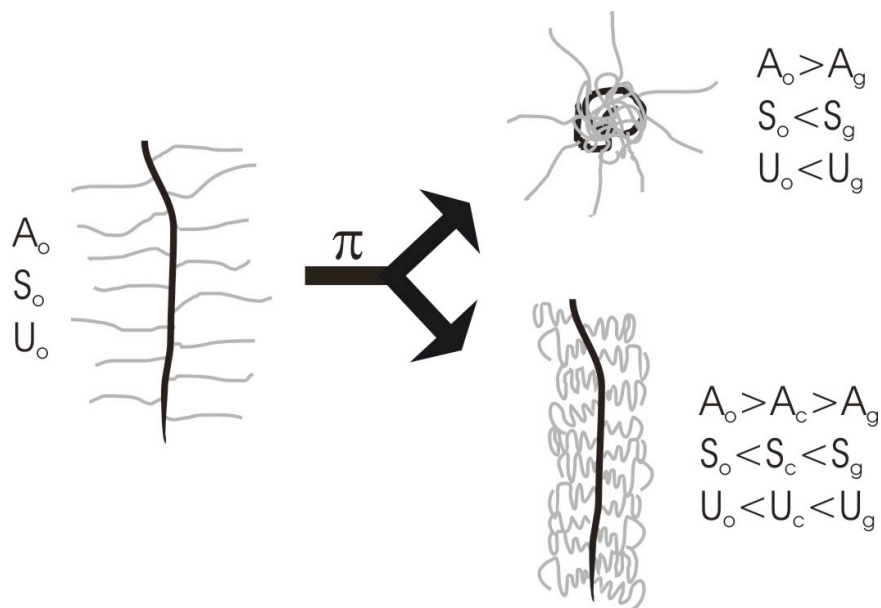


Figure 4.2 Compressed Brush Conformations The ribbon-like brush conformation (top view, left) has a large number of surface contacts, for which it pays a high entropic penalty because the side chains are extended. When compressed the molecule can form either a globule (top view, top right) or a cylinder (top view, bottom right). The globule has the smallest area, which means it sacrifices surface contacts ($U_g > U_o$), but increases its entropy ($S_g > S_o$). The cylindrical conformation occupies an area in between the ribbon and globule, and so it seemingly retains more surface contacts than the globule ($U_c < U_g$) and gains entropy ($S_c > S_o$).

4.2 The Illusive Cylindrical Conformation

Conformational transitions of brush-like macromolecules have been well studied under a variety of conditions and with molecules of varying parameters, such as the star molecules from chapter 2.⁷⁴⁻⁷⁷ The plate-to-globule transition for PBA brushes has been

⁷⁴ Sheiko, S.S.; Prokhorova, S.A.; Beers, K.L.; Matyjaszewski, K.; Potemkin, I.I.; Khokhlov, A.R.; Möller, M.; *Macromolecules* **2001**, *34*, 8354.

observed both by decreasing surface area (lateral compression) and by decreasing surface energy.⁷⁴⁻⁷⁷ Upon either of the aforementioned circumstance, the plate-to-globular transition is driven by the elasticity of the side chains. The spreading parameter for the cap on the corona is zero, but the effective spreading parameter becomes negative when the elasticity of the chains is taken into account. While several variations of backbone-collapsed conformations have been observed, a cylindrical conformation has been predicted to occur with decreasing surface energy, but has remained mostly illusive.⁷⁴ It has been observed only once in a dense film while spreading PBA molecules from a drop on graphite.⁷⁸ Therefore, systematic studies were launched in search of the cylindrical conformation and the conditions of its stability. The conformational behavior of hydrophilic poly(N,N-dimethyl acrylamide) (PDMA) brushes at the air/water (a/w) interface was studied and compared to hydrophobic poly(n-butylacrylate) (pBA) brushes. The PDMA brushes demonstrated the formation of the cylindrical conformation, unlike PBA that formed a globule. It is believed that the observed cylindrical conformation is stabilized by the excluded volume repulsion of the hydrophilic PDMA side chains partially immersed in the water subphase.

⁷⁵ Gallyamov, M.O.; Tartsch, B.; Khoklov, A.R.; Sheiko, S.S.; Börner, H.G.; Matyjaszewski, K.; Möller, M.; *Macromol. Rapid Comm.* **2004**, *25*, 1703.

⁷⁶ Sun, F.; Sheiko, S.S.; Moller, M.; Beers, K.; Matyjaszewski, K.; *J. Phys. Chem. A* **2004**, *108*, 9682.

⁷⁷ Boyce, J.R.; Shirvanyants, D.; Sheiko, S.S.; Ivanov, D.A.; Qin, S.; Börner, H.; Matyjaszewski, K. *Langmuir* **2004**, *20*, 6005.

⁷⁸ Xu, H.; Shirvanyants, D.; Beers, K.L.; Matyjaszewski, K.; Dobrynin, A.V.; Rubinstein, M.; Sheiko, S.S.; *Phys. Rev. Lett.* **2005**, *94*, 237801.

4.3 Synthesis and Characterization

A series of brushes with different length PDMA side chains were synthesized using ATRP as described in chapter 2. The two brushes with the longest side chains had the same backbone, while the brush with the shortest side chains had a different, slightly shorter backbone. The macroinitiator backbones were characterized by GPC-MALLS. The brush molecules themselves were characterized for molecular weight and polydispersity using the AFM-LB technique described in chapter 2. No GPC data was collected for the brushes due to the fact that it is known to be inaccurate for complex molecules and because PDMA does not dissolve easily in the available GPC solvent (THF). Despite the fact that PDMA is hydrophilic and water-soluble, stable monolayers of the molecules are formed on the LB trough, making the AFM-LB analysis possible. The issue of stable PDMA monolayers on a water surface is discussed at length in the following section.

In order to compare the behavior of the hydrophilic PDMA brush to the behavior of a hydrophobic brush, the conformational behavior of a linear brush with PBA side chains is also discussed. The characterization of this brush along with the PDMA series can be found in Table 4.1.

Table 4.1 Molecular Characterization by MALLS-GPC and AFM-LB Techniques

Sample	Macroinitiator		Brush		
	M_n (g/mol) ^a	n_n ^b	M_n (g/mol) ^c	PDI ^d	m_n ^e
PDMA 1	9.01×10^4	340	2.46×10^6	1.20	70
PDMA 2	1.38×10^5	520	5.12×10^6	1.22	97
PDMA 3	1.38×10^5	520	6.36×10^6	1.17	121
PBA	1.23×10^5	465	3.26×10^6	1.14	55

^aNumber average molecular weight determined from GPC-MALLS in THF, $dn/dc = 0.084$.

^bNumber average degree of polymerization of the macroinitiator: $n_n = \frac{M_n}{M_0}$, where $M_0 = 265$ g/mol is the molar mass of BPEM.

^cDetermined by AFM-LB technique (see Chapter 2)

^dSide chain degree of polymerization, $m_n = (M_n^{\text{brush}} - M_n^{\text{backbone}})/n_n m_0$ where m_0 is the monomer molar mass (99 g/mol DMA, 128 g/mol nBA).

The Langmuir-Blodgett trough is a convenient tool for studying these types of transitions in monolayers, as both the surface density of molecules and the surface energy can be easily altered either by closing the barriers (i.e. varying the surface area) or by using a subphase other than pure water. A more detailed discussion of its use can be found in chapter 2. Several of the experiments in this chapter required polymer to remain on the LB trough for long periods of time. In order to minimize evaporation and contamination by organic molecules in the air, a homemade chamber was built around the trough.

4.4 Results and Discussion

4.4.1 The Stability of PDMA Monolayers at the Air/Water Interface: Linear and Brush-like Macromolecules

PDMA is a water soluble polymer. In order to study a water-soluble polymer at the a/w interface, it is first important to assure the stability of monolayers of such a polymer on the water surface. Forming monolayers of water-soluble polymer at the a/w interface is not always possible. PEO is a well-documented water-soluble polymer that forms stable monolayers on water up to a certain surface concentration.^{79,80} As surface concentration increases within the monolayer (i.e. surface pressure increases), small loops within individual polymer chains dissolve into the water subphase, until eventually whole chains dissolve. Hydrophobic end groups can keep PEO from fully dissolving at high pressures, but the resulting layer is brush-like, with the end groups on the surface and the polymer chains dissolved into the subphase. In order to understand the stability of PDMA at the a/w interface, several experiments were performed with both linear and brush molecules.

The stability of monolayers of 2500 g/mol linear PDMA was investigated by running consecutive compression-expansion isotherms on the LB trough and comparing them. The first full isotherm of this low molecular weight PDMA had a maximum pressure around $\pi = 5$ mN/m. Each following cycle had a lower maximum pressure and smaller monomeric areas (See Figure 4.3, left).

⁷⁹ Kawaguchi, M.; Sauer, B.B.; Yu, Hyuk *Macromolecules* **1989**, *22*, 1735.

⁸⁰ Yang, Z.; Sharma, R. *Langmuir* **2001**, *17*, 6254.

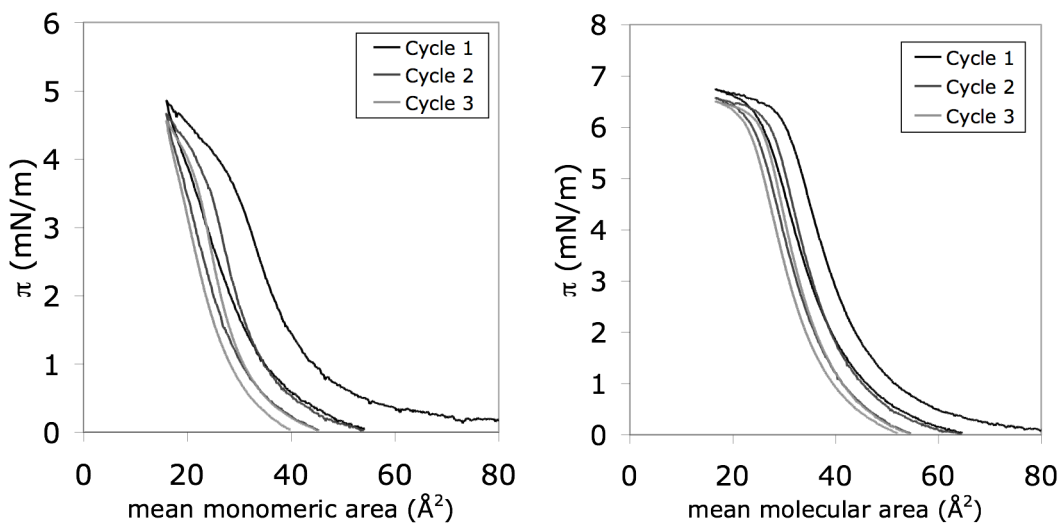


Figure 4.3 Linear PDMA Consecutive Isotherms Three compression-expansion cycles for 2500 g/mol linear PDMA (left) and 231,000 g/mol linear PDMA (right). Several attributes make it clear that polymer is dissolving into the subphase: molecular area decreases with each cycle and none of the cycles trace the previous cycle.

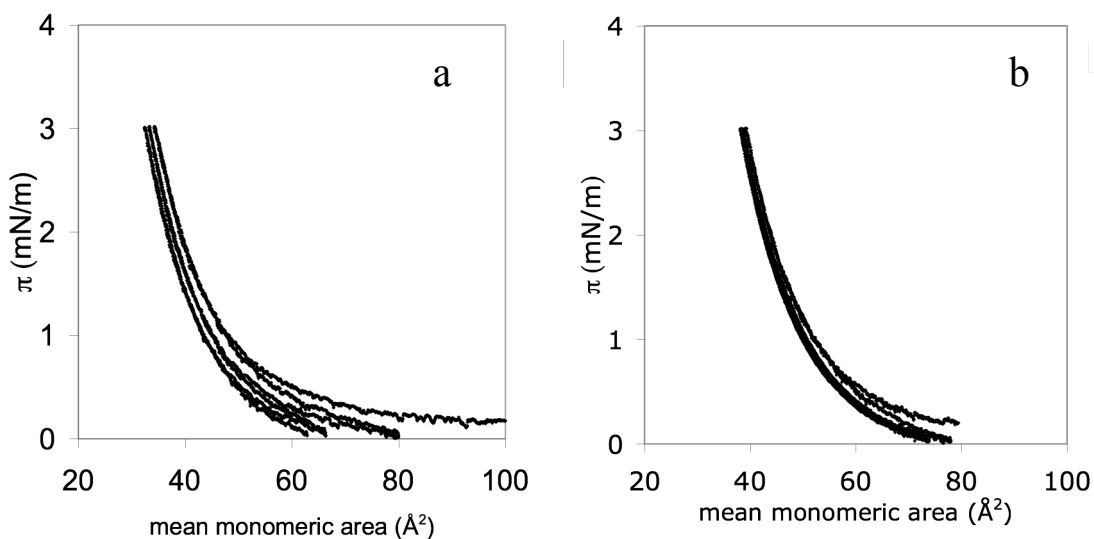


Figure 4.4 Pressure Limited Consecutive Isotherms of Linear PDMA Cycles between 0 – 3 mN/m were run for 2500 g/mol linear PDMA (a) and 231,000 g/mol linear PDMA (b). These cycles with small pressure ranges exhibited similar behavior to full isotherms, with the average monomeric area decreasing with each cycle because of dissolution. However, the minimum MMA decreased slightly with each cycle, but the shift is less than with the lower molecular weight sample. The cycles run consecutively right to left.

Similar cycles run at a pressure interval of 0 – 3 mN/m exhibited similar behavior (Fig. 4.4a), implying that polymer was dissolving when in any dense film. Because these cycles were limited by pressure, the shift was seen in the mean monomeric areas (MMA). Each consecutive cycle shows an onset of pressure increase at a smaller monomeric area than the previous cycle.

Full consecutive isotherms were also run for a higher molecular weight linear PDMA polymer (see Figure 4.3, right). 231,000 g/mol linear PDMA qualitatively had very similar results to the lower molecular weight sample. Each consecutive isotherm had a lower maximum pressure than the one previous, as well as smaller monomeric areas. The higher molecular weight sample did exhibit isotherm properties that suggest a more stable film was formed than with the lower molecular weight. The maximum pressures are significantly larger than for the lower molecular weight sample. The isotherms also exhibit the beginnings of a plateau, indicative of a phase change that would only be possible with some amount of stability within the monolayer. The high molecular weight isotherms also show a small amount of retrace near the maximum pressures, which indicates reversibility. The low molecular weight sample has immediate hysteresis upon expansion.

The high molecular weight PDMA was also run in cycles between 0 and 3 mN/m (see Figure 4.4b). The minimum MMAs also decreased with each cycle of this sample, but the shift was much smaller than for the low molecular sample. This could be evidence of two things: 1) the higher molecular weight polymer is less inclined to dissolve into the subphase, 2) dissolution of the higher molecular weight polymer requires increased pressure.

It is clear from these linear polymer studies that linear PDMA does dissolve into the water subphase when placed on the LB trough. However, the smaller polymer dissolves

much more readily than the larger. Small polymer molecules confined at the a/w interface gain a significant amount of entropy by going into solution. As polymers increase in size that entropic gain gets much smaller, until it becomes negligible compared to energetic contributions from surface adsorption. The behavior of the linear PDMA can be described by the Gibbs isotherm, which relates the surface concentration of a solute to its concentration in solution:

$$\Gamma = \frac{-C}{RT} \frac{d\gamma}{dC} \quad (1)$$

where Γ is the molar surface concentration, C the molar concentration of solute in solution, γ the surface tension, R the gas constant, and T the temperature. The rate of dissolution is proportional to the surface concentration and the surface concentration cannot be greater than a monolayer. This is why significant dissolution is induced with compression of monolayers of linear PDMA as the system seeks an equilibrium arrangement of molecules on the surface and in the subphase.

It is the lack of entropic favorability due to their massive size that makes brush monolayers particularly stable compared to their linear counterparts. As seen in Figure 4.5a, consecutive compression-expansion isotherms for a PDMA brush of intermediate molecular weight, 5.12×10^6 g/mol (sample 2 in Table 4.1), completely overlapped, which means that no polymer dissolved during that time. If an excess of polymer brush was applied to the trough such that multilayers were formed at the highest pressures, isotherms were not identical (see Fig. 4.5b). Rather the lowest pressures decreased with each consecutive run, which is evidence of brush dissolution. Average monomeric areas are also much smaller for this situation compared to the corresponding pressures in the sample where a monolayer is

preserved for the entire isotherm. These smaller monomeric areas also point to multilayer formation and dissolution.

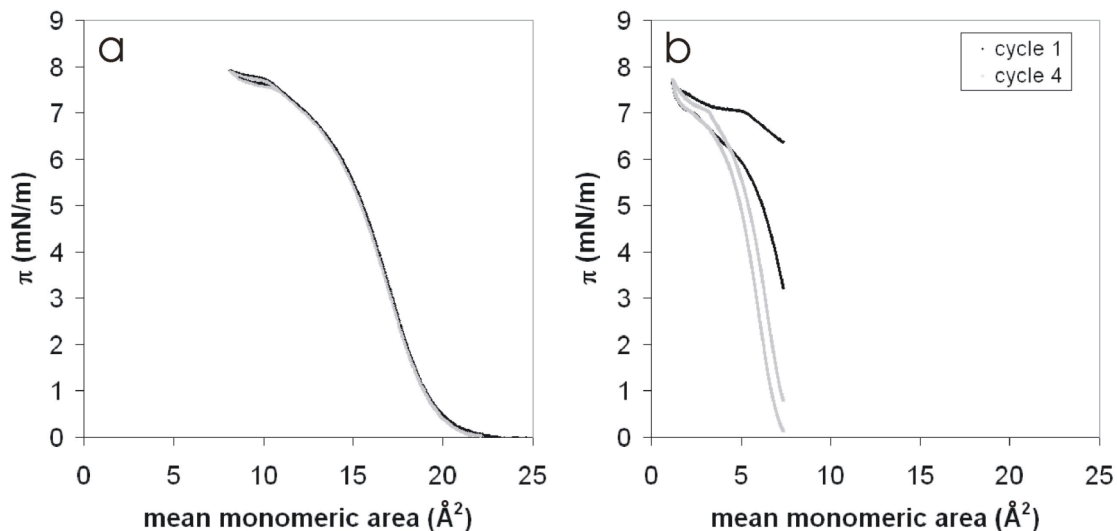


Figure 4.5 PDMA Consecutive Brush Isotherms Two compression-expansion cycles of the 5.12×10^6 g/mol PDMA brush monolayer were nearly identical (a). When an excess of PDMA brush was applied to the LB trough such that multilayers formed at the highest pressures, dissolution occurred (b).

To further verify the PDMA brush preference for the a/w interface as opposed to the subphase, an aqueous solution of 5.12×10^6 g/mol PDMA brush was mixed into the water subphase and the interface was monitored for several days. Isotherms were collected daily and the maximum pressures increased with time. While some of the pressure increase can be attributed to adsorbed impurities from the air, AFM analysis allowed us to show that it was mainly due to PDMA brush that had adsorbed to the interface from the subphase. By transferring a sample from the trough and imaging by AFM, it was determined that by the eleventh day 16% of the polymer that had been mixed into the subphase had adsorbed to the surface of the trough.

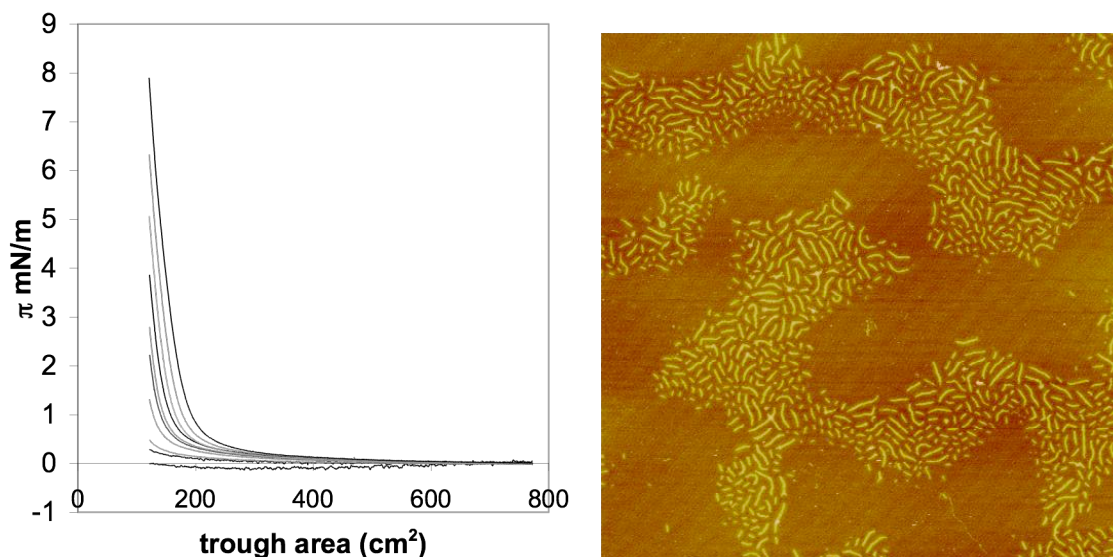


Figure 4.6 Monitoring of a/w Interface for Adsorbing Molecules 5.12×10^6 g/mol PDMA brush polymer dissolved in the subphase gradually returns to the a/w interface over the course of 11 days, illustrated by the increasing maximum pressure of isotherms taken over the course of this time (bottom to top with time). The shape of the isotherms differs from PDMA because of contributions from contaminants adsorbed from the air. On the right is a $4 \times 4 \mu\text{m}^2$ AFM height image taken from the sample transferred on the eleventh day. PDMA brush polymer has clearly adsorbed to the surface; the contaminants from the air are also visible.

Several other less impressive studies were done, which confirmed these earlier results that under monolayer conditions, the PDMA brushes are stable on the water surface. Among these were holding the trough at a certain area with PDMA and watching for pressure changes (there were none) and cycling between two trough areas as opposed to pressure and watching for decreases in pressure (there were none).

It is interesting to note that these soluble brush molecules exhibit very unusual surface-active behavior induced by their architecture. Taking a second look at the Gibb's isotherm, it does not take into account the architecture or even the general size of a molecule. The equation can be expressed differently by substituting mass per unit area and the mass concentration for the molar concentrations:

$$\Gamma = \frac{\text{moles}}{\text{area}} = \frac{m}{M \cdot S} = \frac{\sigma}{M} \quad (2)$$

where m is the mass of polymer, M is the molar mass, σ is the surface area and s is the mass per unit area, and

$$C = \frac{\text{moles}}{\text{volume}} = \frac{m}{M \cdot V} = \frac{c}{M} \quad (3)$$

where V is the volume of the solution and c is the mass concentration of solute in solution.

This now gives a Gibb's isotherm in terms of σ , c , and M

$$\sigma = - \frac{cM}{RT} \left(\frac{\partial \gamma}{\partial c} \right) \quad (4)$$

where σ is the ratio of the monomer mass to the monomeric area times s , the fraction of the surface covered by polymer:

$$\sigma = \frac{M_0}{A_0} s \sim s \quad (5)$$

$$s = \frac{\text{covered area}}{\text{trough area}} \quad (6)$$

The conclusion here is that the fraction of surface area covered by polymer is proportional to the molar mass of the polymer. Therefore, for the same mass concentration in solution, there will be a larger concentration of polymer on the surface for a larger molecular weight species. In other words, larger polymer molecules have a higher "surface activity" than smaller oligomers. This could explain why the larger molecular weight linear PDMA formed stable layers at much lower mass concentration of the solution subphase. In addition, brush monolayers might exhibit a higher kinetic stability than their linear counterparts due to the millipede-like architecture which needs a high cooperativity in the desorption of many quasi-independent side chains in order to dissolve.

To summarize, the architecture of brush molecules seems to enhance the stability of dense monolayers on the a/w interface. This very unusual behavior may be due to some kinetic barrier to dissolution or simply due to an energetic preference for the surface. The fact that molecules in the subphase return to the surface and the Gibb's relation also seems to indicate a preferential surface placement for large molecules seems to suggest that thermodynamically the brush molecules want to be at the interface.

The results of these studies conclude that PDMA brushes form stable monolayers at the a/w interface with no dissolution into the subphase. Therefore, the following studies were done with confidence under monolayer conditions assuming no dissolution.

4.4.2 Conformational Transitions

Combining the AFM and LB techniques provides a facile method for studying single molecule phase transitions, particularly in response to surface energy and lateral pressure/surface density (see chapter 2). Using the combination of these techniques the conformational transitions of both PBA and PDMA brushes were studied for comparison. These two chemically different brushes show surprising differences in behavior that lend insight into the relationship between architecture, chemical composition and function.

4.4.2.1 Poly(n-butyl acrylate) Brushes

To study the conformational behavior of a hydrophobic brush, a PBA brush with backbone degree of polymerization 450 and side chain degree of polymerization 55 was used. The isotherm for a monolayer of PBA brush molecules is similar to that of other fluids, although it exhibits some distinctive features as seen in Figure 4.7. The pressure onset

occurred around a monomeric area of 28 \AA^2 and rose until a critical area of about 20 \AA^2 at which the pressure reached a plateau with $\pi = 21 \text{ mN/m}$. Following this plateau from 20 to 14 \AA^2 , a second plateau was observed with a distinct pressure increase to $\pi = 22.2 \text{ mN/m}$. Upon expansion, hysteresis is observed in the areas corresponding to the two plateaus.

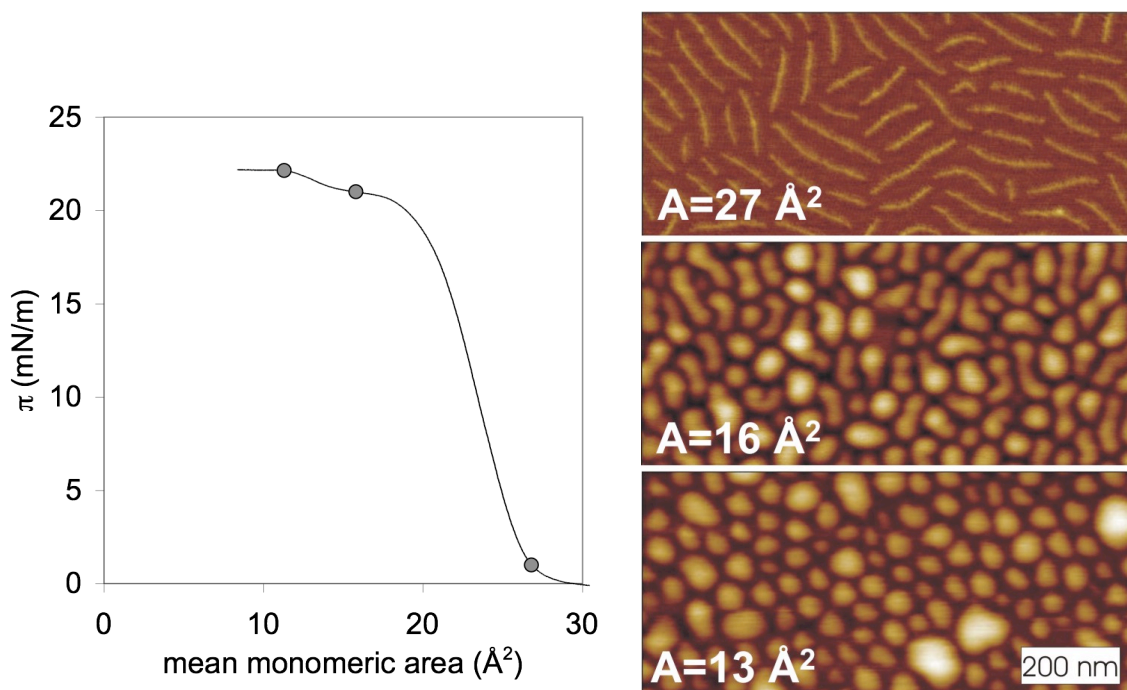


Figure 4.7 PBA Brush Isotherm and Corresponding AFM Height Images The isotherm of PBA brush molecules display two distinct plateaus after a linear rise. The pressures at which samples were taken (1, 21, and 22 mN/m) are marked by grey circles. At low pressures and prior to the plateau, PBA molecules are extended with many of their side chains adsorbed to the surface (top image). Once on the plateau, a coexistence of extended and globular molecules is seen as side chains begin to desorb (middle image). At the beginning of the second plateau, all molecules are globular and some have even begun to aggregate into small multimolecular drops (bottom image).

To visualize conformational changes during compression, LB samples were transferred at compressions corresponding to $\pi = 1, 21,$ and 22 mN/m , imaged by AFM and analyzed. These pressures correspond to four distinct regions of the isotherm: just following

the pressure rise, the steep liquid-like rise, the first plateau, and the second plateau. Figure 4.7 shows AFM height images of samples taken from these three compressions.

Prior to compression at $\pi = 1$ mN/m, the molecules are flat and plate-like (Fig. 4.7 top). The visible bright rod-like backbones are surrounded by a corona of tightly packed extended side chains. Because the side chains adsorb strongly to the water surface and are densely packed, they cause the backbone to be extended, whereas it would otherwise prefer to be coiled. At intermediate pressures like 7 mN/m there are still a majority of side chains adsorbed, keeping the backbone extended. As pressure continues to be increased on the monolayer, there is less and less room for adsorbed side chains. Side chains are forced to desorb from the surface and coil back on the backbone. With fewer side chains adsorbed, the backbone is able to coil and the molecules become more curved. When a sufficient number of side chains have desorbed from the surface, the backbone is able to fully coil and the molecule adopts a globular conformation. At the beginning of the first plateau there is a coexistence of molecules that are still extended and molecules that are globular (Fig. 4.7 middle). As the area decreases along that plateau, the number of extended molecules decreases and the number of globular molecules increases. By the end of the first plateau, all the molecules in the monolayer are globular (Fig. 4.7 bottom). During the second plateau molecules begin to coalesce into multimolecular droplets.

4.3.2.2 Poly(N,N-dimethyl acrylamide) Brushes

PDMA brushes also undergo a conformational change as a result of lateral pressure, but it is surprisingly different from the PBA transition. The isotherm for the PDMA brush differs significantly from that of the PBA due to its differing chemical properties. PDMA

has a much higher surface energy than PBA, so its isotherm covers a smaller range of pressures. While PDMA is a solid at room temperature, being at the a/w interface seems to plasticize the molecules. Therefore, the typical hysteresis seen in the isotherms of crystalline or other solid polymers is not observed for PDMA.

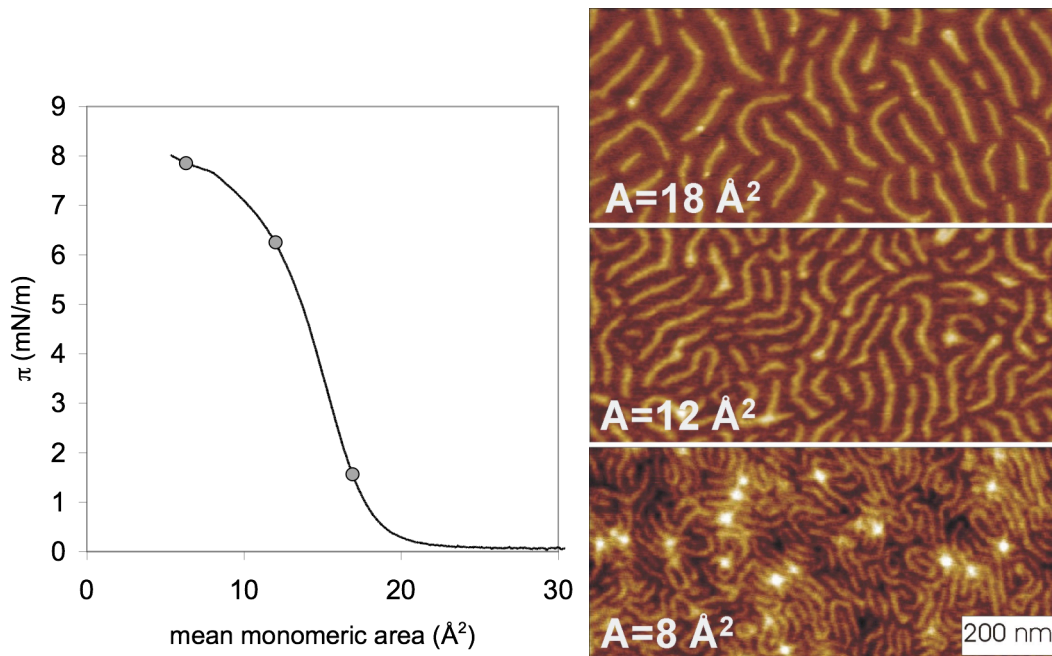


Figure 4.8 PDMA Brush Isotherm and Corresponding AFM Height Images The isotherm of PDMA brush molecules has significantly different features than that of the PBA brush, the most noticeable being a much smaller maximum pressure and the absence of a true plateau. Places where samples were taken are marked by open circles. AFM height images of PDMA brush (2) exhibit a gradual decrease in intermolecular distance with decrease in monomeric area (increase in pressure), transitioning from a plate-like conformation to a cylindrical one.

The isotherm for the PDMA brush increases linearly until about $\pi = 6$ mN/m when the slope begins to gradually change. The pressure never reaches a true plateau, but the slope becomes relatively small and the pressure reaches a maximum around $\pi = 8$ mN/m. Samples were taken at many pressures along the isotherm and imaged by AFM (Figure 4.8). At low pressures the PDMA molecules look almost identical to PBA brushes at low pressures. The

backbone is seen as a bright rod surrounded by the lower lying adsorbed side chains. A large fraction of the side chains are adsorbed to the surface of the water and the backbone is extended, giving the molecule a plate-like shape. As the pressure increases, the distance between molecules gradually decreases, while the contour length of the molecules remains the same. The molecules eventually become very closely packed, adopting a cylindrical shape. At about $\pi = 8$ mN/m multilayer formation begins. No collapse of the backbone was observed.

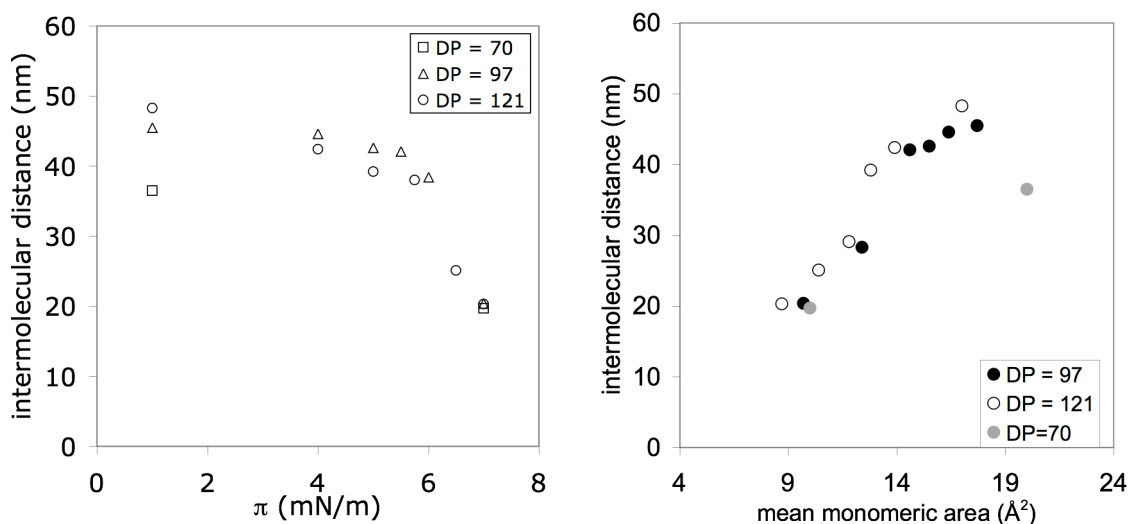


Figure 4.9 Dependence of Intermolecular Distance with Compression The intermolecular distance of PDMA brush molecules as it depends on surface pressure and side chain length. The side chain length has an effect at low pressures, but that effect quickly decreases with an increase in pressure. The dependence of intermolecular distance on MMA is linear with the slope changing slightly with changes in side chain length.

All three of the PDMA brush samples exhibited the same behavior upon monolayer compression. The isotherms were almost identical and the same plate-to-cylinder transition was observed for all. In order to better quantify the conformational transition, contour lengths and intermolecular distances were measured using in-house image analysis software

and the results are summarized in Table 4.2.⁸¹ At very low pressure ($\pi = 1$ mN/m) the intermolecular distances for each sample increase with increasing side chain length as is expected. However, the distances are much smaller than what is observed for PBA brushes of similar side chain degrees of polymerization. At high pressure ($\pi = 7$ mN/m) the intermolecular distance becomes degenerate for every sample at approximately 20 nm. While the contour lengths decreased slightly with increasing pressure, the changes were relatively small, about 10 - 15%. The contour lengths for samples 2 and 3 were approximately the same because they were synthesized from the same backbone. PBA brushes demonstrated completely opposite behavior. The intermolecular distance did not change, but the length contracted considerably, the backbone actually coiling on itself.

Table 4.2 Length Data for Compressed and Uncompressed Brush Monolayers

Sample	$\pi = 1$ mN/m		$\pi = 7$ mN/m	
	d (nm)	l_n (nm)	d (nm)	l_n (nm)
PDMA 1	36.5 ± 0.3	85 ± 5	20.1 ± 0.2	72 ± 2
PDMA 2	45.5 ± 0.3	131 ± 3	20.4 ± 0.2	115 ± 4
PDMA 3	48.3 ± 0.3	127 ± 2	20.4 ± 0.2	114 ± 2
PBA	38.9 ± 0.4	124 ± 2	37.3 ± 0.1	105 ± 1

⁸¹ PEN image analysis program, developed by David Shirvanyants.

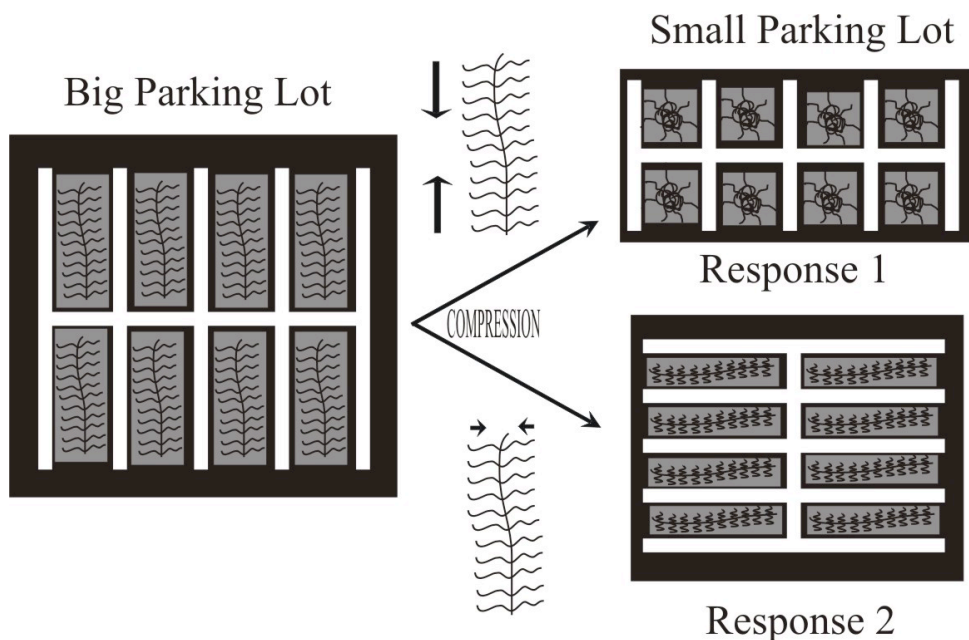


Figure 4.10 Molecular Parking When compressed hydrophobic PBA accommodates the reduction in space by contracting along the backbone. Hydrophilic PDMA exhibits the opposite behavior and contracts its side chains. It can be thought of as a parking lot—the parking lot reduces in size, but has the same number of spots. Therefore, the cars must change their size in order to stay on the lot.

4.4.3 Discussion

There are striking differences in the conformational behavior of the PBA and PDMA brushes despite their identical architecture. Even at very low pressures when the molecules appear almost the same, the intermolecular distances scale differently with respect to the degree of polymerization (DP) of the side chains. PBA brushes have intermolecular distances that are consistent with fully-stretched side chains. The largest PDMA molecules in this study have more than twice the DP of the PBA molecules studied, 120 versus 55, but their intermolecular distance at $\pi = 1$ mN/m were almost the same. The expectation is that a brush with a larger DP would have a correspondingly larger intermolecular distance. This discrepancy that accompanies the change in chemical structure could be accounted for by a difference in monomer size. Indeed, the mean monomeric area calculated from the LB

monolayers for PDMA is significantly smaller than that of PBA. However, theoretically these two monomers should have similar monomeric areas, so the discrepancy is most likely due to some dissolved loops in the PDMA side chains as well as some whole side chains dissolved. This would allow the molecules to occupy less surface area, resulting in smaller than expected intermolecular distances. Unlike the hydrophobic PBA, PDMA does not lose free energy by dissolving into water. At the same time, some side chains can be dissolved, with the molecule still energetically preferring to remain at the interface.

At higher pressures the behavioral differences between the two polymers become much more obvious. The PDMA response to pressure is exactly opposite that of PBA. As they undergo the conformational transition, the PBA molecules maintain an almost constant intermolecular distance, while the contour length of the molecules decreases. This behavior is a result of the competition between the backbone and the side chains. A fraction of side chains that are able to fit remains strongly adsorbed to the surface, maximizing favorable surface contacts; it is these that determine the intermolecular distance. As pressure increases and that adsorbed fraction decreases, the backbone is able to coil more decreasing the contour length. In contrast, the PDMA brushes have a gradually decreasing intermolecular distance and a constant contour length with increasing pressure. The PDMA brush conformation is also determined by the backbone-side chain competition, but the side chains have different preferences because of their hydrophilicity. As the pressure on the film is increased, the polymer has less room on the surface and molecules are forced closer together. The dissolved side chains repel one another due to the good solvent conditions, keeping the backbone extended even at high pressure. PDMA side chains because they are

hydrophilic would much prefer to dissolve into the subphase rather than collapse onto the backbone.

PBA's conformational transition is considered as a first order phase transition. There is coexistence of the two conformations and the transition occurs at constant pressure. PDMA on the other hand exhibits a conformational transition, which is not a conformational phase transition. The change in the molecules' shape occurs gradually with no coexistence and no true plateau in pressure. The effect of the length of the side chains on each transition is quite different. Below a certain side chain length, PBA will no longer undergo a plate-to-globule transition. The curvature of the molecules increases with pressure, but the side chains are not long enough to stabilize the globule conformation. Therefore they remain uncollapsed. The behavior of the PDMA brushes, on the other hand, seems to not have a strong dependence on side chain length. At high pressures the intermolecular distance has no dependence on side chain length, but was the same for every sample. This terminal distance may be related to the grafting density, the interfacial energy, or, most likely, the mounting repulsion of the dissolved side chains. The density profile of polymer near the backbone is the same for every sample having the same intermolecular distance. The density of polymer ultimately determines the molecule's interaction with other molecules, and thus, the intra- and intermolecular conformation. The largest repulsion would occur close to the backbone, determining the intermolecular distance. Beyond these maximum pressures, molecules begin dissolving as they are squeezed out of the film and into the subphase.

4.5 Copolymer Brushes

4.5.1 Characterization

In order to more fully understand this hydrophilic/hydrophobic conformational effect, four different copolymer brushes were studied. The first two brushes had statistical copolymer side chains, the first sample having PBA₃-stat-PDMA₁₇ side chains (15% PBA and 85% PDMA by number) and the second sample having PBA₅₀-block-PDMA₉ side chains (26% PBA and 74% PDMA). The second set of brushes had block copolymer side chains, one with PBA₅₀-block-PDMA₉ side chains and the other with PBA₅₀-block-PDMA₅₀. Analysis of side chain composition was done by gravimetry and GPC-MALLS during and after polymerization. Final molecular weight analysis was done using the AFM-LB technique. Table 4.3 summarizes the characterization data.

Table 4.3 Characterization Data for Copolymer Brushes

Sample	nBA DP ^a	DMA DP ^a	MW (g/mol) ^b
Statistical	3	17	2.45 x 10 ⁶
Statistical	9	26	2.60 x 10 ⁶
PBA-b-PDMA	50	9	6.2 x 10 ⁶
PBA-b-PDMA	50	50	1.28 x 10 ⁷

^aDetermined by gravimetry

^bDetermined by AFM-LB technique (see chapter 2)

4.5.2 Results and Discussion

All four copolymer brushes exhibited the same qualitative conformational behavior as the homopolymer PDMA. At low pressures they were plate-like, and with increasing pressure their intermolecular distance gradually decreased while the contour length remained

relatively constant. However, the dependence of the intermolecular distance on MMA differed for the two types of copolymers, which is clear from the graph in Figure 4.12 of intermolecular distance v. MMA. For comparison, the DP = 97 homopolymer PDMA data is also included on this graph. The block copolymer intermolecular distance depended on MMA with a similar slope to that of the homopolymer brush. The statistical copolymer brushes changed intermolecular distance more slowly with pressure.

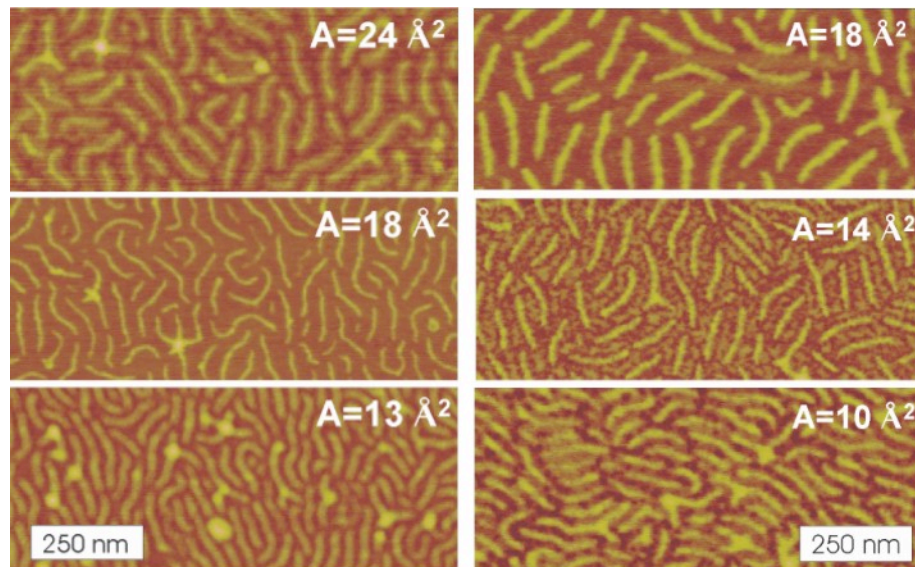


Figure 4.11 Conformational Changes of PBA-PDMA Copolymer Brushes The PBA₉-stat-PDMA₂₆ copolymer (left) and the PBA₅₀-block-PDMA₅₀ copolymer (right) both show gradually decreasing intermolecular distances and the cylindrical conformation at high pressures. Notice how the PDMA block can be seen as brighter areas in between compressed molecules of the block copolymers starting at 14 Å².

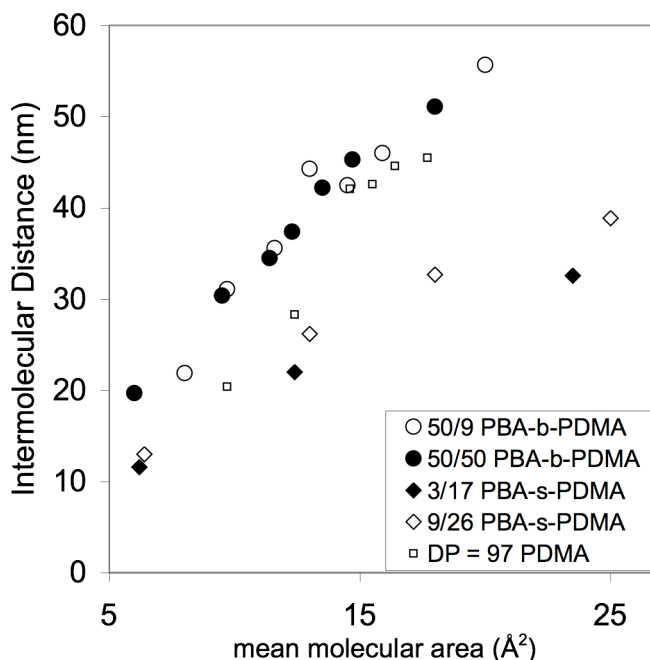


Figure 4.12 Dependence of Intermolecular Distance on MMA The block copolymer brushes have an intermolecular distance that scales closely with MMA to that of the homopolymer PDMA, but the stabilization of the brush seems to be enhanced by the inner PBA block. The intermolecular distance trend for the statistical copolymers varies significantly from the homopolymer PDMA, changing more slowly.

The differing dependence of the intermolecular distance of the statistical copolymers on MMA begins to show that this qualitatively identical behavior somehow differs in mechanism. The pressure/area isotherms of the two different types of copolymers further support a potential difference in the mechanism of the conformational transition. The block copolymer isotherms first traced the shape of the PDMA isotherm up to about $\pi = 8$ mN/m and then followed the shape of the PBA isotherm to $\pi = 24$ mN/m. This suggests that at lower pressures, the brushes behave according to PDMA with the PDMA block of the adsorbed side chains dissolving into the subphase more or less completely by $\pi = 8$ mN/m. Above 8 mN/m the brushes show a PBA-like dependence on pressure, but the backbone is not able to collapse because of the dissolved PDMA block. In turn, the PBA block keeps the

molecules from dissolving into the subphase at high pressures, and thus stabilizes them at the interface.

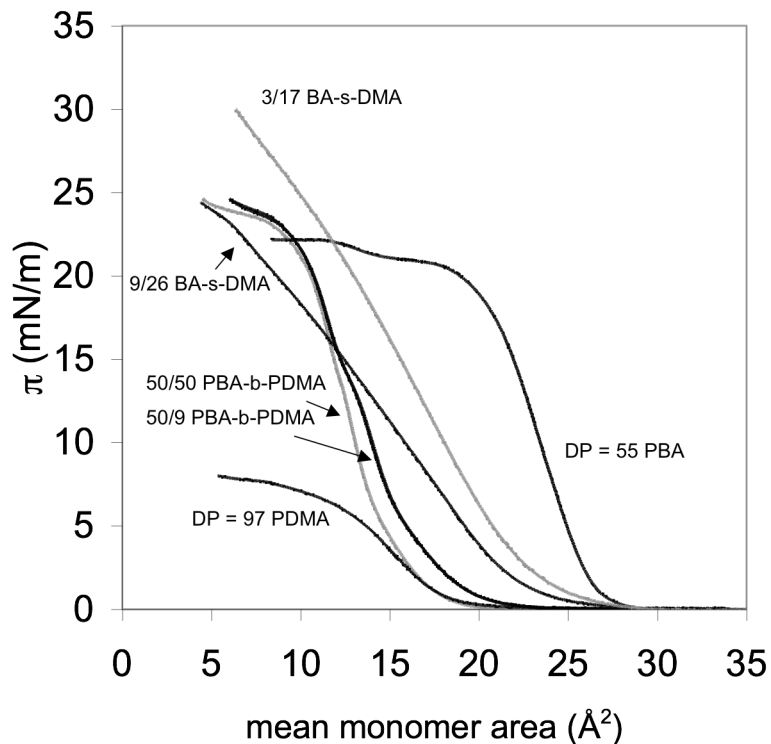


Figure 4.13 Copolymer and Homopolymer Isotherms Copolymer isotherms are significantly different from their homopolymer components. Block copolymer isotherms resemble an addition of the two, while statistical copolymer isotherms seem to have nothing in common with either component's.

The statistical copolymers have isotherms that do not resemble PBA or PDMA brush isotherms. They increase linearly with a smaller slope than PBA to a maximum pressure higher than that of PBA. In like manner, there are no similarities to the PDMA isotherm, which exhibits much smaller maximum pressures and a curved shape. The statistical copolymers also exhibit larger MMAs than PDMA at low pressures. The random placement of the nBA monomer through the side chains allows them to act as anchors, keeping the side chains from fully dissolving into the subphase. At the same time, sections of PDMA in the

side chains are able to loop in the water, providing the repulsion needed to keep the backbone extended. The random placement of these two opposite-behaving monomers results in side chains that cannot leave the water surface. They cannot fully dissolve into the subphase, nor can they desorb from the surface onto the backbone. This combination results in the anomalous isotherm behavior as molecules are literally forced to move closer together, while being much more restricted than their homopolymer counterparts.

4.6 Conclusions

Hydrophilic and hydrophobic macromolecular brush polymers have significantly different conformational behavior at the a/w interface due to their difference in chemical composition. Hydrophobic PBA brushes undergo a first order phase transition from a plate-like to a globular conformation from $\pi = 1$ mN/m to $\pi = 21$ mN/m, with constant intermolecular distance and gradually decreasing contour length. Unlike PBA, hydrophilic PDMA brush gradually changes from a plate-like to a cylindrical conformation from $\pi = 1$ mN/m to $\pi = 7$ mN/m, with gradually decreasing intermolecular distance and constant contour length. The width of the final cylindrical conformation does not depend on side chain length. Brushes with side chains that were copolymers of nBA and DMA resulted in behavior that qualitatively appeared to be the same as that of PDMA homopolymer brushes, but the isotherms of which had MMA dependencies on pressure that revealed mechanisms that differed slightly from that of the homopolymer, particularly with the brushes having statistical copolymer side chains. The block copolymer side chains were stabilized on the water surface by the PBA block after the PDMA block had dissolved into the subphase. The

random placement of both monomers in the statistical side chains resulted in chains that were trapped at the interface even with the application of pressure.

Chemical composition clearly has a strong effect on the functional behavior of cylindrical brush polymers. By changing the hydrophilicity of the polymer, a completely new surface conformation was observed. Using copolymerization expands the more subtle details of the molecule's behavior, showing that what is happening intramolecularly is more complicated than simply the observed conformation. These subtleties could be used for surfaces with nano-selective domains, for the growth of nanowires or nanoparticles, or to stabilize coatings. The cylindrical conformation alone provides another shape for patterning on a sub 30 nm length scale.

CHAPTER 5

THE MIXING OF CHEMICALLY DIFFERENT MACROMOLECULAR BRUSHES

5.1 Polymer Mixing

The process of two-component mixing is governed by the energy of interaction between the two species and the entropy of the system. In an ideal mixture, whether two species will mix depends on the sign of the free energy of mixing, $\Delta F_{\text{mix}} = \Delta U_{\text{mix}} - T\Delta S_{\text{mix}}$, a negative change in energy favoring mixing and a positive change opposing mixing. Two species in a mixed system will take on one of three possible arrangements: phase separation, mixing, or ordered mixing (see Fig. 5.1). Disordered mixing of any level is driven by an entropy increase, which decreases with an increase in molecular size; this is why polymer molecules almost always phase separate. Ordering is a type of mixing that leads to a decrease in entropy. As such, it actually has more in common with phase separation than with ordinary mixing. If one considers perfect phase separation (two domains) and perfect ordering with no defects, there can be only one arrangement of the molecules in each situation. Therefore, both phase separation and ordering have negligible entropic contributions and so must be entirely energy driven. In the case of phase separation, the energy change upon mixing, $\Delta U_{\text{mix}} \cong (2u_{\text{AB}} - u_{\text{AA}} - u_{\text{BB}})$ is positive, promoting fewer AB contacts. In the case of ordered mixing, $\Delta U_{\text{mix}} < 0$ favoring more contacts between A and B species. In both cases, non-zero mixing entropy will perturb the molecular arrangement, resulting in a mixture of A-rich and B-rich domains.

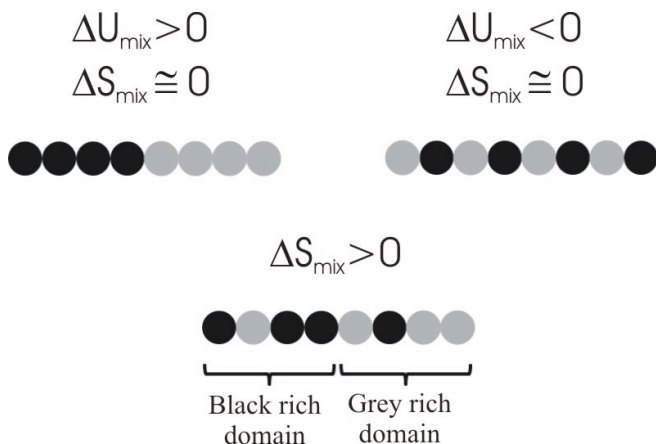


Figure 5.1 Possible States of Two-Component Mixing Phase separation ($\Delta U_{\text{mix}} > 0$) usually occurs in mixed polymer systems due to their large size ($\Delta S_{\text{mix}} \cong 0$). There are two scenarios for mixing: a small positive ΔU_{mix} that can be overcome by entropy (gives a mixture of black-rich and grey-rich domains) or a large negative ΔU_{mix} (gives perfect ordering). In general, polymers and other large molecules with either phase separate (state 1) or order (state 2) since they have no entropic incentive to randomly mix.

It is well known that, generally, chemically different species phase separate when mixed together due to a positive energy of interaction, unless entropy is large enough to compensate. In the case of polymers, entropy is always negligible because of their large size, resulting in phase separation even for a positive energy of interaction that is very small. A variety of methods have been developed to overcome this obstacle.^{82,83} At the most basic level, polymers can sometimes be forced to combine by physically mixing molten polymer or reacting unlike polymers together. Chemical modification of otherwise immiscible polymers by introducing functional groups induces mixing via specific interactions such as hydrogen bonding or ion-ion interactions. Other strategies have been developed to encourage the mixing of polymers by lowering the interfacial tension between the two phases with a third component, such as diblock or graft copolymers. Even with these many

⁸² Leibler, Ludwik; *Prog. Polym. Sci.* **2005**, *30*, 898.

⁸³ Koning, C.; Van Duin, M.; Pagnouille, C.; Jerome, R. *Prog. Polym. Sci.* **1998**, *23*, 707.

modifications, most polymer blends remain incompatible and it is often a challenge to find and implement the correct strategy to sufficiently incorporate a pair of chemically different polymers.

Mixing often becomes even more difficult for two dimensional polymer blends, which exhibit properties that differ from the three-dimensional bulk system. Going from a 3D to a 2D system introduces a kinetic barrier which opposes mixing. Interactions at the polymer/substrate interface as well as the polymer/air interface can strongly effect the miscibility of two component polymer films.⁸⁴ Most of the recent studies on 2D blend systems have been concerned with understanding how to control the final morphology of phase separated mixed films, as opposed to increasing miscibility.^{85,86} The results show that the volume fraction of each polymer, the sample preparation technique used, and the substrate all effect the final phase morphology.⁸⁷ However, these phase morphologies are often metastable and macroscopically phase separate upon annealing.

In general, most mixed polymer systems in both thin films and bulk are forced to mix by kinetic means or by introducing some kind of stabilizer that alters the interaction energies. Most polymer pairs do not have a thermodynamic incentive to mix. This study found that by changing the polymer architecture, normally immiscible polymers mix in a monolayer. Here it is demonstrated that hydrophilic PDMA and hydrophobic PBA mix at the air/water interface when the macromolecular architecture is changed from linear to brush-like.

⁸⁴ Budkowski, A.; Bernaski, A.; Cyganik, P.; Raczkowska, J.; Penc, B.; Bergues, B.; Kowalski, K.; Rysz, J.; Janik, J. *Macromolecules* **2003**, *36*, 4060.

⁸⁵ Chung, H.-J.; Wang, H.; Composto, R.J. *Macromolecules* **2006**, *39*, 153.

⁸⁶ Lioa, Y.; You, J.; Shi, T.; An, L.; Dutta, P. K. *Langmuir* **2007**, *23*, 11107.

⁸⁷ Li, X.; Han, Y.; An, L. *Polymer* **2003**, *44*, 8155.

Furthermore, the mixing was shown to transform into an alternating pattern upon increasing the surface concentration of adsorbed molecules. In addition, mixtures of linear polymers and linear and brush polymers were studied to better understand the mechanism of the brush-brush mixing.

5.2 Polymers Studied

The molecules primarily used in this study were the 5.12×10^6 g/mol PDMA brush molecules and the 3.26×10^6 g/mol PBA brush molecules (see Table 5.1). Besides the aforementioned brush molecules, a number of polymers were used in this study and are summarized in Table 5.1. Three PDMA brushes and the smaller two PBA brushes were synthesized as described in chapter 2. The largest PBA brush was synthesized via a similar technique, but using an emulsion polymerization. All brushes had an approximately 100% grafting density. The linear PBA, PDMA, poly(dimethyl siloxane) (PDMS) samples were all purchased from a polymer supplier. The perfluoropolyether (PFPE) was provided by the DeSimone group. Table 5.1 contains the molecular weight and side chain degree of polymerization data for all the polymers studied.

Table 5.1 Molecular Weight Data for Polymers Studied

Sample	Architecture	M_n (g/mol) ^a	m_n ^b
PDMA 1	linear	2.50×10^3	--
PDMA 2	linear	2.31×10^5	--
PBA 1	linear	1.44×10^3	--
PBA 2	linear	3.11×10^3	--
PBA 3	linear	4.12×10^4	--
PBA 4	linear	7.70×10^4	--
PBA 5	linear	2.26×10^5	--
PBA 6	linear	1.13×10^6	--
PDMS	linear	8.0×10^3	--
PFPE	linear	4.0×10^3	--
PDMA 1	brush	2.46×10^6	70
PDMA 2	brush	5.12×10^6	97
PDMA 3	brush	6.36×10^6	121
PBA 1	brush	9.97×10^5	38
PBA 2	brush	3.26×10^6	55
PBA 3	brush	4.69×10^6	80

^adetermined by the AFM-LB technique described in chapter 2

^bside chain degree of polymerization

Each of these polymers exhibits different properties due to their differences in chemical composition. The chemical composition of each monomer unit is shown in Figure 5.2.

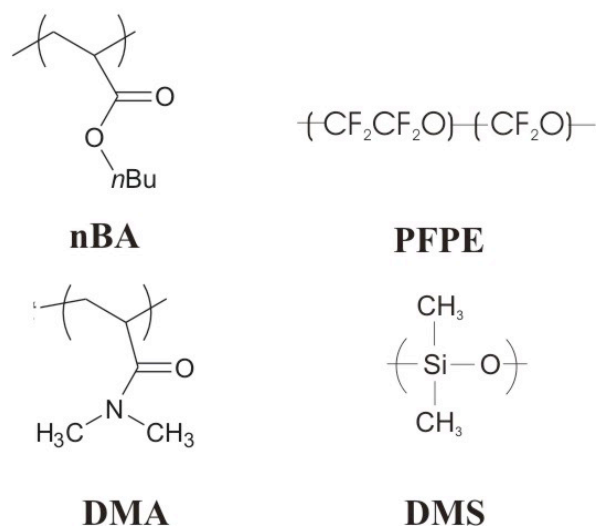


Figure 5.2 Chemical Structures of the Monomers Used Four different polymers were used in this study that had significant variation in chemical composition.

5.3 The Phenomenon

5.3.1 Linear Polymer Mixing

The behavior of two-component linear polymer systems is well studied and there are but a few special pairs of polymers that will mix without spontaneously phase separating. It still seemed important to observe the mixing behavior in two dimensions for the pair of corresponding linear polymers used in the brush studies. Mixing experiments were carried out for two sets of linear polymer molecules. One set had a relatively low molecular weight with 2500 g/mol PDMA and 3100 g/mol PBA. The high molecular weight set was 231,000 g/mol PDMA and 226,000 g/mol PBA. Polymer was applied to the LB trough in two different ways. First, both the PDMA and the PBA polymer were dissolved into the same chloroform solution in a 50/50 by number concentration. This premixed solution was then applied to the trough. Second, separate solutions of the PDMA and PBA polymers were

applied consecutively to the trough. All the linear studies were done by compressing the polymer to 1 mN/m, transferring to mica, and imaging by AFM.

When applied from the premixed solution, the low molecular weight polymers formed a mixed monolayer with small domains on the order of 10 nm (left image, Fig. 5.3). The disparity in chemical structure of the two polymers results in a difference in physical properties. Therefore each has a distinct interaction with the AFM tip and shows up differently in the phase image and sometimes even in the height image. The fact that the polymers are distinguishable is a great benefit of the AFM technique. The high molecular weight linear polymers exhibited much larger phase separated domains than the low molecular weight (right image, Fig. 5.3). It is expected that lower molecular weight species mix more readily than high molecular weight ones, because they gain more entropy in so doing.

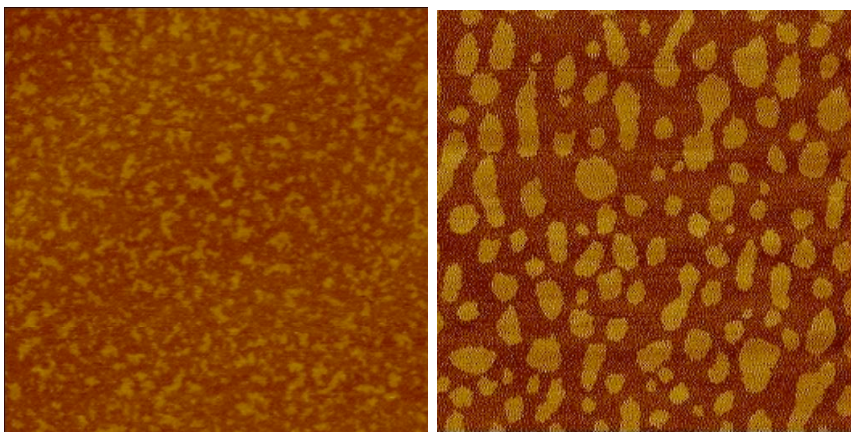


Figure 5.3 Linear Mixtures from Premixed Solutions The mixture of 2500 g/mol PDMA and 3110 g/mol PBA on the left has small domains of each type of polymer (height image, 1 x 1 μm). The mixture of 231,000 g/mol PDMA and 226,000 g/mol PBA on the right exhibits much larger domains, the PDMA domains appearing brighter than those of the PBA (height image, 5 x 5 μm).

To determine the equilibrium arrangement of the high molecular weight mix and rule out possible metastable states, the premixed polymer mixture was applied to the trough and

allowed to sit some amount of time before a monolayer was compressed. The surface concentration was kept low, so that there was room for the molecules to diffuse on the surface. At the end of the allotted time, the barriers were closed until a monolayer formed and was then transferred and imaged by AFM. Trials were done at times from 0 to 50 hours. The polymers remained phase separated and the size of the domains increased with time. The PDMA molecules formed domains in a matrix of PBA. The PDMA domain size was measured using the Nanoscope III software. The graph in Figure 5.4 shows the increase of domain size from 0 to 50 hours. This increase in domain size proves that the system energetically prefers to be phase separated rather than mixed. Hypothesizing from these results, one would expect the order of magnitude more massive macromolecular brushes to phase separate even more readily than the linear polymer.

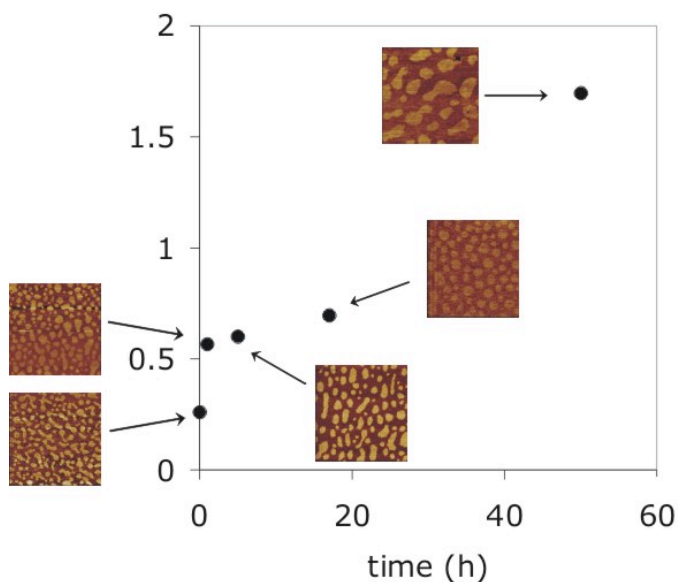


Figure 5.4 PDMA Domain Size in Linear Mixture with Time The domain size of 231,000 g/mol linear PDMA in 226,000 g/mol linear PBA more than tripled over two days, illustrating its preference for phase separation. 5 x 5 μm AFM phase images correspond to the data points, the lighter spots being PDMA and the darker areas PBA.

5.3.2 Brush Polymer Mixing

Mixing of PDMA and PBA brushes demonstrated strikingly different behavior. Unlike linear polymers of the same chemical structure, polymer brushes mixed completely yielding a molecularly alternating structure. Brush-brush experiments were carried out in a similar manner to the linear-linear trials, but with surprising results. A solution of both the PDMA and the PBA brush polymers was made and placed on the LB trough. The arrangement of molecules in the monolayer was observed at several pressures between 1 and 8 mN/m. From pressure 1 mN/m to pressure 5 mN/m, the monolayers consisted of small domains of approximately 1 to 5 PDMA or PBA brush molecules (Fig. 5.5A-B). In this pressure range the intermolecular distance decreased slightly with increasing pressure, but little change was observed in the degree of mixing. From pressure 6 mN/m to 7 mN/m a change occurred. The small domains were replaced by an alternating structure, each molecule having two neighbors of the other type of molecule. The difference between molecules was discernable because of AFM's sensitivity to differences in physical properties. The two types of polymers look very different in AFM phase images, PBA appearing dark and PDMA appearing light (see Figure 5.6, inset).

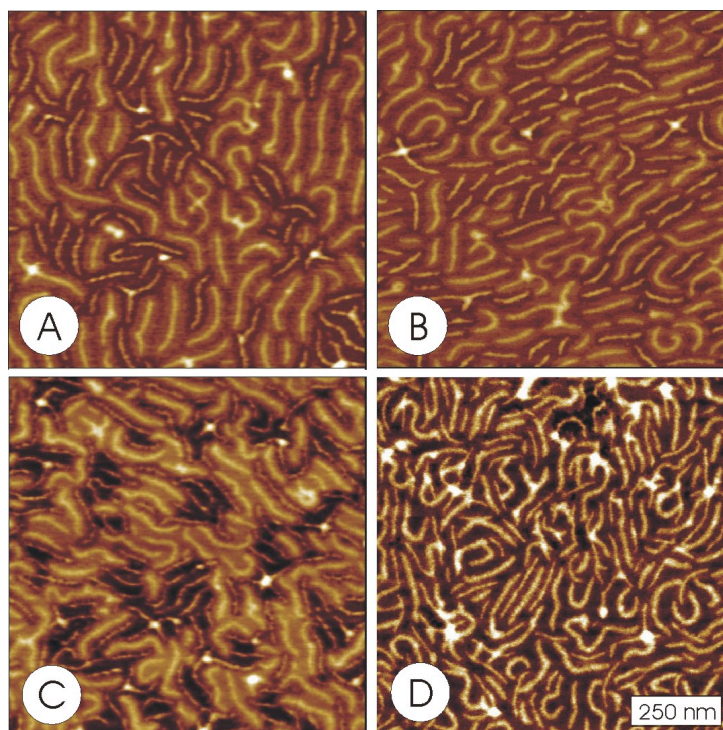


Figure 5.5 AFM Height Images of Mixed Monolayers at Different Lateral Pressures
Mixed monolayers of 5.12×10^6 g/mol PDMA and 3.26×10^6 g/mol PBA brushes gradually became more mixed with pressure. (A) $\pi = 1$ mN/m, (B) $\pi = 3$ mN/m (C) $\pi = 6$ mN/m (D) $\pi = 7$ mN/m In (A) – (C) PBA molecules have dark coronas and PDMA molecules are bright.

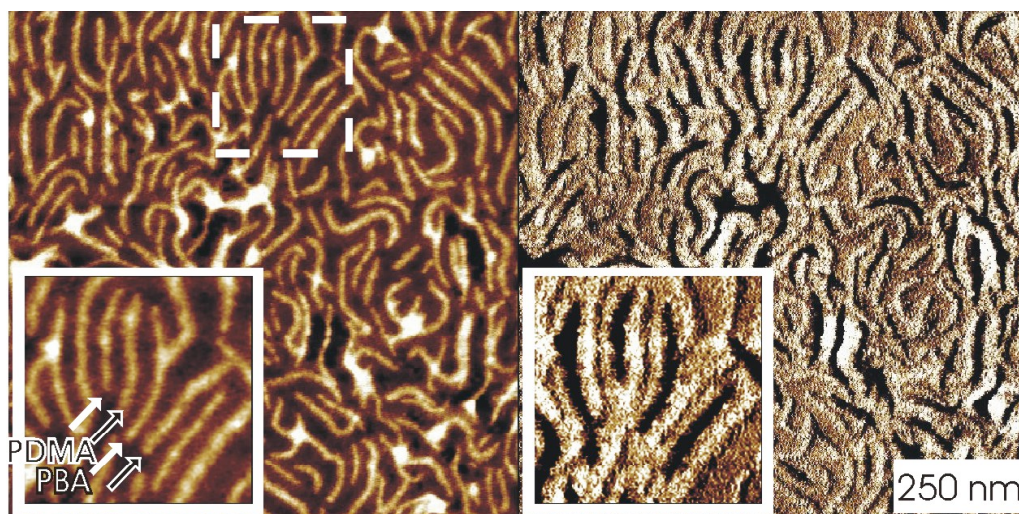


Figure 5.6 Phase Contrast Between PBA and PDMA Phase imaging (right) allows the PDMA and PBA molecules in this $\pi = 7$ mN/m sample to be distinguished and alternation to be seen. In the phase image, the PBA molecules are dark and the PDMA molecules are bright.

5.4 Effects on Mixing

The mixing and ordering behavior of the PDMA and PBA brushes is quite unusual and necessitated further study to determine if the behavior changed with the specific parameters of the molecules or if the architecture of both species was important for the particular result.

5.4.1 Brush Mixtures with Varying Side Chain Lengths

In order to understand the dependence of mixing on side chain length, a series of films were prepared with brushes of different side chain lengths. The first set used the 5.12×10^6 g/mol PDMA brush (side chain DP = 97 (from above experiments)) and three different PBA brushes with side chain DP = 38, 55 (from above experiments) and 80. The second set used the 3.26×10^6 g/mol PBA brush (side chain DP = 55 (from above)) and three different PDMA brushes with side chain DP = 70, 97 (from above), and 121. All films were made from 50/50 by number premixed solutions and compressed to $\pi = 7$ mN/m before transferring and imaging by AFM.

Images from the first set of monolayers are presented in Figure 5.7. Visually, the PBA brush with the smallest side chains seemed to exhibit amazing alternation. The phase images in particular showed the contrast well. However, the intermolecular distance data was strange (see Figure 5.8). The total intermolecular distance was the same as the intermolecular distance just for the PBA molecules. This did not seem to make sense in light of the stunning AFM images. In the places where a PBA molecule is bordered by another PBA molecule, the intermolecular distance is very small, around 20 nm or less. The very small PBA-PBA distances pulled the average significantly down from the alternating distance. The largest PBA brush visually shows some alternation, but does not appear as

orderly as with the DP = 55 PBA brush. The arrangement of this pair of molecules was very sensitive to pressure, overlapping very easily. Several overlapping molecules can be seen in Figure 5.7. It seems that the long side chains of the PBA molecules may allow them to “slide” over the PDMA molecules, many of the side chains of which are under the water surface. This would not only explain the ease of overlapping, but also the smaller PDMA intermolecular distance in this film compared to those with the smaller PBA brushes. Overall, an increase in the length of the PBA side chains facilitates a decrease in the total intermolecular distance of the system. This could be because of PBA’s greater attraction to the water surface becoming dominant, resulting in a quasi-bilayer with PDMA side chains underneath the PBA ones.

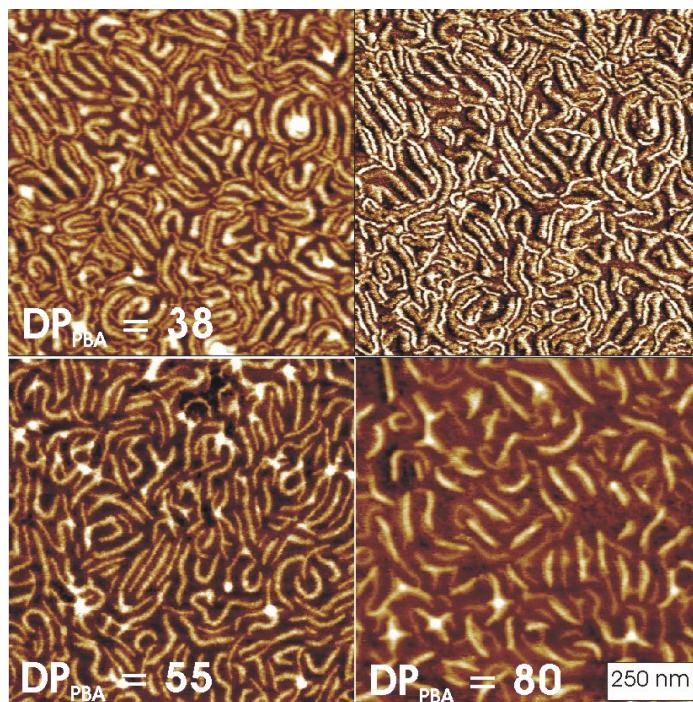


Figure 5.7 AFM Height Images of Mixed Monolayers with Different Side Chain Length PBA Brushes All PBA brushes exhibited an alternating structure with 5.12×10^6 g/mol PDMA (DP = 97). The smallest 9.97×10^5 g/mol PBA brush mix was particularly striking, which can be seen in height (top left) and phase (top right) images. The 4.69×10^6 g/mol PBA brush seemed to facilitate more overlapping of molecules along with alternation.

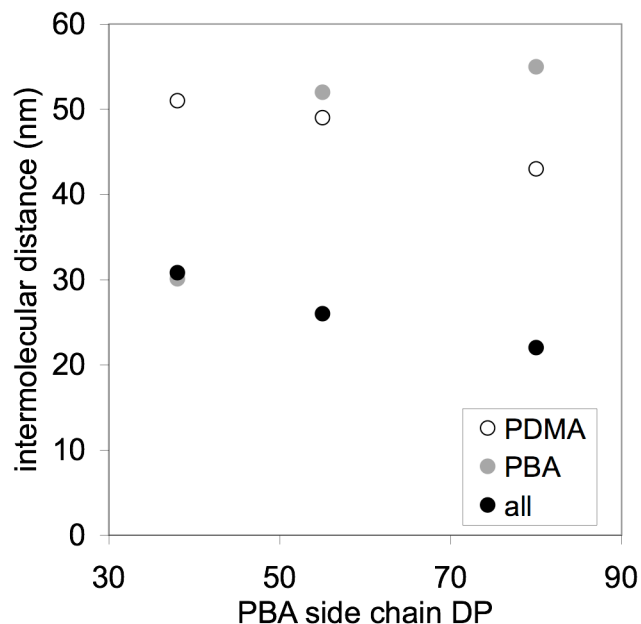


Figure 5.8 Intermolecular Distances of All Species in Monolayers with Different Side Chain Length PBA Brushes The total intermolecular distance for the mixed films at 7 mN/m decreases with an increase in PBA side chain length. This may be due to the PBA molecules actually “sliding” over the PDMA molecules, allowing the PDMA to get closer together.

Figure 5.9 shows representative AFM images from the second set of monolayers prepared by varying the side chain length of the PDMA and holding the PBA molecule constant. Varying the PDMA side chain length had a much weaker effect on intermolecular distances (see Figure 5.10). The total intermolecular distance did not change significantly over the DP range, while both individual component distances increased slightly. This may be due to the fact that the PDMA side chains can loop or dissolve into the water, adjusting how many side chains remain on the surface. In this way both the surface confined and the dissolved side chains regulate the intermolecular distance.

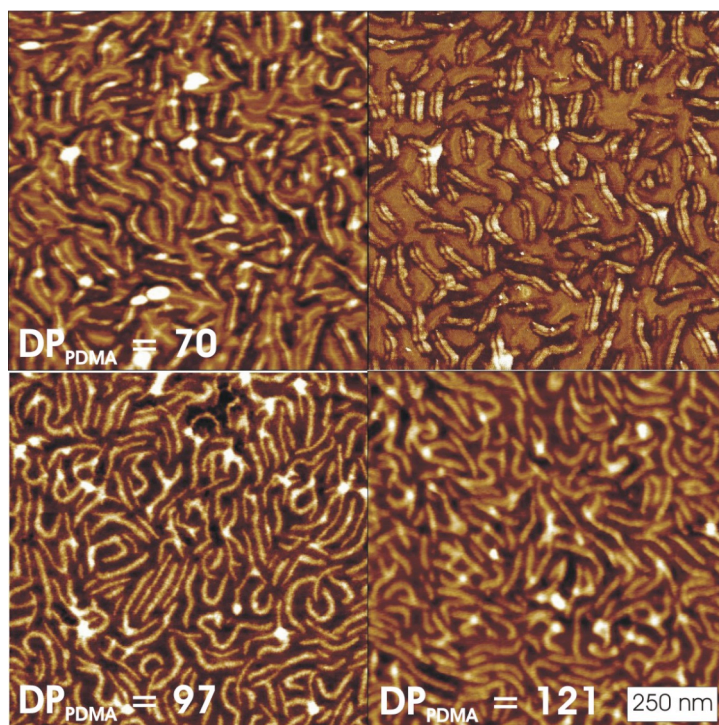


Figure 5.9 AFM Images for Mixed Monolayers with Different Side Chain Length PDMA Brushes AFM height images of 3.26×10^6 g/mol, DP = 55 PBA brush mixed with three different PDMA brushes (top left, height for DP = 70; top right, phase for DP = 70). All combinations exhibited alternation.

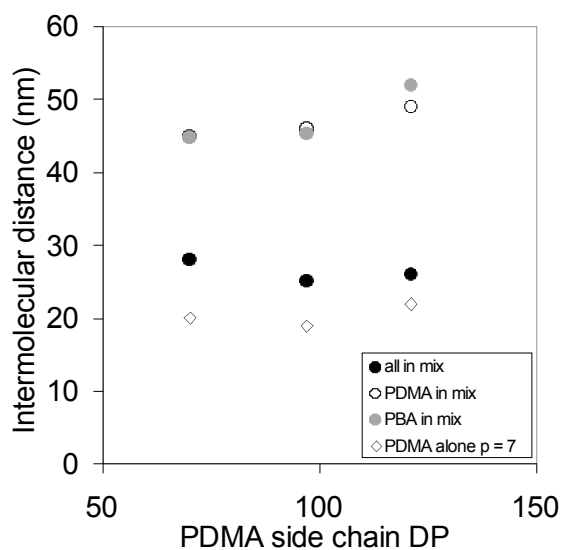


Figure 5.10 Intermolecular Distances Between All Species with Different Side Chain Length PDMA Brushes Changing the PDMA side chain length does not effect the intermolecular distances of the system as strongly as when changing the PBA side chain length. The total intermolecular distance for each system was approximately the same. The total intermolecular distance in the mix is still greater than that of PDMA by itself at 7 mN/m

5.4.2 Linear and Brush Mixtures

To further probe the mechanism of this phenomenon and to determine the link to polymer architecture, two samples were prepared in the premixed fashion and compressed to monolayers. The first sample was 3.26×10^6 g/mol PBA brush (side chain DP = 55) and 231,000 g/mol linear PDMA and the second was 5.12×10^6 g/mol PDMA brush (side chain DP = 97) and 226,000 g/mol linear PBA. In both samples the linear polymer was in excess. In the first sample, the PBA brush made small domains in a network-like structure and there was no indication of any linear PDMA penetrating between the brushes (see Fig. 5.11). In the second sample, the linear PBA clearly penetrated the PDMA brushes, as seen in height and phase images (see Fig. 5.12). Taking intermolecular distance measurements and comparing them to measurements of the brush alone at the same pressure provided further evidence that PBA was in between the PDMA brushes.

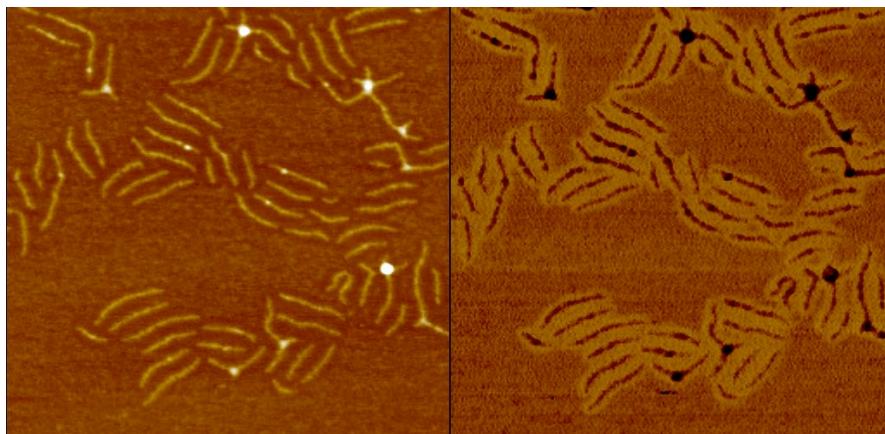


Figure 5.11 AFM Height and Phase Image of Linear PDMA with PBA Brushes The bright backbones of the 3.26×10^6 g/mol PBA brushes stand out in 2.31×10^5 g/mol linear PDMA in the height image (left). In the phase image (right) it is clear that the darker PDMA does not penetrate between the paler side chains of the PBA brushes.

The experiment was repeated with linear PBA of several different molecular weights from 1500 to 1.1×10^6 g/mol and the PDMA brush. In every experiment the linear PBA

inserted itself between the PDMA brush molecules. Surprisingly, the distance between neighboring PDMA molecules was independent of the molecular weight of the linear PBA. In every sample there was an excess of linear polymer, but the PDMA brushes always formed islands with linear PBA evenly incorporated. The intermolecular distance between brushes was always approximately 50 nm. Linear poly(dimethyl siloxane) with PDMA brush also exhibited the same behavior with an average 50 nm intermolecular distance. The one anomaly was with linear perfluoropolyether (PFPE) and PDMA brush. This sample showed dramatic mixing with intermolecular distances greater than 70 nm. This behavior may be unusual due to the unusual nature of PFPE and its extremely low surface energy. Some height images seem to suggest that the PFPE may actually be covering the PDMA brush, which changes the system considerably.

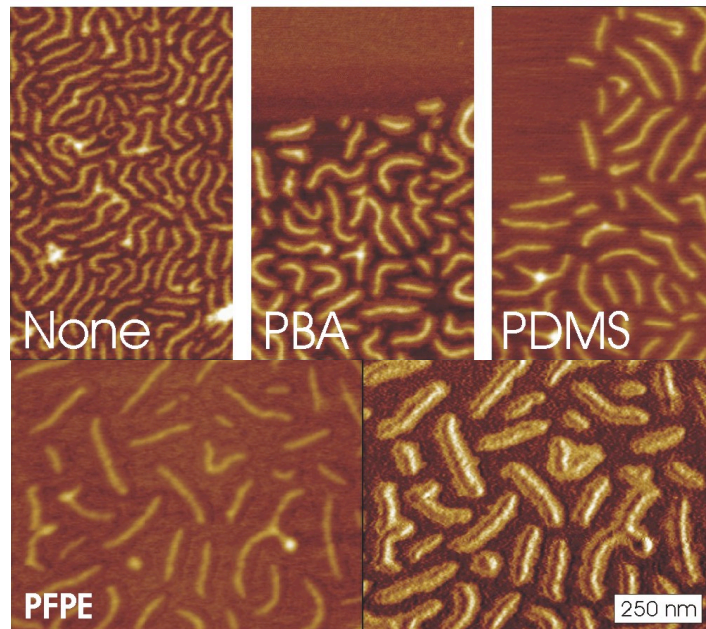


Figure 5.12 Monolayers of Various Linear Polymers Mixed with PDMA Brush AFM height images of 5.12×10^6 g/mol PDMA brush with 3110 g/mol PBA (top middle), 8000 g/mol PDMS, and 4000 g/mol PFPE at 7 mN/m. The image on the bottom right is the phase image corresponding to the height image on the left of the PDMA brush and linear PFPE. The side chains are obscured in the height image, but are made visible in the phase. The top left image is 5.12×10^6 g/mol PDMA brush alone at 7 mN/m.

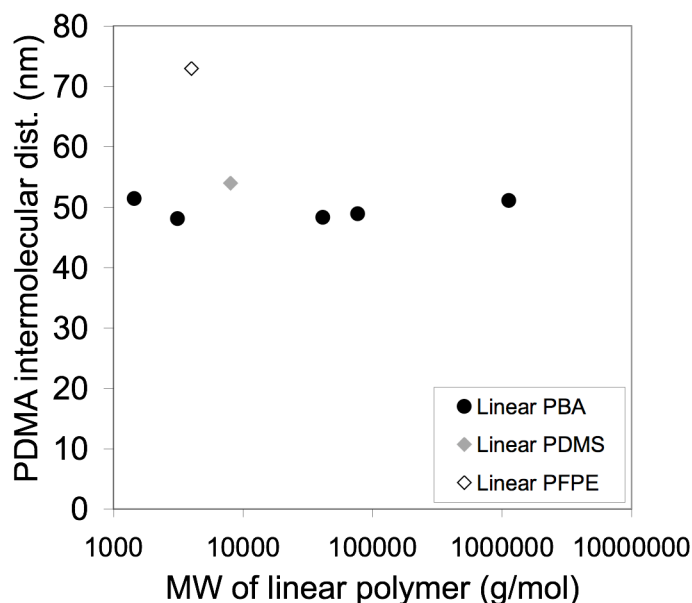


Figure 5.13 The Dependence of PDMA Brush Intermolecular Distance on the Molecular Weight of the Linear Polymer 5.12×10^6 g/mol PDMA brush intermolecular distance did not depend on the molecular weight of the linear polymer it was mixed with. However, the drastic difference in chemical composition of the linear PFPE increased the intermolecular distance significantly.

5.5 Mixing Kinetics and Analysis of Composition

Because of the possibility of the mixed and alternating structures being kinetically trapped, metastable arrangements, samples were prepared differently to observe the molecules' behavior with time and determine their equilibrium arrangement. These trials were different from the ones discussed previously for linear samples in that the polymers were applied separately. Separate chloroform solutions of the 3.26×10^6 g/mol PBA and 5.12×10^6 g/mol PDMA molecules were applied to the LB trough and allowed to remain an amount of time before the barriers were closed and a monolayer transferred. At short times up to 7 hours, there were large domains greater than tens of microns of PBA and PDMA molecules with some smaller areas containing both types of molecules. With increasing time the mixed areas grew larger, while the single polymer phases decreased in size. By 15 hours

the monolayer was completely homogeneously mixed with no single polymer phases remaining. This made it clear that the mixing observed was not a kinetic anomaly, but that it was the thermodynamically preferred state.

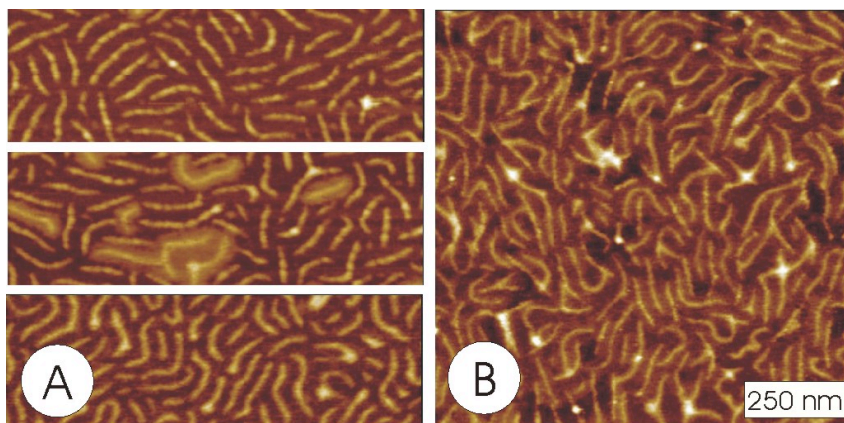


Figure 5.14 AFM Height Images of Brush Monolayers Mixed with Time 5.12×10^6 g/mol PDMA and 3.26×10^6 g/mol PBA brush polymers that are phase separated mix with time. At time zero (A) there are large phase separated domains of PBA and PDMA and some small areas with a low level of mixing. The top image shows a domain of PBA molecules, the middle image a mixed domain, and the bottom image a PDMA domain. By 15 hours (B) the entire monolayer is mixed. Both (A) and (B) are at $\pi = 7$ mN/m.

To quantify the image data, in house software⁸⁸ was employed that measures the contour length and curvature of the molecules, as well as intermolecular distances. Contour lengths can be found using a cutoff height related to the color table of the image, or drawn by hand. Chemically different polymers can be labeled with different colored contours and thereby distinguished by the program. Nearest neighbors are then found using a Delaunay triangulation using the points that make up the marked contour lengths of the molecules. This method of triangulation connects all the points in such a way that the resulting triangles cannot be made smaller by connecting any two other points. After the triangulation the program discards all edges that connect points within the same molecule. It then counts how many triangle edges connect points of the same or different colors on different molecules.

⁸⁸ PEN, David Shirvanyants

Comparing the total number of same color and different color connections can then easily be used to calculate the fractions of like and unlike neighbors as a function of total molecule length. These values give information about the type of mixing within the monolayers. The simplest way to look at a mixed system is to compare it with the results of a randomly mixed system. A random two-component mixture with 50% of each component would exhibit a 0.5 fraction of unlike pairs and 0.25 of each type of like pairs. A larger fraction of unlike pairs suggests that the system is moving toward an ordered state, whereas a smaller fraction suggests that the system is moving toward a phase separated state. A perfectly alternating arrangement would have a fraction of 1 for unlike pairs and 0 for like pairs.

For the monolayers compressed from the premixed solution (section 5.3.2), the fraction of unlike pairs remained approximately constant at 0.30 from 1 mN/m to 5 mN/m (See Fig. 5.15, left graph). At 6 mN/m there was a clear change as the alternating pattern began and the fraction of unlike pairs rose to 0.47. The unlike pair fraction reached a maximum of 0.56 at 7 mN/m. For the equilibrium studies, the fraction of unlike pairs at 7 mN/m grew with time from 0.04 at one hour to 0.54 at 15 hours (see Fig. 5.15, right graph). The equilibrium state at 15 hours is nearly identical to the premixed arrangement. A 0.54 fraction of unlike pairs suggests slightly more than random mixing, but by eye, the images appear to be almost completely alternating. The monolayers are certainly not perfect crystals, but there are clear grains of order. The grain boundaries could affect nearest neighbor results, making the system less ordered on a large scale. In addition, the molecules are flexible and thus exhibit some curvature, which interrupts alternation.

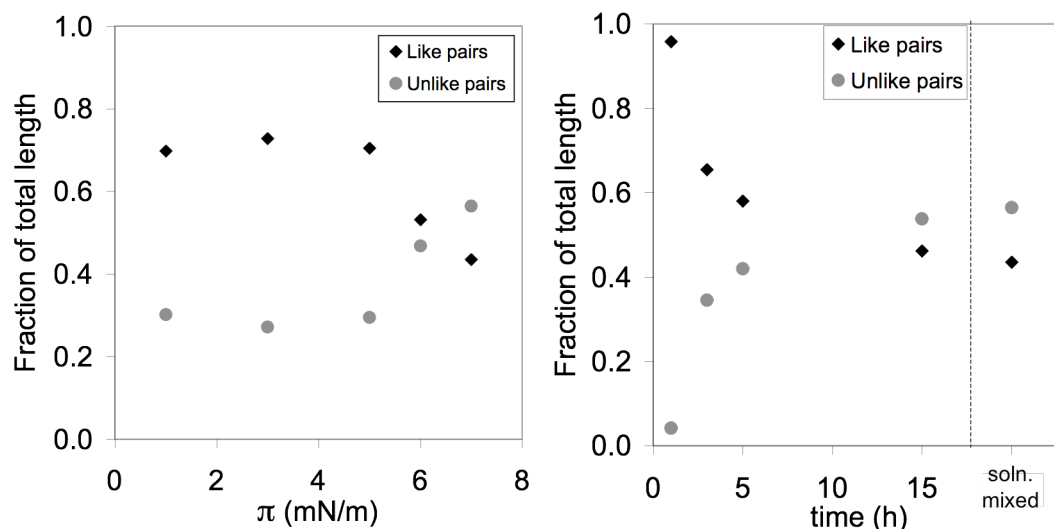


Figure 5.15 Fractions of Like and Unlike Polymer Pairs in Monolayers at Different Pressures and Times Ordering increased with pressure in the premixed monolayers (left) and with time in the postmixed monolayers (right). This is evident by the increase in unlike pairs of molecules and the decrease in like pairs of molecules. All time-dependent data are for $\pi = 7$ mN/m.

Intermolecular distance measurements are a very simple analytical method that can also help quantify the patterning behavior of the mixed films. Comparing the intermolecular distance of all molecules with the intermolecular distance of individual components can show, on average, how far molecules of each type are from one another. For a randomly mixed film, the average intermolecular distance should be in between the individual component intermolecular distances. For a perfectly alternating pattern, the average intermolecular distance would be half that of the individual component intermolecular distances, which would be the same value for both species. In single component films at 1 mN/m, both the PDMA and the PBA brush have an intermolecular distance of about 50 nm; at 7 mN/m PBA still has approximately a 50 nm intermolecular distance, while PDMA's is about 20 nm. In figure 5.16, at 1 mN/m the average intermolecular distance for all molecules is smaller than for both individual species, but only by about 10 nm. The average

intermolecular distances for the individual species are also larger than for a single component sample. This gives some indication of enhanced mixing, but not of any clear patterning. A similar trend is followed until 7 mN/m when the total intermolecular distance becomes approximately half that of the intermolecular distance of the individual species, which is indicative of alternation. The intermolecular distances of the individual species, however, are not equal, which supports the conclusion from the nearest neighbor data that the alternation is not perfect.

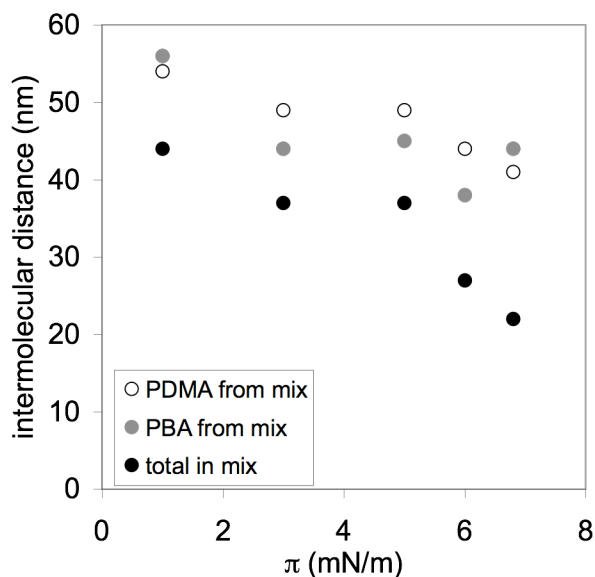
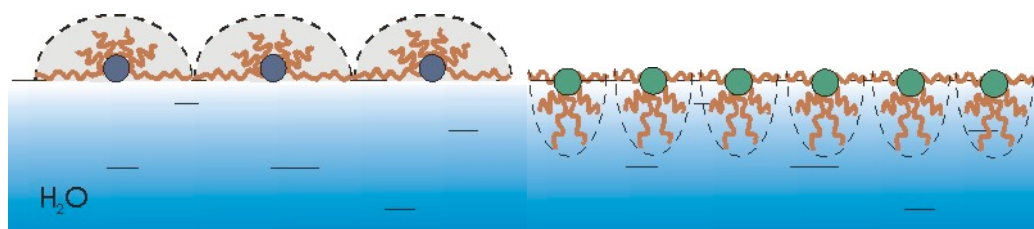


Figure 5.16 Intermolecular Distances Between All Species in the Premixed Brush Monolayer The total intermolecular distance between molecules in the mixed monolayer makes a big jump at 6 mN/m. By 7 mN/m the total intermolecular distance is approximately half that of the individual species, indicating an alternating pattern.

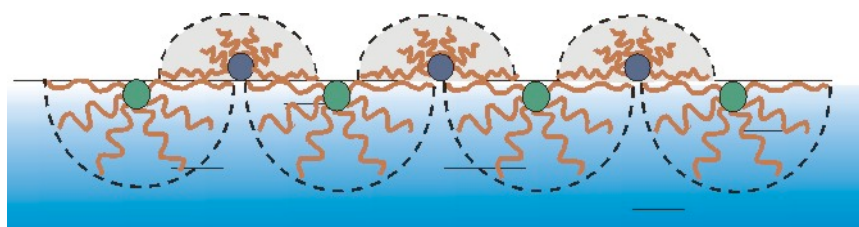
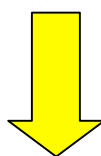
A more sophisticated analysis is probably necessary to take all the variables into account in this somewhat complex system. What is clear, however, is that the system is not phase separated, which is what is expected from a mixture of two chemically different polymers, and there is some degree of ordering within the layer. This must be related to the brush architecture, since linear polymer of the same chemical structure phase separates.

5.6 Discussion

The explanation for this seemingly strange mixing behavior between chemically different polymers is a matter of energetics. While entropy is always present, it is very small. Energetics have to be driving the rearrangement of molecules, because an alternating pattern is among the lowest entropy arrangements for a two component system. It is most likely that the brush structure combined with the water surface changes the energy within the system, causing the mixed state to be the thermodynamically favorable state. Extrapolating from the results discussed in Chapter 4, it is reasonable to assume that some of the side chains from each PDMA molecule are dissolving into the water, while the molecule remains at the interface. Because water is a good solvent for PDMA, there is a net repulsion between side chains of neighboring molecules. This repulsion is relieved by the insertion of linear polymer or a PBA brush molecule between the PDMA molecules.



Phase Separated PBA Brush and PDMA Brush



Two Component Mixed System

Figure 5.17 Scheme of Polymer Brushes at the Air/Water Interface This schematic shows a side view of brush molecules on a water surface at 7 mN/m. PBA brushes have a blue backbone and PDMA brushes have a green backbone. Single component PDMA at 7 mN/m experiences significant repulsion from dissolved side chains, which results in its cylindrical morphology. Phase separated at a fixed surface area, these molecules have a higher energy than if they mixed. When a transition is made to a mixed state, the repulsion experienced by the PDMA is relieved as the molecules can be farther apart and the total energy of the system is lowered.

One of the curious issues that remains unexplained is the 50 nm intermolecular distance that was consistently observed regardless of the second polymer's molecular weight or architecture (PFPE being the only exception). If mixing is truly favored energetically, PDMA brush molecules should disperse in an excess of another polymer to maximize mixing entropy. At this point it is unclear what is stabilizing the polymers at this particular distance.

It is possible that line tension, i.e. the attraction between the expanded PDMA brushes, stabilizes the intercalated structure. Therefore the system resists negative or positive deviations from this particular distance, hence the islands of PDMA brush in an excess of linear polymer. It is also possible that what is observed is an asymmetric phase separation into PDMA brush-rich and linear polymer-rich domains with very little concentration of PDMA in the linear-rich domains. In addition to thermodynamic stability, one may regard the 50 nm distance as a metastable state with a local energy minimum that would take large amounts of time to move from.

What is clear is that this is a very unusual system that offers a way to mix chemically different species in thin films. From what is understood, many of the PDMA side chains are dissolved into the water, while the PBA side chains that are desorbed and collapsed onto the backbone. This results in a system that in a sense is phase separated in the z-direction with PBA on the water surface and PDMA below it and mixed in the x-y direction.

5.5 Conclusion

The brush architecture facilitated the mixing of two chemically different polymers, PBA and PDMA, that otherwise phase separate. Not only did they mix, but the molecules also ordered in an alternating structure due to the intermolecular interactions between the hydrophilic PDMA brushes. In addition, a large variety of linear polymers (PBA, PDMA, PFPE) was able to mix with chemically incompatible brush polymer, also as a result of the brush architecture. The hydrophilic nature of the PDMA combined with the brush architecture and being on the surface of water resulted in repulsion between brushes of the same type, allowing brush or linear polymer of a second type to be inserted between them.

The stability of the alternating morphology is still under investigation. Both thermodynamic (line tension) and kinetic (interfacial translation of large molecules) factors are considered as possible stabilizing agents.

CHAPTER SIX

CONCLUSION

Flexible molecular brushes have exhibited extraordinary conformation and phase behavior that is largely a result of their brush-like architecture. The unusual behavior was especially evident on substrates when studying single adsorbed molecules and dense monolayers. The following major achievements and discoveries have been made.

1. Molecular Imaging: new techniques for characterization of complex macromolecules. New characterization techniques were developed for characterization of molecular weight, molecular conformation, and molecular ordering. The techniques are based on the imaging of individual molecules by AFM in direct space. In combination with the Langmuir-Blodgett technique, we determined number average molecular weight, characterize length distribution of individual arms of star-like macromolecules, and observed local ordering of soft disk-like molecules. This approach was further enhanced by using the soft-lithography techniques which extended the application field to 3D objects.

- Resolving branched architecture comprised of backbone, arms, and side chains. Here, molecular imaging was shown to be an indispensable tool for polymer chemists as it confirms synthetic strategies of complex molecular architectures and also offers accurate molecular characterization.

- Soft-lithography enabled accurate measurements of the height of soft nanometer-sized objects such as macromolecules, colloidal particles, and drops. We measured the true height and evaluated sample deformation due to contact with the AFM tip and due to contact with the PFPE molding precursor.
- Local ordering of collapsed disk-like molecular stars was observed and quantified using developments to in house image analysis software. The replication via soft-lithography also allowed an additional view of the ordered film without deformation due to the tip-sample interactions.

2. New molecular conformation. A new conformation of brush-like macromolecules was observed. Unlike hydrophobic brushes that form globules on low energy substrates, hydrophilic poly(dimethyl acrylamide) brushes demonstrated a cylindrical conformation. It is believed to be stabilized by the repulsion of dissolved side chains.

- Monolayers of hydrophilic brushes at the air/water interface exhibited unusual stability with respect to dissolution into the water subphase. Compared to small molecules and even large polymer chains, brush monolayers are virtually “insoluble” due to their strong attraction to the interface and large size resulting in small changes in mixing entropy.
- Upon lateral compression these hydrophilic brushes rather than collapsing like their hydrophobic counterparts, were observed to stay extended, contracting along the short axis of the molecule forming a cylinder rather than

a globule. This conformation had previously only been observed once in a spreading film.

- The conformations of block and statistical copolymer brushes of n-butyl acrylate and dimethyl acrylamide were dominated by the ability of the DMA to dissolve into the subphase. Therefore all copolymer molecules exhibited the cylindrical conformation at high compression. However, the surface-anchoring character of the nBA monomer units resulted in much larger changes in surface energy than with PDMA homopolymer.

3. New mixing behavior. Hydrophilic and hydrophobic brush polymers were found to mix in a monolayer, unlike their linear counterparts which phase separate.

The mixing was enhanced by lateral compression, the molecules forming an alternating pattern within the film. The hydrophilic PDMA brush also was observed to mix with a variety of linear polymers. It is thought that this unusual mixing behavior is due to the repulsion of dissolved PDMA side chains altering the energetics of the system making mixing energetically favorable.

- Linear polymers phase separate. Premixed solutions of linear PBA and linear PDMA left on the LB trough for times up to 50 hours showed an increase in domain size, confirming for this pair of polymers the general fact that polymers do not mix.
- PBA and PDMA brushes mixed in a monolayer and formed an alternating structure with pressure. The same structure was formed from a less mixed one when the polymers were placed separately on the trough and allowed to

diffuse for 24 hours. Changing the length of the brush side chains had small effects on the structure of the films, but the ordering was still observed.

- PBA linear polymers with a range of molecular weights all penetrated between PDMA brush polymers in a layer. Linear PDMS and PFPE exhibited the same behavior.
- This highly unusual behavior was attributed to the repulsion of dissolved PDMA side chains creating a well of sorts for another polymer to fill in order to minimize its own energy. This could only happen as a result of the tethered brush structure.

Further work needs to be done to better understand the mechanism of mixing and how changing the chemical composition changes a brush molecules' interaction in its environment. One of the most important experiments toward this end would be x-ray scattering of the layer while on the LB trough. This would provide information about the structure of a cross-section of the layer, helping to understand what is really going on the underside of the layer. A very recently developed technique of using the AFM tip to do apertureless scanning near-field optical microscopy (ASNOM) could also benefit this project. With ASNOM an IR spectrum is measured at every point on the AFM topography image. Therefore, it is possible to identify chemically different species in an image by mapping these spectra over the topography. Then exact locations of each type of polymer could be determined. Theoretically, concentration/density data could also be obtained, but it would be technically challenging to achieve. If the technical challenges could be overcome, knowing how much of each type of polymer is in specific locations would increase the understanding

of where each type of side chain is primarily going. There are a variety of other simple experiments that could be done, including mixing other types of polymers with PDMA brush. To know whether this mixing is a universal phenomenon based on the hydrophilic character of the molecules, it would be good to try similar experiments to the ones reported here using a brush synthesized from a different hydrophilic monomer like PEO.

In addition, theoretical simulations and calculations could be very helpful for learning more about the thermodynamic source for particular brush conformations and exactly why mixing occurs under the observed conditions.

The data collected from the studies presented in this dissertation have broadened the understanding of both the conformational behavior and the functional behavior of macromolecular brush molecules. It has brought us one step closer to linking molecular architecture, chemical composition, and behavior of polymer molecules. With continued studies, both experimental and theoretical, macromolecular brush polymers could be applied to a variety of technologies in ways that other materials cannot.

REFERENCES

- Bansil, R.; Stanley, E.; LaMont, J.T. *Annu. Rev. Physiol.* **1995**, *57*, 635.
- Barthlott, W.; Neinhuis, C. *Planta* **1997**, *202*, 1.
- Bartlett, P. *J. Chem. Phys.* **1998**, *109*, 10970.
- Basire, C.; Ivanov, D.A. *Phys. Rev. Lett.* **2000**, *85*, 5587.
- Birshtein, T.M.; Borisov, O.V.; Zhulina, E.B.; Khokhlov, A.R.; Yurasova, T.A. *Polym. Sci. U.S.S.R.* **1987**, *29*, 1293.
- Boyce, J.R.; Shirvanyants, D.; Sheiko, S.S.; Ivanov, D.A.; Qin, S.; Börner, H.; Matyjaszewski, K. *Langmuir* **2004**, *20*, 6005.
- Boyce, J.R.; Sun, F.C.; Sergei, S.S. in “Responsive Polymer Materials: Design and Applications” by Sergei Minko (Ed.), 1-26 (**2006**). (and references therein)
- Bromberg, L.E.; Barr, D.P. *Biomacromol.* **2000**, *1*, 325.
- Burchard, W. *Adv. Polym. Sci.* **1999**, *143*, 113.
- Cha, M.C.; Fertig, H.A. *Phys. Rev. B* **1994**, *50*, 14368.
- Chaikin, P.M.; Lubensky, T.C. “Principles of Condensed Matter Physics” Cambridge, Univ. Press, 1995.
- Chen, L.; Yang, B.L.; Wu, Y.; Yee, A.; Yang, B.B. *Biochemistry* **2003**, *42*, 8332.
- Elli, S.; Ganazzoli, F.; Timoshenko, E.G.; Kuznetzov, Y.A.; Connolly, R. *J. Chem. Phys.* **2004**, *120*, 6257.
- Essentials of Glycobiology; Varki, A.; Cummings, R.; Esko, J.; Freeze, H.; Hart, G.; Marth, J., Eds.; Cold Spring Harbor Laboratory Press: Cold Spring Harbor, NY, 1999.
- Fischer, K.; Schmidt, M. *Macromol. Rapid Commun.* **2001**, *22*, 787.
- Fredrickson, G.H. *Macromolecules* **1993**, *26*, 2825.

- Gallyamov, M.O.; Tartsch, B.; Khokhlov, A.R.; Sheiko, S.S.; Börner, H.G.; Matyjaszewski, K.; Möller, M.; *Macromol. Rapid Comm.* **2004**, *25*, 1703.
- Gerle, M.; Fischer, K.; Roos, S.; Müller, A.H.E.; Schmidt, M.; Sheiko, S.S.; Prokhorova, S.; Möller, M. *Macromolecules* **1999**, *32*, 2629.
- <http://botweb.uwsp.edu/Anatomy/non-secretorytrichomes.htm> (accessed September 2005).
- Israelachvili, J. *Intermolecular & Surface Forces* 2nd ed., Academic Press: London, 2006.
- Jay, G.D.; Haberstroh, K.; Cha, C.-J. *Connet. Tissue. Res.* **1992**, *28*, 71.
- Kaneider, N.C.; Dunzendorfer, S.; Wiedermann, C.J. *Biochemistry* **2004**, *43*, 237.
- Khalatur, P.; Khokhlov, A. R.; Prokhorova, S. A.; Sheiko, S. S.; Moller, M.; Reineker, P.; Shirvanynts, D.; Starovoitova, N. *Eur. Phys. J. E* **2000**, *1*, 99.
- Khalsa, P.S.; Eisenberg, S.R. *J. Biomechanics* **1997**, *30*, 589.
- Khokhlov, A.R.; Möller, M.; *Macromolecules* **2001**, *34*, 8354.
- Khokhlov, A.R.; Semenov, A.N. *Physica A* **1981**, *108*, 546.
- Kofke, D.A.; Bolhuis, P.G. *Phys. Rev. E* **1999**, *59*, 618.
- Kreutzer, G. *et al. Macromolecules* **2006**, *39*, 4506.
- Lecommandoux, S.; Chécot, F.; Borali, R.; Schappacher, M.; Deffieux, A. *Macromolecules* **2002**, *35*, 8878.
- Li, C.; Gunar, N.; Fischer, K.; Janshoff, A.; Schmidt, M. *Angew. Chem. Int. Ed.* **2004**, *43*, 1101.
- Li, Z.; Hou, W.-S.; Bromme, D. *Biochemistry* **2000**, *39*, 529.
- Matyjaszewski, K.; Qi, S.; Boyce, J.R.; Shirvanyants, D.; Sheiko, S.S. *Macromolecules* **2003**, *36*, 1843.
- Maynor, B.W.; LaRue, I., Hu, Z., Rolland, J.P.; Pandya, A.; Fu, Qiang; Liu, Jie; Spontak, R.J.; Sheiko, S.S.; Samulski, R.J.; Samulski, E.T.; DeSimone, J.M. *Small* **2007**, *3*, 845.
- Nakamur, Y.; Wan, Y.; Mays, J.W.; Iatrou, H.; Hadjichristidis, N. *Macromolecules* **2000**, *33*, 8323.
- Nelson, D.R.; Rubinstein, M.; Spaepen, F. *Phil. Mag. A* **1982**, *46*, 105.

Neugebauer, D.; Carson, B.E.; Sheiko, S.S.; Matyjaszewski, K. *Polym. Prep. (Am. Chem. Soc., Div. Polym. Chem.)* **2003**, *44*, 510.

Neugebauer, D.; Zhang, Y.; Pakula, T.; Sheiko, S.S.; Matyjaszewski, K. *Macromolecules* **2003**, *36*, 6746.

Onsager, L. *Ann. N.Y. Acad. Sci.* **1949**, *51*, 627.

Percec, V.; Ahn, C.-H.; Ungar, G.; Yeardley, D.J.P.; Möller, M.; Sheiko, S.S. *Nature* **1998**, *391*, 161.

Potemkin, I. I.; Khokhlov, A. R.; Reineker, P. *Eur. Phys. J. E* **2001**, *4*, 93. Potemkin, I.I.; Khokhlov, A.R.; Sheiko, S.S. *Macromolecules* **2004**, *37*, 3918.

Prokhorova, S. A.; Sheiko, S. S.; Mourran, A.; Moller, M.; Beginn, U.; Zipp, G.; Ahn, C.-H.; Percec, V. *Langmuir* **2000**, *16*, 6862.

Rathgeber, S.; Pakula, T.; Wilk, A.; Matyjaszewski, K.; Beers, K.L. *J. Chem. Phys.* **2005**, *122*, 124904/1.

Rolland, J.P.; Hagberg, E.C.; Denison, G.M.; Carter, K.R.; DeSimone, J.M.; *Angew. Chem. Int. Ed.* **2004**, *43*, 5796.

Rolland, J.P.; Van Dam, R.M.; Schorzman, D.A.; Quake, S.R.; DeSimone, J.M.; *J. Am. Chem. Soc.* **2004**, *126*, 2322.

Rouault, Y.; Borisov, O.V. *Macromolecules* **1996**, *29*, 2605.

Saariaho, M.; Ikkala, O.; Szleifer, I.; Erukhimovich, I.; ten Brinke, G. *J. Chem. Phys.* **1997**, *107*, 3267.

Saariaho, M.; Ikkala, O.; ten Brinke, G. *J. Chem. Phys.* **1999**, *110*, 1180.

Saariaho, M.; Subbotin, A.; Szleifer, I.; Ikkala, O.; ten Brinke, G. *Macromolecules* **1999**, *32*, 4439.

Santen, L.; Krauth, W. Los Alamos National Laboratory, Preprint Archive, Condensed Matter (2001), 1-4, arXiv:cond-mat/0107459.

Schaefgen, J. R.; Flory, P. J. *J. Am. Chem. Soc.* **1948**, *70*, 2709.

Scott, J.E. *Biochemistry* **1996**, *35*, 8795.

Seog, J.; Dean, D.; Plaas, A.H.K.; Weng-Palms, S.; Grodzinsky, A.J.; Ortiz, C. *Macromolecules* **2002**, *35*, 5601.

Shirvanyants, D. PEN Image Analysis Program

Sheiko, S.S.; Prokhorova, S.A.; Beers, K.A.; Matyjaszewski, K.; Potemkin, I.I.; Khokhlov, A.R.; Möller, M. *Macromolecules* **2001**, *34*, 8354.

Sheiko, S.S.; Sumerlin, B.S.; Matyjaszewski, K. *Prog. Poly. Sci.* **2008**, (*submitted*) (and references therein)

Shulz, G.V.Z. *Phys. Chem.* **1939**, *B43*, 25.

Simon, W.H. *J. Biomech* **1971**, *7*, 379.

Subbotin, A.; Saariaho, M.; Stepanyan, R.; Ikkala, O.; ten Brinke, G. *Macromolecules* **1999**, *32*, 4439.

Sumerlin, B.S.; Matyjaszewski, K. in “Macromolecular Engineering: Precise Synthesis, Materials Properties, Applications” by Krzysztof Matyjaszewski, Yves Gnanou, and Ludwik Leibler (Eds.), v.2, 1103-1136 (**2007**). (and references therein)

Sun, F.; Sheiko, S.S.; Moller, M.; Beers, K.; Matyjaszewski, K.; *J. Phys. Chem. A* **2004**, *108*, 9682.

Terao, K.; Nakamura, Y.; Norisuye, T. *Macromolecules* **1999**, *32*, 711.

Tsubaki, K.; Kobayashi, H.; Sato, J.; Ishizu, K. *J. Colloid Interface Sci.* **2001**, *241*, 275.

Xu, H.; Shirvanyants, D.; Beers, K.L.; Matyjaszewski, K.; Dobrynin, A.V.; Rubinstein, M.; Sheiko, S.S.; *Phys. Rev. Lett.* **2005**, *94*, 237801.

Yuan, J.; Xu, Y.; Schumacher, M.; Schmalz, H.; Müller, A.H.E. *Polym. Prepr. (Am. Chem. Soc., Div. Polym. Chem.)* **2008**, in press